NATIONAL ADVISORY COMMITTEE FOR AERONAUTICS

TECHNICAL NOTE

No. 1339

WIND-TUNNEL INVESTIGATION OF THE EFFECT OF POWER AND FLAPS ON THE STATIC LONGITUDINAL STABILITY AND CONTROL CHARACTERISTICS OF A SINGLE-ENGINE HIGH-WING AIRPLANE MODEL

By John R. Hagerman

Langley Memorial Aeronautical Laboratory
Langley Field, Va.

Washington
July 1947

NATIONAL ADVISORY COMMITTEE FOR AERONAUTICS

TECHNICAL NOTE NO. 1339

WIND-TUNNEL INVESTIGATION OF THE EFFECT OF POWER AND FLAPS ON THE STATIC LONGITUDINAL STABILITY AND CONTROL CHARACTERISTICS OF A SINGLE-ENGINE HIGH-WING AIRPLANE MODEL

By John R. Hagerman

SUMMARY

An investigation was conducted to determine the effect of power and full-span slotted flaps on the longitudinal stability and control characteristics of a single-engine high-wing airplane. The model combinations investigated included three power conditions - namely, propeller off, propeller windmilling, and power on - tested with flap neutral, single slotted flap, and double slotted flap.

The results of the investigation revealed that deflection of the double slotted flap produced almost twice as much lift increment as did the deflection of the single slotted flap. The application of power greatly increased the lift increments and tail-off lift-curve slopes. The application of power decreased the stability of the model for all three flap configurations. Elevator deflection required to trim was greatly increased with increase in flap deflection. The application of power decreased the amount of negative elevator required to trim the model for all three flap configurations. Deflecting the flaps reduced the maximum wing loading that may be used with power off without exceeding a sinking speed of 25 feet per second. Deflecting the flaps required an increase in power to maintain an indicated sinking speed of 25 feet per second at a given wing loading.

INTRODUCTION

The development and use of high-powered engines have introduced pronounced and important effects upon the stability and control characteristics of the airplane. Previous papers have shown that the propeller had some effect on the characteristics even when in the windmilling condition. The direct effects of the propeller, such as thrust, torque, and normal force, act on the airplane through the propeller shaft. The indirect effects, which may be larger, result from the interaction of the propeller slipstream with the component parts of the airplane. When power is applied, the effect is much greater. Some of the effects of power are shown in references 1 and 2. Reference 1 also presents an analytical study of the contributions of power to longitudinal stability.

High-lift devices, especially flaps, also have a pronounced influence on the stability and control characteristics of the airplane. Flaps are known to increase the difficulty of obtaining longitudinal trim and stability for all flight conditions and to increase the adverse effects of power in many cases. The use of more effective high-lift flaps may be expected to aggravate these difficulties with the possibility that the flaps may be of primary concern as regards longitudinal stability and control.

The location of the wings also has pronounced effects on the stability of the airplane. High-wing airplanes tend to have more longitudinal stability at medium and high lift coefficients than low-wing airplanes (references 3 and 4).

Up to the present time knowledge of the effects of power on airplane stability is incomplete and does not permit quantitative predictions. The literature (see bibliography) contains almost nothing on power effects with deflected flaps or with different wing position. The present systematic investigation of the interrelated effects of power, flaps, and wing position was therefore started in 1941. Longitudinal and lateral stability and control data were obtained for a basic model (fig. 1) with different configurations. The present paper covers the investigation of the longitudinal stability and control of the model as a high-wing airplane. It has been necessary to limit the analysis to qualitative considerations.

COEFFICIENTS AND SYMBOLS

The results of the tests are presented in the form of standard NACA coefficients of forces and moments. Pitching-moment coefficients are given about the center-of-gravity location shown in figure 1 (26.7 percent M.A.C.). The data are referred to the stability axes, which are a system of axes having their origin at the center of gravity and in which the Z-axis is in the plane of symmetry and perpendicular to the relative wind, the X-axis is in the plane of symmetry and perpendicular to the Z-axis, and the Y-axis is perpendicular to the plane of symmetry. The positive directions of the stability axes, of the angular displacements of the airplane and control surfaces, and of the hinge moments are shown in figure 2.

The coefficients and symbols are defined as follows:

C_L	lift coefficient (Z/qS)
ΔC_L	increment in lift coefficient due to flap deflection
C_{L_α}	slope of lift curve, per degree
C_{L_t}	horizontal-tail lift coefficient (L_t/q_tS_t)
C_X	longitudinal-force coefficient (X/qS)
C_m	pitching-moment coefficient (M/qSc')
C_{m_o}	tail-off pitching-moment coefficient
$C_{m_{eff}}$	tail-off pitching-moment coefficient about the effective tail-off neutral point
C_{m_t}	pitching-moment coefficient provided by the tail $\left(C_{m_{tail\ on}} - C_{m_{tail\ off}}\right)$
C_{h_e}	elevator hinge-moment coefficient $(H/qb_e'\bar{c}_e^2)$
T_c'	effective thrust coefficient based on wing area (T_{eff}/qS)
Q_c	torque coefficient $(Q/\rho V^2D^3)$
V/nD	propeller advance-diameter ratio
η	propulsive efficiency $\left(T_{eff}V/2\pi nQ\right)$
V_t	horizontal-tail volume coefficient $\left(S_tl_t/Sc'\right)$
Z	lift
X	longitudinal force
L	rolling moment, pound-feet
N	yawing moment, pound-feet
M	pitching moment about Y-axis, pound-feet
L_t	horizontal-tail lift, positive upward, pounds
H	hinge moment, pound-feet

T_{eff} propeller effective thrust, pounds

Q propeller torque, pound-feet

q free-stream dynamic pressure, pounds per square foot $\left(\frac{\rho V^2}{2}\right)$

q_t effective average dynamic pressure at tail as determined from pitching-moment data, pounds per square foot

S wing area (9.44 sq ft on model)

S_t horizontal-tail area (1.92 sq ft on model)

c airfoil section chord, feet

c' wing mean aerodynamic chord (M.A.C.) (1.36 ft on model)

$\bar{c}_e$ elevator root-mean-square chord back of hinge line (0.264 ft on model)

b wing span (7.458 ft on model)

b_e' elevator span along hinge line (2.546 ft on model)

l_t tail length measured from center of gravity to quarter-chord point of horizontal-tail mean aerodynamic chord

V air velocity, feet per second

D propeller diameter (2.00 ft on model)

n propeller speed, rps

ρ mass density of air, slugs per cubic foot

α angle of attack of fuselage center line, degrees

α_t angle of attack of tail chord line

ϵ effective angle of downwash at the tail as determined from pitching-moment data, degrees

ψ angle of yaw, degrees

i_t angle of stabilizer with respect to fuselage center line, positive when trailing edge is down, degrees

δ	control-surface deflection with respect to chord of fixed surface, degrees
β	propeller blade angle at 0.75 radius (25° on model)
n_o	tail-off neutral point, percent wing mean aerodynamic chord; distance of tail-off neutral point behind leading edge of wing mean aerodynamic chord
n_p	neutral point, percent wing mean aerodynamic chord; distance of neutral point behind leading edge (center-of-gravity location for neutral stability in trimmed flight)
V_i	indicated airspeed, miles per hour $\left(\sqrt{\sigma}V/1.467\right)$
V_S	sinking speed, feet per second
V_{S_i}	indicated sinking speed, feet per second $\left(\sqrt{\sigma}V_S\right)$
σ	ratio of air density at altitude to air density at sea level

Subscripts:

a	aileron
b	trimmed conditions with center of gravity at the neutral point
e	elevator
eff	effective
r	rudder
t	horizontal tail

MODEL AND APPARATUS

The tests were conducted in the Langley 7- by 10-foot tunnel described in references 5 and 6. The test body is a $\frac{1}{5}$-scale model of a fighter-type airplane (fig. 1). The wing design characteristics are given in table I. No landing gear was used for these tests, inasmuch as the effect of landing gears on longitudinal stability is known to be small.

The wing was fitted with a 40-percent-chord double slotted flap covering 93 percent of the span. This flap was designed from the data of reference 7. For the flap-neutral tests the flap was retracted and the gaps were faired to the airfoil contour with modeling clay. For the single-slotted-flap tests, the front flap was retracted and faired to the airfoil contour with modeling clay. The rear flap, which represented the flap for a single-slotted-flap configuration, had a 25.66-percent chord and was maintained at a setting of 30° for the single-slotted-flap tests. For the double-slotted-flap tests, the rear flap was set at 30° relative to the front flap which in turn was set at 30° relative to the wing. With flaps deflected there was about $\frac{1}{32}$-inch clearance between the end of the flap and the fuselage.

During the preliminary stages of the investigation it became apparent that a conventional horizontal tail surface would be inadequate to provide longitudinal trim when the double slotted flap was used. As a result, the horizontal tail shown in figures 1 and 3 was designed for the present tests. (See tables I and II.) The present horizontal tail has an inverted Clark Y airfoil section and is equipped with a fixed leading-edge slot. The slot had a constant chord but was located to approximate the best slot shape given in reference 8. For the flap-neutral and single-slotted-flap stabilizer and elevator tests, the slot was filled in and faired to the contour of the tail. The slot was left open for one stabilizer setting during single-slotted-flap tests for comparative purposes. The tail slot was left open for the double-slotted-flap tests.

Tests were made to determine the characteristics of the horizontal tail for use in the determination of the angle of downwash and the dynamic-pressure ratio at the tail. For these tests the tail unit was mounted in the Langley 7- by 10-foot tunnel as shown in figure 4.

The 2-foot-diameter, three-blade, right-hand metal propeller was set for a blade angle of 25° at 0.75 radius for all tests. The dimensional characteristics of the propeller are given in figure 5. The power for the model propeller was obtained from a 56-horsepower water-cooled induction motor mounted in the fuselage nose. The propeller speed (rpm) was measured by means of an electric tachometer accurate to within 0.2 percent.

Elevator hinge moments were measured by means of an electric strain gage mounted in the stabilizer.

TESTS AND RESULTS

Test Conditions

The tests were made in the Langley 7- by 10-foot tunnel (reference 5) at dynamic pressures of 12.53 pounds per square foot for power-on tests with the double slotted flap and 16.37 pounds per square foot for all other tests. These dynamic pressures correspond to airspeeds of about 70 and 80 miles per hour. The corresponding test Reynolds numbers were 875,000 and 1,000,000, based on the wing mean aerodynamic chord of 1.36 feet. Because of the turbulence factor of 1.6 for the tunnel, effective Reynolds numbers (for maximum lift coefficients) were about 1,400,000 and 1,600,000.

Corrections

All power-on data have been corrected for tares caused by the model support strut. No power-off tares were obtained because they have been found to be relatively small and erratic on similar models with flaps deflected; thus, omission of the power-off tares is not believed to change the results very much. The test results for the isolated horizontal tail were corrected for tares obtained by testing the tail assembly with the horizontal tail removed. Jet-boundary corrections that include the effect of slipstream have been applied to the angles of attack, the longitudinal-force coefficient, and the tail-on pitching-moment coefficients. The corrections were computed from reference 9 as follows:

$$\Delta\alpha = 57.3\delta_w\frac{S}{C}C_L$$

$$\Delta C_X = -\delta_w\frac{S}{C}C_L^2$$

$$\Delta C_m = -57.3\left(\frac{\delta_T}{\sqrt{q_t/q}} - \delta_w\right)\frac{S}{C}\frac{\partial C_m}{\partial i_t}C_L$$

where

δ_w jet-boundary correction factor at wing (0.1125)

δ_T total jet-boundary correction at tail (varies between 0.20 and 0.21)

S model wing area (9.44 sq ft)

C tunnel cross-sectional area (69.59 sq ft)

$\frac{\partial C_m}{\partial i_t}$ rate of change in pitching-moment coefficient per degree change in stabilizer setting as determined in tests

q_t/q ratio of effective dynamic pressure over the horizontal tail to free-stream dynamic pressure

All corrections were added to the test data.

Test Procedure

Propeller calibrations were made by measuring the longitudinal-force coefficient for a range of propeller speeds with the model at zero angle of attack, flap neutral, and tail removed. The effective thrust coefficient T_c' was then determined from the relation

$$T_c' = C_{X_{\text{propeller operating}}} - C_{X_{\text{propeller removed}}}$$

The motor torque was also measured from which propeller efficiency was computed. The results of the propeller calibration are shown in figure 6.

The variation of the effective thrust coefficient T_c' with the lift coefficient C_L used for the tests is given in figure 7. A straight-line variation was used because it is a close approximation to the variation for airplanes with constant-speed propellers operating at constant power. Preliminary runs were made by setting the propeller speed to obtain a given value of T_c' and then varying the angle of attack α until the value of C_L, corresponding to the set value of T_c' indicated in figure 7, was read on the scale. The results were then cross-plotted to obtain a curve of propeller speed against angle of attack. All subsequent power-on tests with the same flap setting were also made at the angles of attack corresponding to the aforementioned propeller speeds.

The use of a straight-line variation of T_c' with C_L implies that the propeller efficiency is proportional to the speed; for this case the value of $\eta\sqrt{C_L}$ was taken as 0.98. Although this assumption requires propeller efficiencies that would never be reached at low lift coefficients on an actual airplane, the error in T_c' is small because the values of T_c' are small. The value of T_c' for the tests with the propeller windmilling was about -0.005. The approximate amount of engine horsepower represented for various model scales and wing loadings is given in figure 8.

Because of an error in part of the investigation of the double-slotted-flap configuration, some of the data are omitted. The data presented herein are composed of both stabilizer and elevator tests plotted in the same figure. Neutral points were determined from these data where possible, but the stability parameters were not obtainable.

Method of Analysis

Neutral points.- A neutral point is a center-of-gravity location for which $\frac{dC_m}{dC_L}$ is zero and the airplane is trimmed. For the power-on case, $\frac{dC_m}{dC_L}$ is evaluated with the appropriate variation of T_c' with C_L. The neutral points were determined by the method of tangents developed in references 10 and 11. The use of this method provides the locations of neutral points but does not show qualitatively the individual aerodynamic factors (longitudinal-stability parameters) affecting the locations. When the neutral point is behind the center of gravity the airplane is statically stable. The symbol n_p is used to refer either to the neutral point or to its distance from the leading edge. Phrases such as "increase in n_p," "n_p moves rearward," and "increase in stability" have the same significance in the discussion.

The following equation, although laborious for the solution of neutral points, shows the relative significance of the several aerodynamic factors. The derivation of this equation is found in the appendix of reference 12. The neutral points were computed by the method of tangents of reference 10 and checked by the present equation which is accurate within ±2 percent.

$$n_p = n_c + \frac{V_{t_b} \frac{dC_{L_t}}{d\alpha_t} \frac{q_t}{q} \left(1 - \frac{d\epsilon}{d\alpha}\right)}{\left(\frac{dC_L}{d\alpha}\right)_b (1 - P)} + \frac{C_{m_{eff}}}{C_{L_b}\left(\frac{1}{P} - 1\right)}$$

where

V_{t_b} horizontal-tail volume coefficient for the center of gravity at the neutral point

$\dfrac{dC_{L_t}}{d\alpha_t}$ isolated-tail lift-curve slope

q_t/q effective dynamic-pressure ratio

$\left(\dfrac{dC_L}{d\alpha}\right)_b$ trim lift-curve slope of complete airplane (for derivation see appendix of reference 12)

$$\left[\frac{dC_{L_{tail\ off}}}{d\alpha}\left(1 + \frac{n_p - n_o}{l_t/c}\right)\right]$$

P power parameter $\left[\dfrac{\dfrac{d(q_t/q)}{dC_{L_b}}}{\dfrac{q_t/q}{C_{L_b}}}\right]$

$C_{m_{eff}}$ pitching-moment coefficient about the effective tail-off aerodynamic center n_o

$\dfrac{d\epsilon}{d\alpha}$ rate of change of downwash angle with angle of attack

C_{L_b} trim lift coefficient of complete airplane

Dynamic-pressure ratio.- For the method of determining the effective dynamic-pressure ratio q_t/q and the effective downwash angle at the tail ϵ, see the appendix of reference 12. These values are obtained from the contribution of the tail to the pitching moment and are not necessarily those that would be obtained from flow surveys.

Presentation of Results

A short outline of the figures showing the test results is as follows:

DISCUSSION

Lift Characteristics

Because the tests were not carried through maximum lift, a comparison of the maximum lift coefficient of the model with the maximum lift coefficient from section data was not possible.

Effect of flaps.- The double-slotted-flap configuration produced almost twice as much lift-coefficient increment as the single-slotted-flap configuration without power. (See table III.) The increments for both configurations were increased by power, but the double-slotted-flap configuration produced the greater increase. The greater increments in lift due to the double slotted flap are caused by greater thrust coefficients at the higher lift coefficients. The results are in general accord with theory.

Effect of power.- Application of power resulted in substantial increases in tail-off lift-curve slopes and tail-off lift coefficients for all flap configurations (table III). The largest increases were obtained for the double-slotted-flap configuration. The increases in lift coefficient are caused by the increased velocity over the part of the wing in the slipstream. The increases in lift-curve slope are caused partly by the growth of this increased velocity with angle of attack according to the thrust-coefficient variation $T_c' = 0.161C_L$. This action of the propeller slipstream upon the lift-curve slope and lift-coefficient increment is characteristic of airplanes employing tractor-propeller arrangements. (See bibliography.) The flap provides greater increments of lift during power-on operation if immersed in the slipstream. Values of the trim-lift increment of the complete airplane are lower than tail-off lift increments of table III because of the large down loads required by the tail.

Effect of wing position.- A comparison of the model tested as a low-wing airplane (reference 12) and the model tested as a high-wing airplane (present paper) showed that the high-wing model produced slightly higher lift-curve slopes. The lift increments caused by power and flaps, however, were about the same for both models.

Elevator-Fixed Stability

Effect of flaps.- A study of the neutral-point curves in figures 13(a) and 13(b) indicates an increase in stability with an increase in lift coefficient for all flap configurations investigated. This increase is noted in most high-wing airplane data and is largely due to the rearward movement of n_o with lift coefficient. (See figs. 16(a) and 16(b).)

A comparison of the data for the flap-neutral and single-slotted-flap configurations showed a forward movement of the neutral point over the lift-coefficient range. This forward movement may be largely attributed to the forward shift of n_o and also the increase in $(dC_L/d\alpha)_b$. (See figs. 16(a) and 16(b).) The effect of the double slotted flap compared to the single slotted flap showed very little change in neutral-point location at the lift coefficients for both flap configurations.

The large forward shift of n_o is presumed to be componsated by an increase in $\left(\frac{dq_t/q}{dC_L}\right)_b$. With the application of power the neutral point showed the tendency to move forward with increasing lift coefficient for the three flap configurations investigated. (See fig. 15.) This increase in n_p may also be traced to the increase in n_o. (See fig. 16(c).) A comparison of the flap-neutral and the single-slotted-flap configurations showed a loss in stability at the same lift coefficient. The comparison of the single-slotted-flap and double-slotted-flap configurations, however, showed an increase in stability at the lift coefficients. The loss in stability caused by the single slotted flap may be traced to the increase of $(dC_L/d\alpha)_b$ and the decrease of both q_t/q and $\left[\frac{d(q_t/q)}{dC_L}\right]_b$ (See fig. 16(c).) The increase in stability resulting from the double slotted flap is incompletely explained because of the lack of data, but an inspection of the tail-off pitching-moment curve of figure 11(c) suggests that n_o is largely responsible.

Effect of power.- The greatest stability (most rearward n_p), in agreement with references 1 and 2, was obtained with the propeller off. (See fig. 14.) Addition of the windmilling propeller for all three flap configurations reduced the stability appreciably. Application of power brought a greater reduction. By far, the greatest reduction occurred at high lift coefficients with the double slotted flap deflected.

With the propeller windmilling and flap neutral (fig. 14), the loss in stability at low lift coefficients is traced to the slightly forward shift of n_o and at higher lift coefficients, to the large increase of $d\epsilon/d\alpha$ with increasing lift coefficient. (See fig. 17(a).) The forward shift of n_o caused by adding the propeller is explained by the fact that a pitched propeller produces a normal force similar to a small fixed horizontal airfoil. The loss in stability resulting from the application of power is primarily caused by the large increase of $d\epsilon/d\alpha$ and $(dC_L/d\alpha)_b$, both of which more than offsets the increase in q_t/q and $\left[\frac{d(q_t/q)}{dC_L}\right]_b$.

The effects of power on the single-slotted-flap configuration are similar to those on the flap-neutral configuration but are larger. (See fig. 14.) An increase in n_o is more than offset by increases in $(dC_L/d\alpha)_b$ and $d\epsilon/d\alpha$. (See fig. 17(b).)

The over-all effect of power, relative to the propeller-off case, on the double-slotted-flap configuration is destabilizing as for the single-slotted-flap configuration but is much larger. (See fig. 14.) The forward n_p-shift reaches about 20 percent mean aerodynamic chord at high lift coefficients. (See fig. 15.) Data for the propeller-windmilling case as well as for several of the stability parameters $\left(\frac{d\epsilon}{d\alpha}, \frac{q_t}{q}, \text{ and } \left[\frac{d(q_t/q)}{dC_L}\right]_b\right)$ investigated with propeller off and power on are unavailable. The stability parameters n_o and $(dC_L/d\alpha)_b$, however, show an increase with power as did the single-slotted-flap configuration but this increase is much larger than it is for the double-slotted-flap configuration.

Effect of wing position.– A comparison of the longitudinal stability of the low-wing model (reference 12) with that of the high-wing model showed that for medium and high lift coefficients the high-wing model was more stable for all power and flap conditions. For low lift coefficients the low-wing model was more stable. This fact is a characteristic difference between low-wing and high-wing airplanes.

The high-wing position with flap neutral exhibited a greater destabilizing effect of power than the low-wing position. For the single-slotted-flap configuration the low-wing position showed better stability characteristics with power at low lift coefficients but poorer stability characteristics with power at high lift coefficients.

Elevator-Free Stability

The effects of flap deflection and power on the elevator-free stability, in general, are similar to the effects on elevator-fixed stability. The results show that, in all cases (figs. 13 and 14), the elevator-free neutral point is slightly forward of the elevator-fixed neutral point (between 1 and 6 percent M.A.C.) and indicates a tendency of the free elevator to float with the relative airstream at the tail.

Longitudinal Control and Trim

Effect of flaps.– A study of the elevator test results for the propeller-off condition (figs. 19(a), 20(a), and 11(a)) indicates that the neutral-flap condition will require an elevator deflection of about -20° to trim the model at the maximum lift coefficient for the center of gravity at which the model was tested (26.7 percent M.A.C.). The single-slotted-flap condition at the same stabilizer setting would require a much greater negative elevator deflection for trim at the maximum lift coefficient because the negative tail load required for trim is increased as a result of the increase in tail-off pitching moment due to flaps. The amount of negative elevator required for trim was reduced for the tests to a reasonable value of -11° by adjusting the stabilizer setting downward 8.3°.

Deflection of the double slotted flap causes a large wing-diving moment and an increased downwash at the tail. The resultant downward increment in tail load is insufficient to offset this diving moment. An elevator deflection of about -24°, therefore, will be required to trim the model at the maximum lift coefficient. This deflection is close to the usual limit of negative elevator travel. If the incidence setting of -1.3° were maintained, therefore, the elevator control would probably be insufficient should the center of gravity be shifted forward or should the model be in proximity of the ground. A negative increase in tail incidence through the use of an adjustable stabilizer would improve this condition. Forward center-of-gravity travel, however, would still be seriously limited because the horizontal tail is on the verge of stalling even with the tail slot open.

A comparison of elevator test results with propeller off (figs. 19(a), 20(a), and 11(a)) and with propeller windmilling (figs. 19(b), 20(b), and 11(b)) shows small and negligible differences in the elevator deflections required for trim. The most noticeable difference occurs with the double-slotted-flap configuration; with the propeller windmilling less negative elevator is required for trim than with the propeller off. This difference is due both to the propeller-fin effect and to the corresponding increased downwash at the tail.

A study of the elevator test results for the power-on condition (figs. 19(c), 20(c), and 11(c)) reveals a similarity with the power-off condition discussed previously. The negative elevator deflections required to trim for the flap-neutral and single-slotted-flap configurations were somewhat less with power on but, with the double slotted flap deflected, the elevator deflection required to trim was slightly greater. A negative increase in tail incidence through the use of an adjustable stabilizer would improve this condition.

Effect of power.- The test results for the flap-neutral and single-slotted-flap configurations indicated smaller negative elevator deflections for trim with power on than with propeller off. In the case of the neutral flap, the power effects increase the dynamic-pressure ratio and slightly increase the downwash. (See fig. 17(a).) Inasmuch as a slight downward tail load is required for trim, the increase in dynamic pressure and in downwash act to reduce the negative elevator required for trim. In the case of the single-slotted-flap configuration, figure 20 shows that more down load on the tail is required to trim with power. The increased downwash and dynamic-pressure ratio at the tail, however, tend to reduce the negative elevator required for trim.

The application of power to the model for the double-slotted-flap configuration resulted in a sharp increase in tail-off pitching moment (fig. 11(c)) and, consequently, greater negative tail loads are required to trim. Unless an adjustable stabilizer were provided, the model would have insufficient elevator to maintain control up to the maximum lift coefficient. The proximity of the ground would aggravate the situation and a more negative stabilizer or elevator would be required.

Effect of wing position.- A comparison was made of elevator effectiveness ($dC_{L_t}/d\delta_e$ and $d\alpha_t/d\delta_e$) for the low-wing model (reference 12) and for the present high-wing model. The low-wing model showed the better effectiveness with the flap-neutral configuration; whereas the models showed about the same effectiveness with the single-slotted-flap configuration. The comparison of the low-wing and high-wing models could not be carried to the double-slotted-flap configuration because of the incompleteness of the high-wing data, but the available data suggest that the high-wing model should have a slightly higher elevator effectiveness.

Tuft Studies

Figures 21(a) and 21(b) show the results of tuft studies on the wing with the double slotted flaps extended. With the propeller windmilling (fig. 21(a)) the rear flap was almost completely stalled throughout the angle-of-attack range. The front flap and the main part of the wing, however, did not show any stall characteristics until higher angles of attack were reached. When the main part of the wing started to stall, the rear flap unstalled. When power is applied (fig. 21(b)), most of the center part remains unstalled throughout the angle-of-attack range. This effect of slipstream is in accord with previous experience. It is not known, however, whether the rear flap will stall when on a full-scale airplane.

The wing tips are shown to stall first. This undesirable condition, however, may be considerably affected by the Reynolds number as well as by tunnel-wall effect. Computations indicate that the induced upwash at the wing caused by the tunnel walls increased the effective angle of attack of the tip about $0.3C_L{}^{\circ}$, thus giving the wing an effective washin.

Landing Characteristics

For the purpose of computing landing characteristics, the drag against lift data of the present investigation (effective Reynolds number, 1,600,000) were extrapolated to an effective Reynolds number of 8,000,000 (approximately full scale). The original and the extrapolated curves of C_D against C_L for zero pitching moment are plotted in the lower part of figure 22. With these curves are plotted calculated curves of C_D, required to ensure a sinking speed of 25 feet per second, against C_L for various wing loadings. Another set of curves plotted in the upper part of figure 22 gives V_i against C_L for the same wing loadings.

An example will illustrate the estimation of landing characteristics from figure 22: Select the desired lift coefficient (for example, $C_L = 1.0$) and note the value of C_D measured on the appropriate curve. Next note the value of C_D required on the curve for the desired wing loading (for example, 40 lb/ft^2) for this same value of C_L. If $C_{D_{measured}}$ is less than $C_{D_{required}}$, the sinking speed will be less than 25 feet per second; and if $C_{D_{measured}}$ is more than $C_{D_{required}}$, the sinking speed will be more than 25 feet per second. If $C_{D_{measured}}$ is negative, a climb is indicated.

It was found that a wing loading of approximately 90 pounds per square foot could be attained without exceeding the recommended maximum sinking speed of 25 feet per second (reference 13) with power off and either flap neutral or single slotted flap deflected. (See fig. 22.) With the double slotted flap deflected, a wing loading of approximately 40 pounds per square foot may be attained without exceeding a sinking speed of 25 feet per second.

With the application of power, corresponding to the horsepower on figure 8, for flap neutral and single slotted flap deflected, the airplane will tend to gain altitude over most of the lift range. With the double slotted flap deflected, wing loadings as high as 200 pounds per square foot may be attained without exceeding a sinking speed of 25 feet per second. (See fig. 22.)

The power required to maintain an indicated sinking speed of 25 feet per second (reference 13) at $0.85C_{L_{max}}$ (estimated for effective Reynolds number of 8,000,000) at various wing loadings is shown in figure 23 for three different model scales (1/4, 1/5, and 1/8 scale). This figure, derived from the model data of figure 22, also shows the wing loadings that may be attained without exceeding the recommended sinking speed with power off. With the application of flaps the power must be increased to avoid exceeding the recommended sinking speed at a given wing loading.

CONCLUSIONS

The results of the longitudinal stability and control investigation of a powered model of a single-engine high-wing airplane with full-span single and double slotted flaps and an elevated horizontal tail are in general accord with previous experience with powered models and with qualitative theoretical considerations. In particular, the results indicate that:

Lift characteristics:

1. Deflection of the double slotted flap produced almost twice as much lift-coefficient increment as did the deflection of the single slotted flap.

2. The application of power greatly magnified both the lift increments and tail-off lift-curve slopes.

Longitudinal stability:

1. The application of power decreased the stability of the model for all three flap configurations.

Longitudinal control and trim:

1. Elevator deflection required to trim with power off was increased with increase in flap deflection.

2. The application of power decreased the amount of negative elevator required to trim for all three flap configurations.

Landing characteristics:

1. Deflecting the flaps reduced the maximum wing loading that may be used with power off without exceeding a sinking speed of 25 feet per second.

2. Deflecting the flaps required an increase in power to maintain an indicated sinking speed of 25 feet per second at a given wing loading.

Effect of wing position:

1. The present high-wing model produced slightly higher lift-curve slopes than the corresponding low-wing model discussed in NACA TN No. 1239.

2. The high-wing model was more stable at medium and high lift coefficients; whereas the low-wing model was more stable at low lift coefficients.

3. With flap neutral the elevator effectiveness was better on the low-wing model than on the high-wing model; however, the data available indicated that with an increase in flap deflection the elevator effectiveness might become better on the high-wing model.

Langley Memorial Aeronautical Laboratory
National Advisory Committee for Aeronautics
Langley Field, Va., April 28, 1947

REFERENCES

1. Millikan, Clark B.: The Influence of Running Propellers on Airplane Characteristics. Jour. Aero. Sci., vol. 7, no. 3, Jan. 1940, pp. 85-103. (Discussion, pp. 103-106.)

2. Recant, Isidore G., and Swanson, Robert S.: Determination of the Stability and Control Characteristics of Airplanes from Tests of Powered Models. NACA ARR, July 1942.

3. Sherman, Albert: Interference of Tail Surfaces and Wing and Fuselage from Tests of 17 Combinations in the N.A.C.A. Variable-Density Tunnel. NACA Rep. No. 678, 1939.

4. Wallace, Arthur R., and Turner, Thomas R.: Wind-Tunnel Investigation of Effect of Yaw on Lateral-Stability Characteristics. V - Symmetrically Tapered Wing with a Circular Fuselage Having a Horizontal and a Vertical Tail. NACA ARR No. 3F23, 1943.

5. Harris, Thomas A.: The 7 by 10 Foot Wind Tunnel of the National Advisory Committee for Aeronautics. NACA Rep. No. 412, 1931.

6. Wenzinger, Carl J., and Harris, Thomas A.: Wind-Tunnel Investigation of an N.A.C.A. 23012 Airfoil with Various Arrangements of Slotted Flaps. NACA Rep. No. 664, 1939.

7. Harris, Thomas A., and Recant, Isidore G.: Wind-Tunnel Investigation of NACA 23012, 23021, and 23030 Airfoils Equipped with 40-Percent-Chord Double Slotted Flaps. NACA Rep. No. 723, 1941.

8. Weick, Fred E., and Wenzinger, Carl J.: The Characteristics of a Clark Y Wing Model Equipped with Several Forms of Low-Drag Fixed Slots. NACA Rep. No. 407, 1932.

9. Swanson, Robert S., and Schuldenfrei, Marvin J.: Jet-Boundary Corrections to the Downwash behind Powered Models in Rectangular Wind Tunnels with Numerical Values for 7- by 10-Foot Closed Wind Tunnels. NACA ARR, Aug. 1942.

10. Schuldenfrei, Marvin: Some Notes on the Determination of the Stick-Fixed Neutral Point from Wind-Tunnel Data. NACA RB No. 3I20, 1943.

11. Schuldenfrei, Marvin: Some Notes on the Determination of the Stick-Free Neutral Point from Wind-Tunnel Data. NACA RB No. 4B21, 1944.

12. Wallace, Arthur R., Rossi, Peter F., and Wells, Evalyn G.: Wind-Tunnel Investigation of the Effect of Power and Flaps on the Static Longitudinal Stability Characteristics of a Single-Engine Low-Wing Airplane Model. NACA TN No. 1239, 1947.

13. Gustafson, F. B., and O'Sullivan, William J., Jr.: The Effect of High Wing Loading on Landing Technique and Distance, with Experimental Data for the B-26 Airplane. NACA ARR No. L4K07, 1945.

BIBLIOGRAPHY

Harris, R. G.: Forces on a Propeller Due to Sideslip. R.&M. No. 427, British A.C.A., 1918.

Glauert, H.: The Stability Derivatives of an Airscrew. R &M. No. 642, British A.C.A., 1919.

Koning C.: Influence of the Propeller on Other Parts of the Airplane Structure. Vol. IV of Aerodynamic Theory, div. M, W. F. Durand, ed., Julius Springer (Berlin), 1935, pp. 361-430.

Weinig, F.: Die Strömungsverhältnisse im Schraubenstrahl. Jahrb. 1936 der LGL, R. Oldenbourg (Munich), pp. 29-56.

Smelt, R., and Davies, H.: Estimation of Increase in Lift Due to Slipstream. R. & M. No. 1788, British A.R.C., 1937.

Flügge-Lotz, I., and Küchemann, D.: Zusammenfassender Bericht über Abwindmessungen ohne und mit Schraubenstrahl. Jahrb. 1938 der deutschen Luftfahrtforschung, R. Oldenbourg (Munich), pp. I 172 -I 193. (Available as R.T.P. Translation No. 870, British Ministry of Aircraft Production.) Contains bibliography on general power effects.

Helmbold H. B.: Untersuchungen über den Einfluss des Luftschraubenstrahls auf den Abwind und die Höhenleitwerkswirkung. Luftfahrtforschung, Bd. 15, Lfg. 1/2, Jan. 20, 1938, pp. 3-8.

Muttray, H.: Untersuchungen über den Abwind hinter einem Trapezflügel mit Rumpf und Schraube. Luftfahrtforschung, Bd. 15, Lfg. 3, March 20, 1938, pp. 101-122. (Available as NACA TM No. 876, 1938.)

Stüper, J.: Einfluss des Schraubenstrahls auf Flügel und Leitwerk. Luftfahrtforschung, Bd. 15, Lfg. 4, April 6, 1938, pp. 181-205. (Available as NACA TM No. 874, 1938.)

Franke, A., and Weinig, F.: Tragflügel und Schraubenstrahl. Luftfahrtforschung, Bd. 15, Lfg. 6, June 6, 1938, pp. 303-314. (Available as NACA TM No. 920, 1939.)

Flügge-Lotz, I, and Solf, K.: Strömungsaufnahmen eines durch einem Tragflügel gestörten Schraubenstrahles. Luftfahrtforschung, Bd. 17, Lfg. 6, June 20, 1940, pp. 161-166.

Goett, Harry J., and Pass, H. R.: Effect of Propeller Operation on the Pitching Moments of Single-Engine Monoplanes. NACA ACR, May 1941.

v. Baranoff, A.: Effect of the Propeller Slipstream on Downwash. R.T.P. Translation No. 1555, British Ministry of Aircraft Production. (From Luftfahrtforschung, Bd. 19, Lfg. 1, Jan. 20, 1942, p. 1-10.)

Pass, H. R.: Wind-Tunnel Study of the Effects of Propeller Operation and Flap Deflection on the Pitching Moments and Elevator Hinge Moments of a Single-Engine Pursuit-Type Airplane. NACA ARR, July 1942.

Ribner, Herbert S.: Propellers in Yaw. NACA ARR No. 3L09, 1943. Contains bibliography on propeller fin effect.

Goett, Harry J., and Delany, Noel K.: Effect of Tilt of the Propeller Axis on the Longitudinal-Stability Characteristics of Single-Engine Airplanes. NACA ACR No. 4E29, 1944.

Ribner, Herbert S.: Notes on the Propeller and Slipstream in Relation to Stability. NACA ARR No. L4I12a, 1944.

TABLE I

MODEL WING AND TAIL-SURFACE DATA

	Wing	Horizontal tail	Vertical tail
Area, sq ft	9.440	1.920	1.250
Span, ft	7.458	2.542	1.508
Aspect ratio	5.91	3.36	1.81
Taper ratio	0.445	0.438	-----------
[a]Dihedral, deg	1.9	0	-----------
Root section	NACA 2215	Clark Y (Inverted)	NACA 0009
Tip section	NACA 2209	Clark Y (Inverted)	NACA 0004.5
[b]Angle of incidence at root, deg	1.0	-1.3, 7	-1.50
[b]Angle of incidence at tip, deg	1.0	-1.3, 7	-1.50
M.A.C., ft	1.360	----------	-----------
Root chord, ft	1.800	1.141	1.272
Theoretical tip chord, ft	0.800	0.500	-----------

[a]Dihedral measured with respect to chord plane.
[b]Angle of incidence measured with respect to fuselage center line.

NATIONAL ADVISORY
COMMITTEE FOR AERONAUTICS

TABLE II

MODEL CONTROL-SURFACE DATA

	Elevator	Rudder	Flap
Percent span	99.5	99.1	93.0
Area behind hinge line, sq ft	0.621	0.506	-----
Balance area, sq ft	0.131	Minimum	-----
Root-mean-square chord behind hinge line, ft	0.264	0.353	-----
Distance to hinge line from normal center of gravity, ft	3.721	3.611	-----

TABLE III

TAIL-OFF LIFT CHARACTERISTICS

Flap	Operating condition	C_L (Tail off, $\alpha = 0^\circ$)	ΔC_L (Tail off, $\alpha = 0^\circ$)	C_{L_α} ($\alpha = 0^\circ$)
Neutral	Propeller off	0.17	--------	0.076
Single slotted	Propeller off	1.17	1.00	.083
Double slotted	Propeller off	2.04	1.87	.086
Neutral	Propeller windmilling	.16	--------	.076
Single slotted	Propeller windmilling	1.17	1.01	.083
Double slotted	Propeller windmilling	2.07	1.91	.085
Neutral	Power on, $T_c' = 0.161\ C_L$	.15	--------	.080
Single slotted	Power on, $T_c' = 0.161\ C_L$	1.23	1.08	.098
Double slotted	Power on, $T_c' = 0.161\ C_L$	2.46	2.31	.134

NATIONAL ADVISORY
COMMITTEE FOR AERONAUTICS

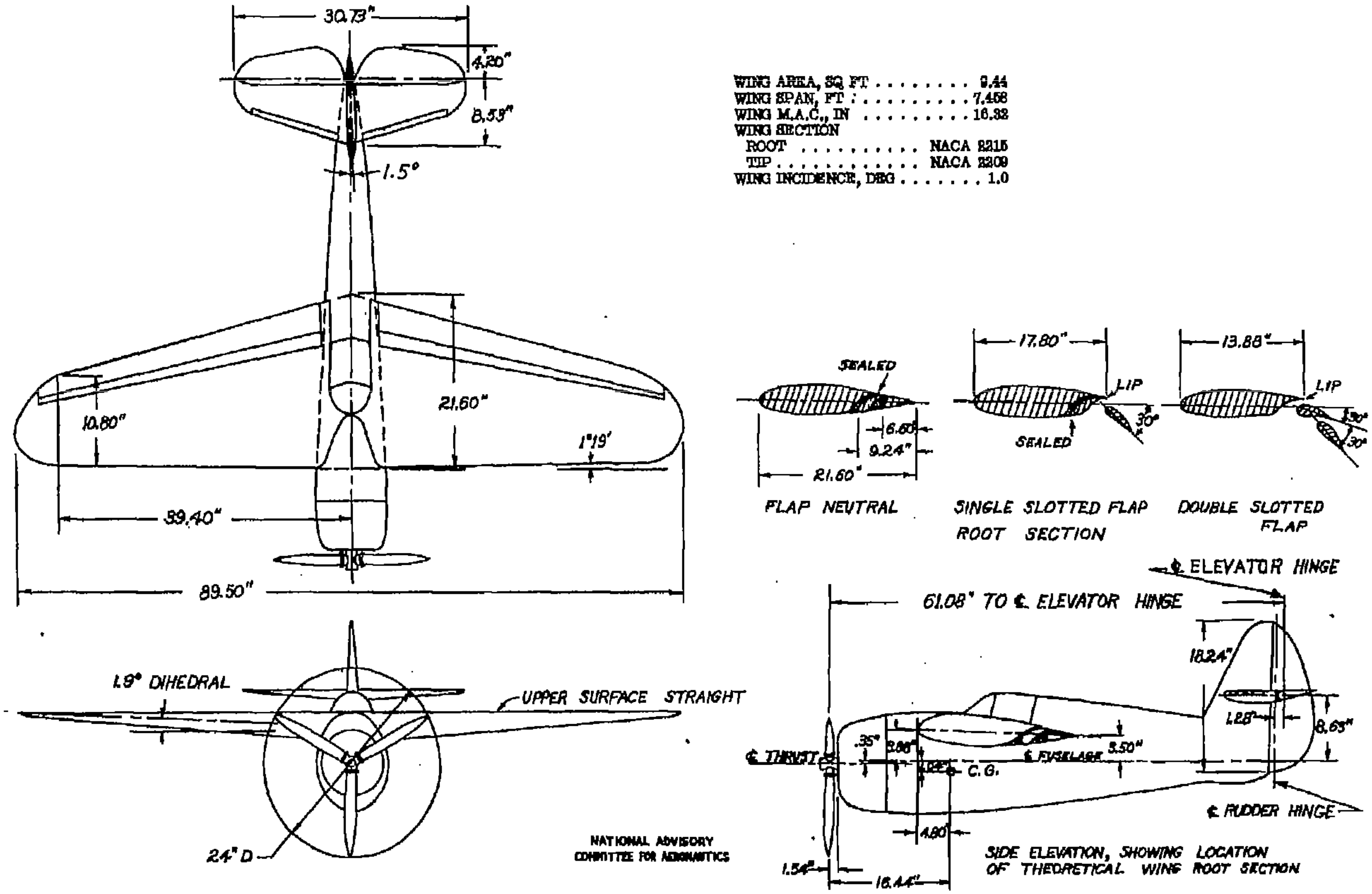

Figure 1.- Three-view drawing of the $\frac{1}{5}$-scale model as a single-engine high-wing airplane.

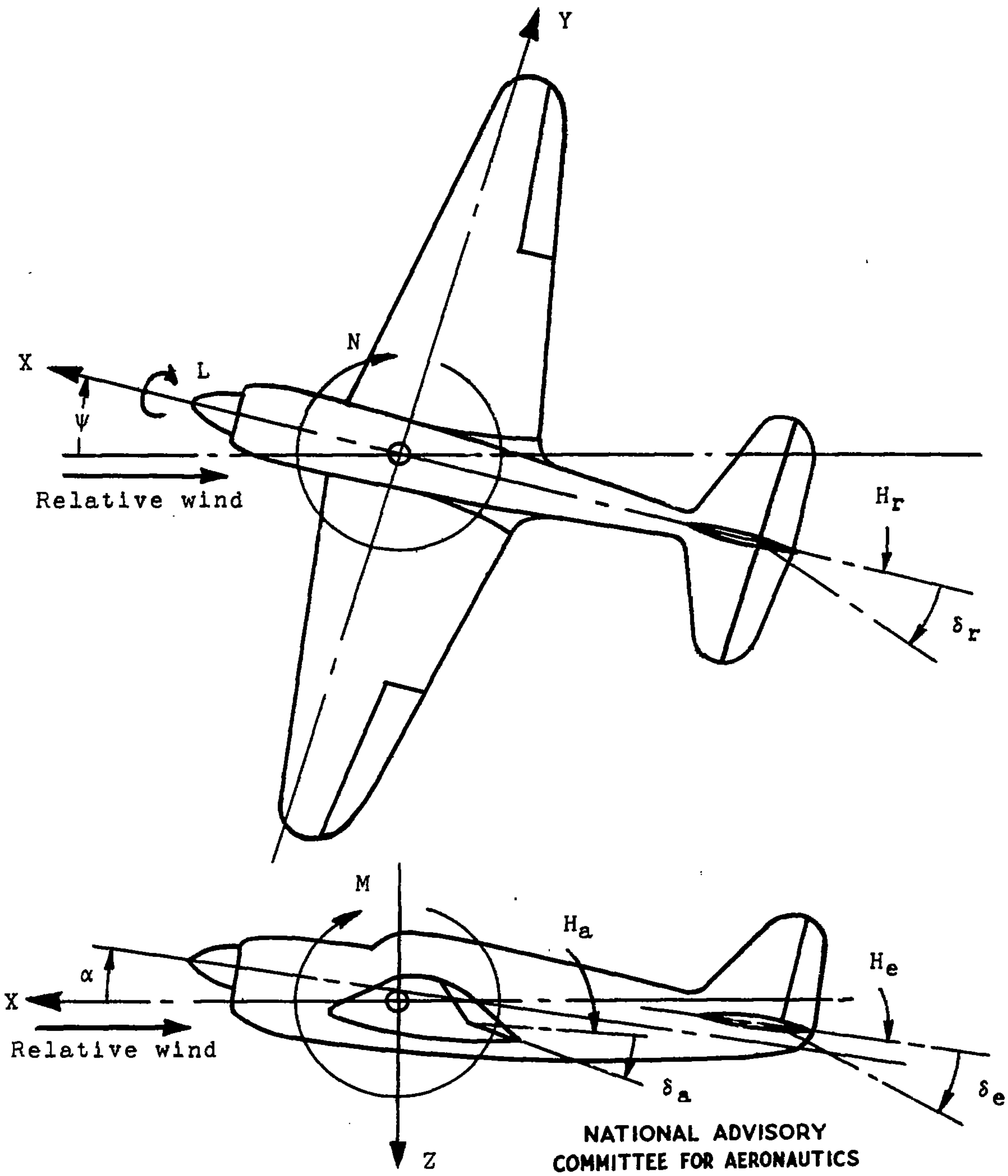

Figure 2.- System of axes and control-surface hinge moments and deflections. Positive values of forces, moments, and angles are indicated by arrows. Positive values of tab hinge moments and deflections are in the same directions as the positive values for the control surfaces to which the tabs are attached.

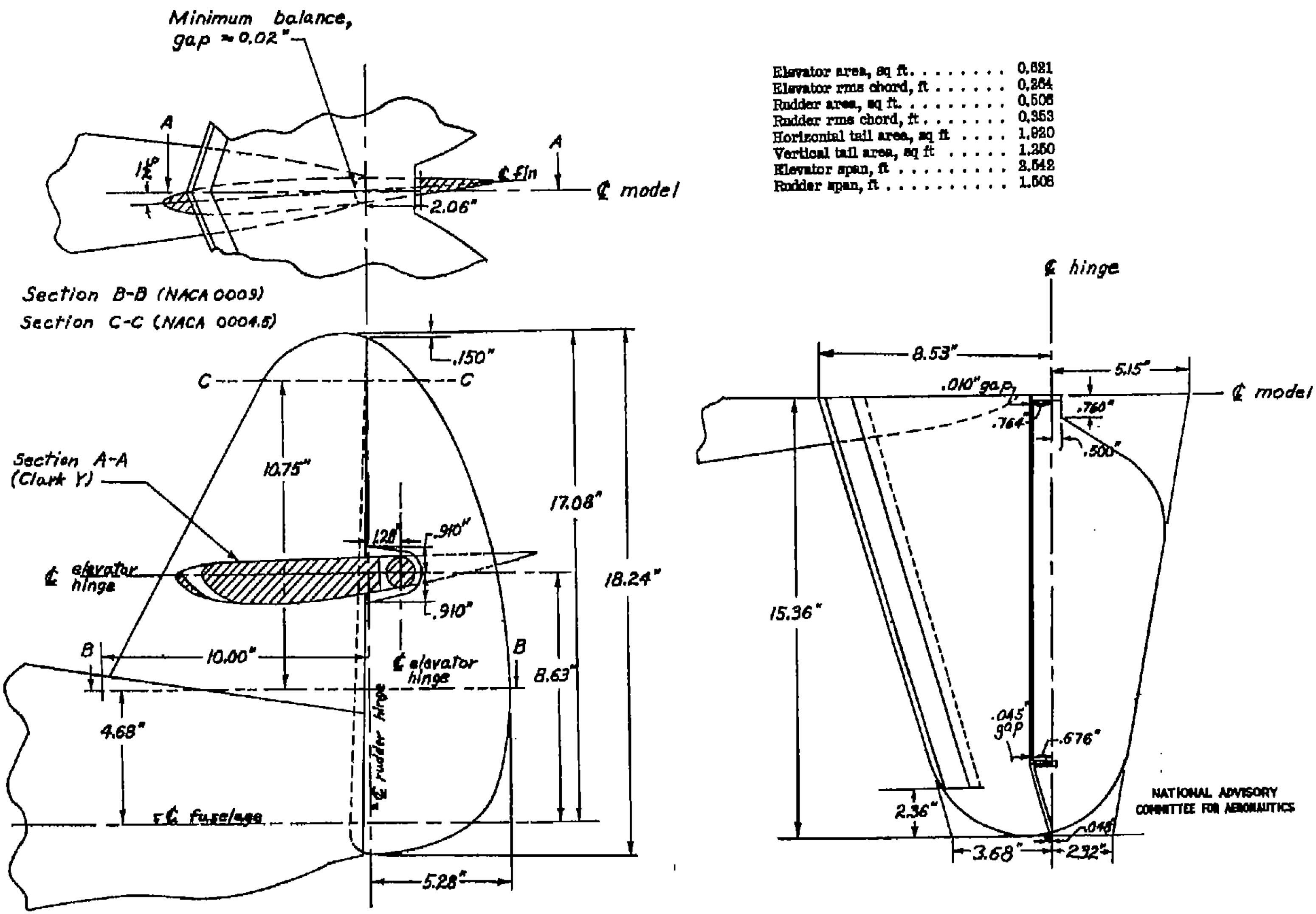

Elevator area, sq ft.	0.621
Elevator rms chord, ft	0.264
Rudder area, sq ft.	0.506
Rudder rms chord, ft	0.353
Horizontal tail area, sq ft	1.920
Vertical tail area, sq ft	1.250
Elevator span, ft	2.542
Rudder span, ft	1.506

Figure 3.- Details and dimensions of the vertical and horizontal tails.

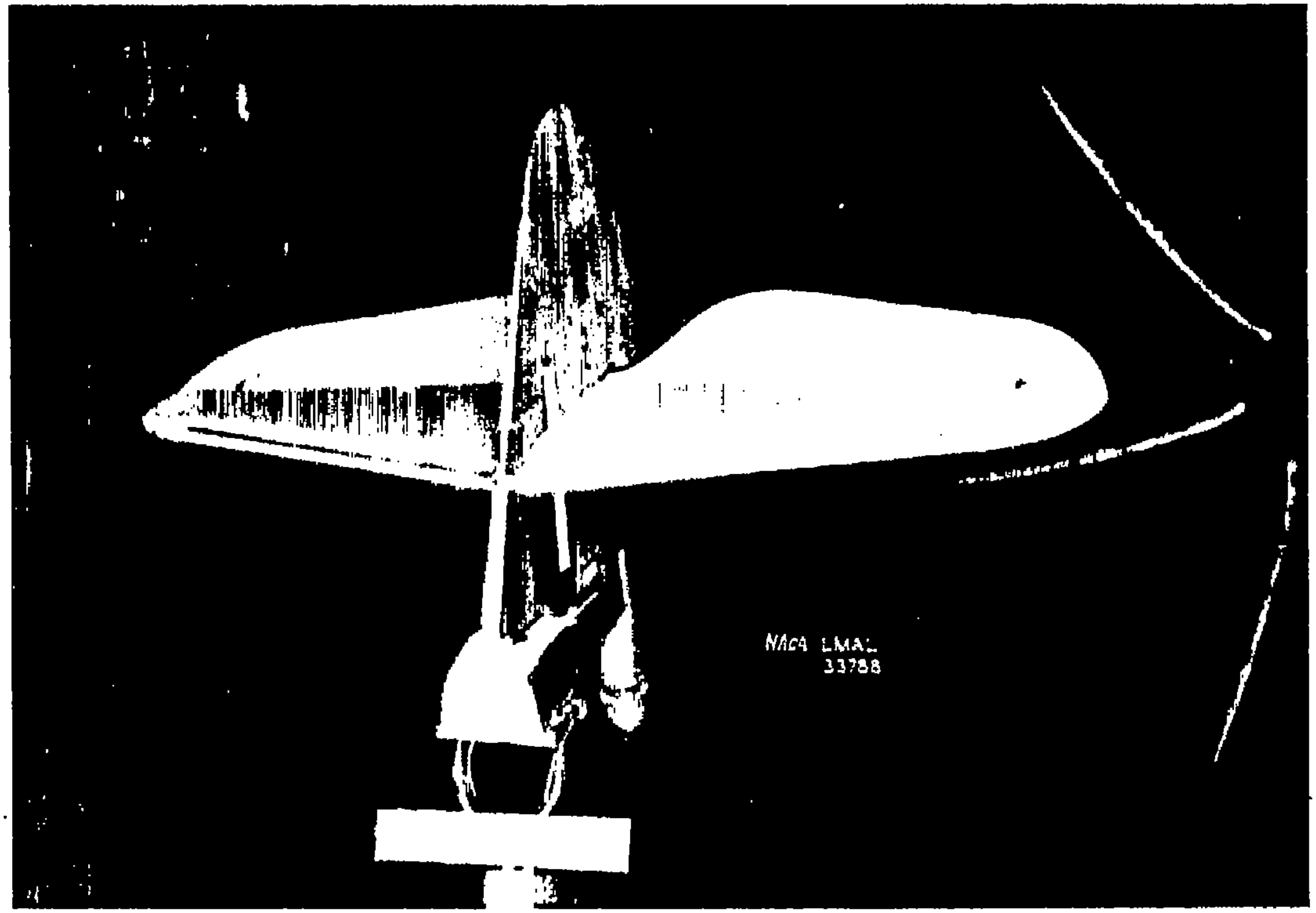

Figure 4.- Isolated tail assembly mounted in Langley 7- by 10-foot tunnel.

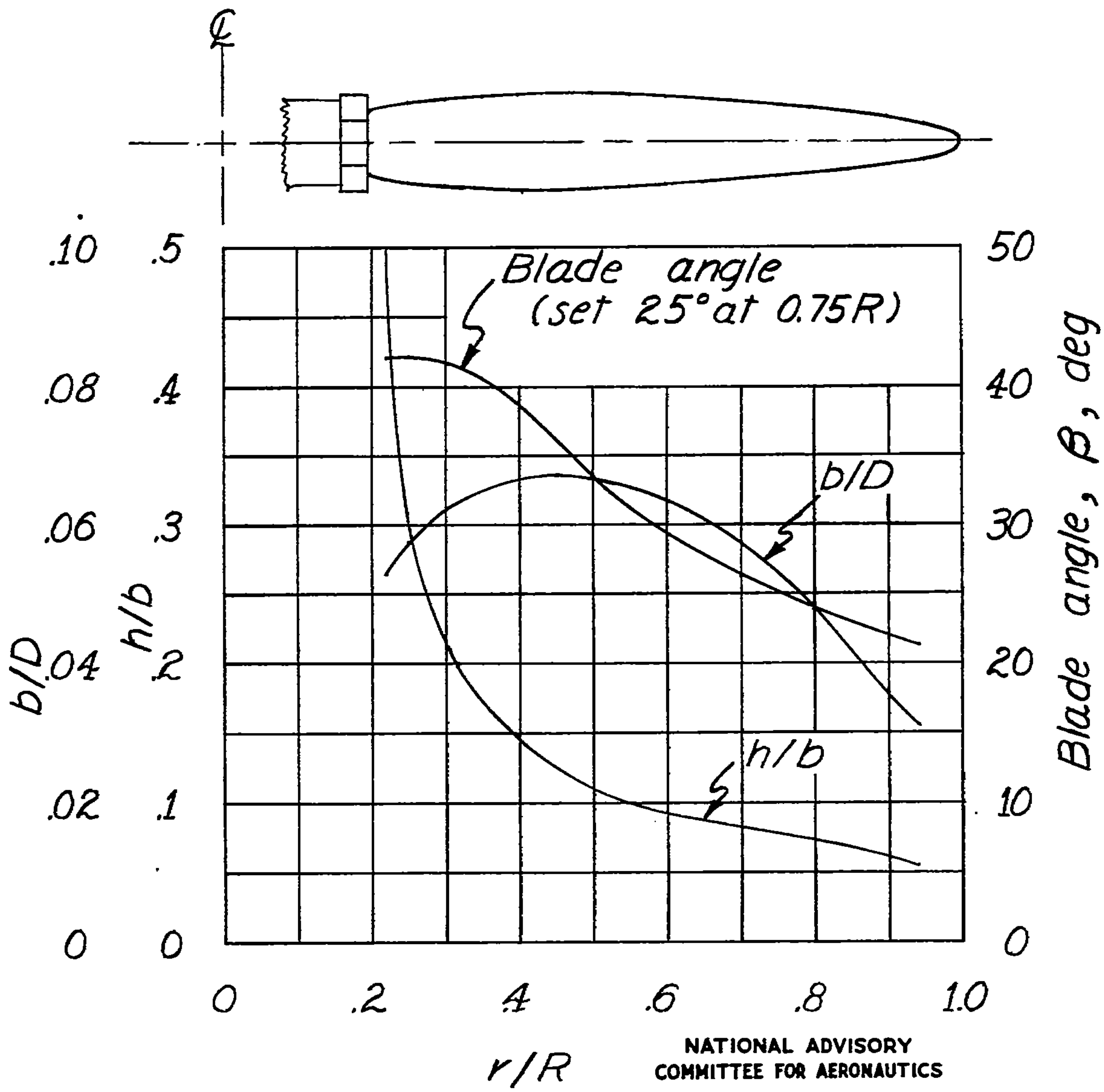

NATIONAL ADVISORY COMMITTEE FOR AERONAUTICS

Figure 5.- Plan-form and blade-form curves for the model propeller. D, diameter; R, radius to tip; r, station radius; b, section chord; h, section thickness; RAF 6 airfoil section.

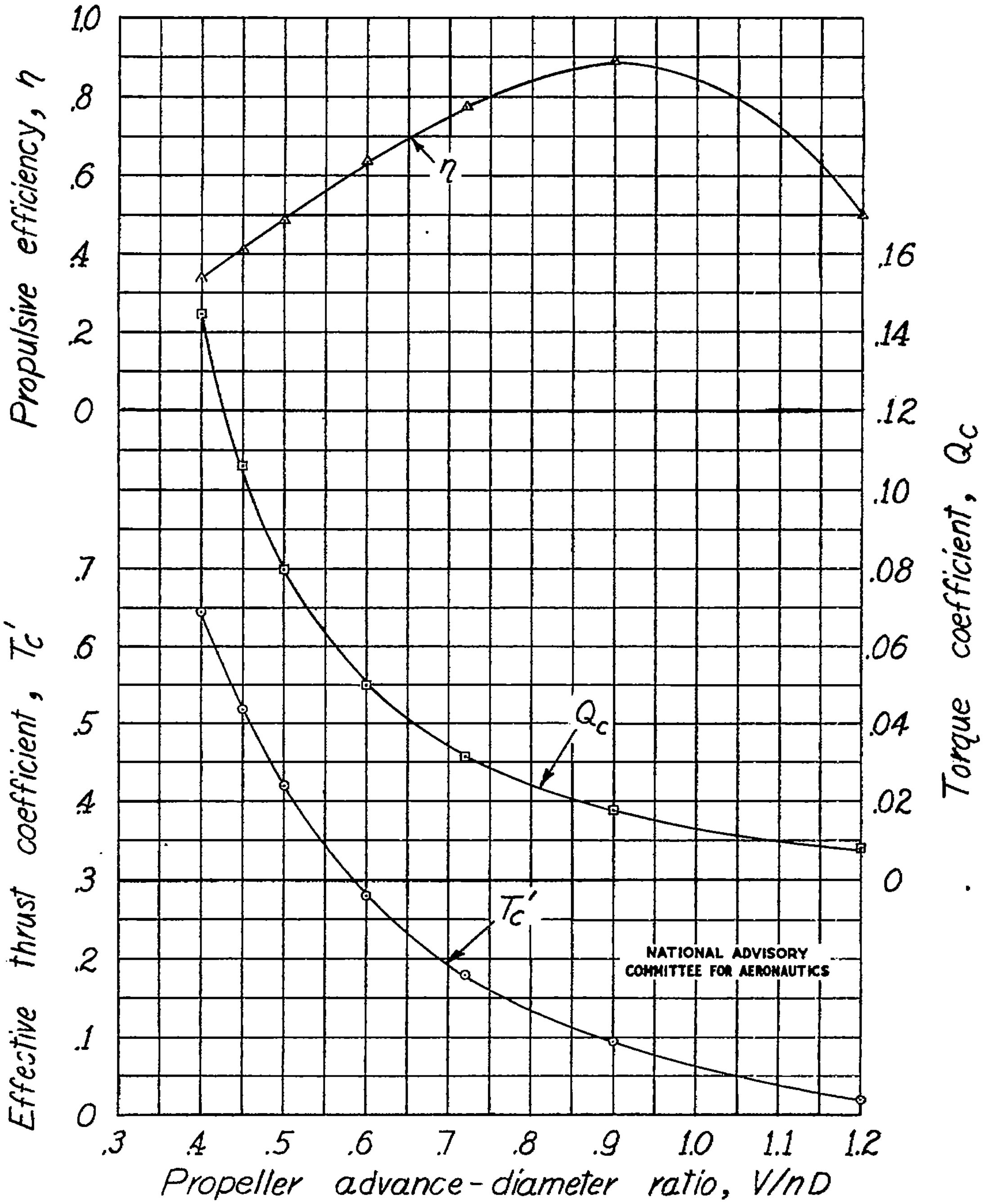

Figure 6.- Effective thrust coefficient, torque coefficient, and efficiency as functions of propeller advance-diameter ratio for the model as a high-wing airplane. D = 2.0 feet; β = 25°.

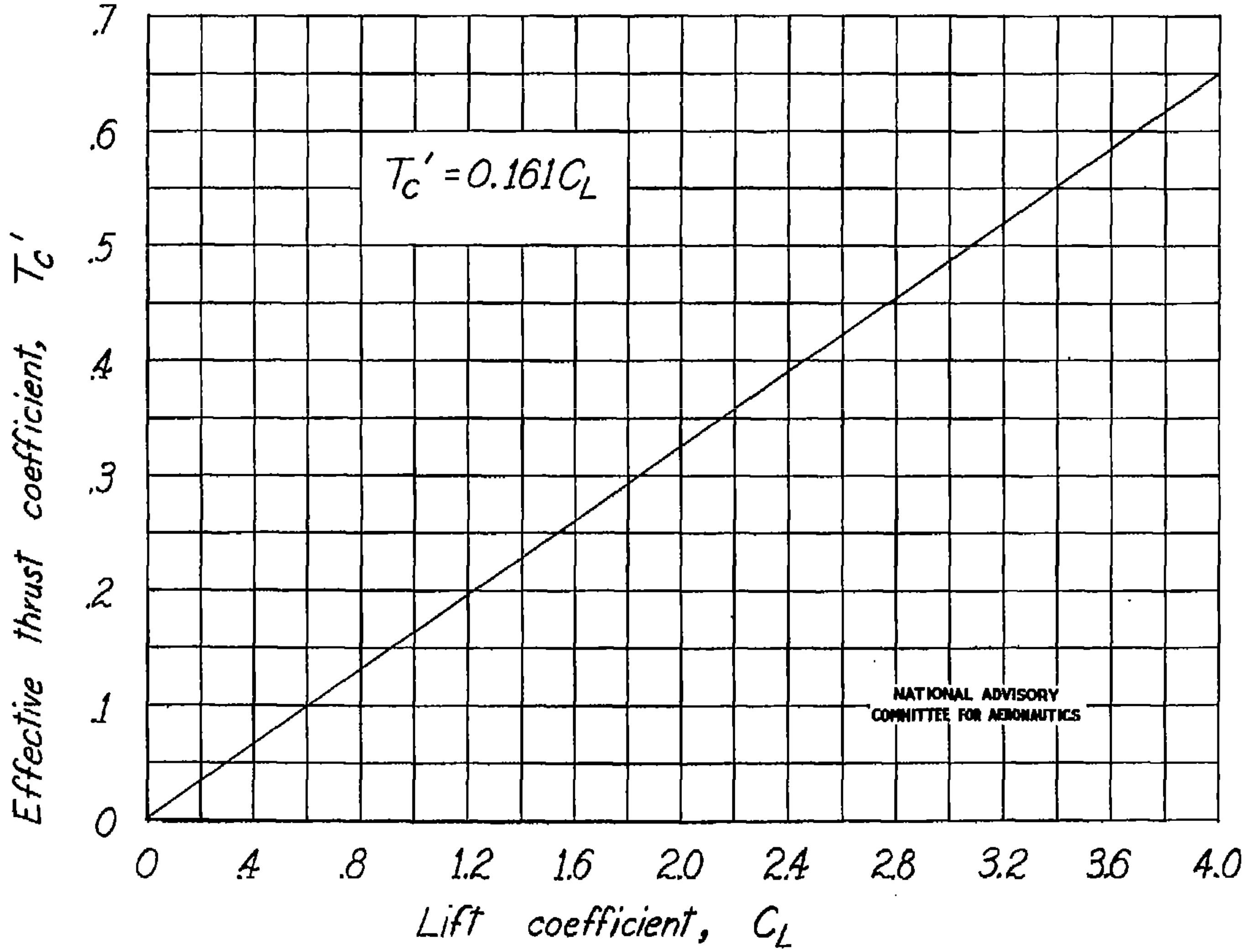

Figure 7.- Variation of effective thrust coefficient with lift coefficient for power-on tests.

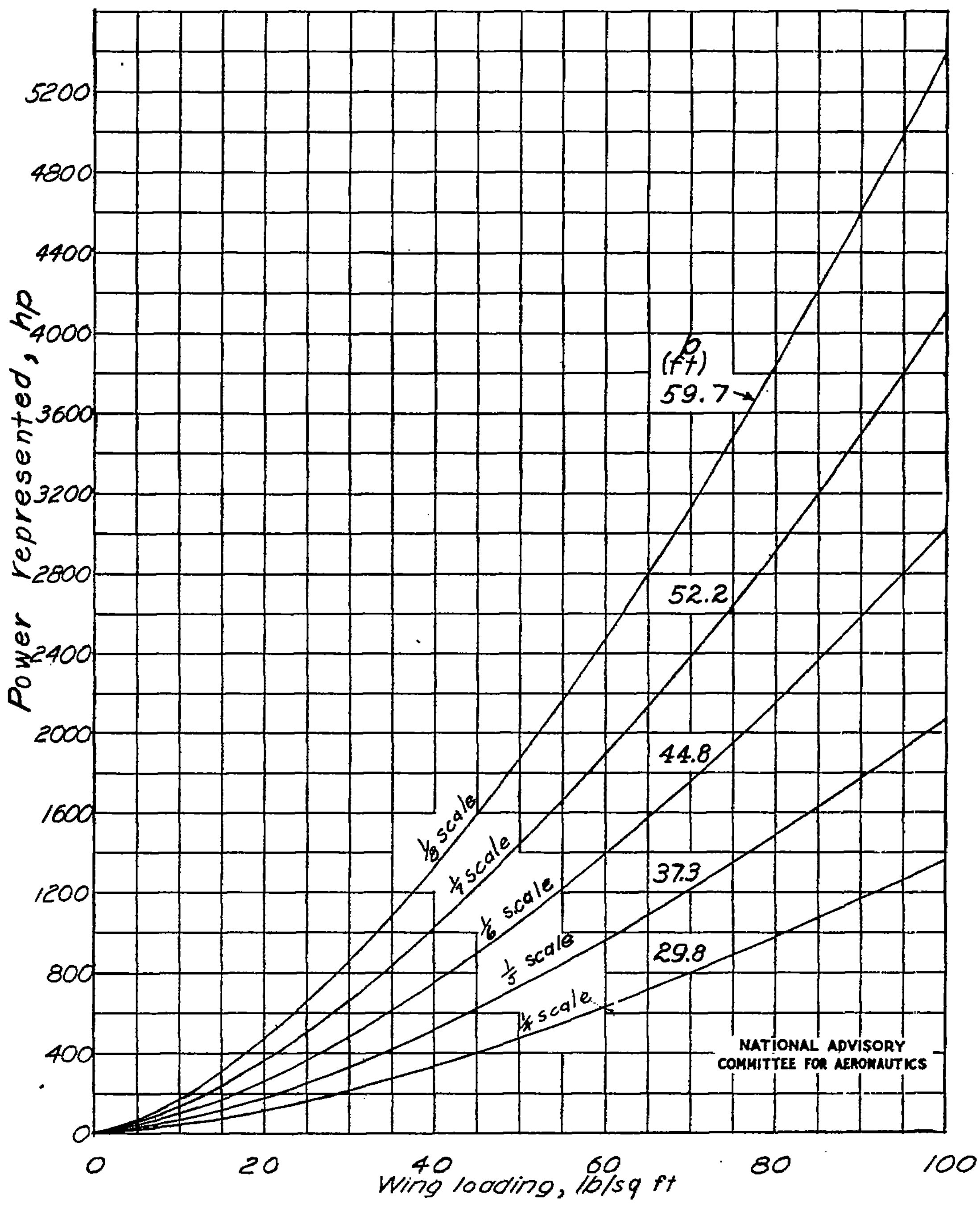

Figure 8 - Variation of approximate horsepower represented with airplane wing loading for various model scales.

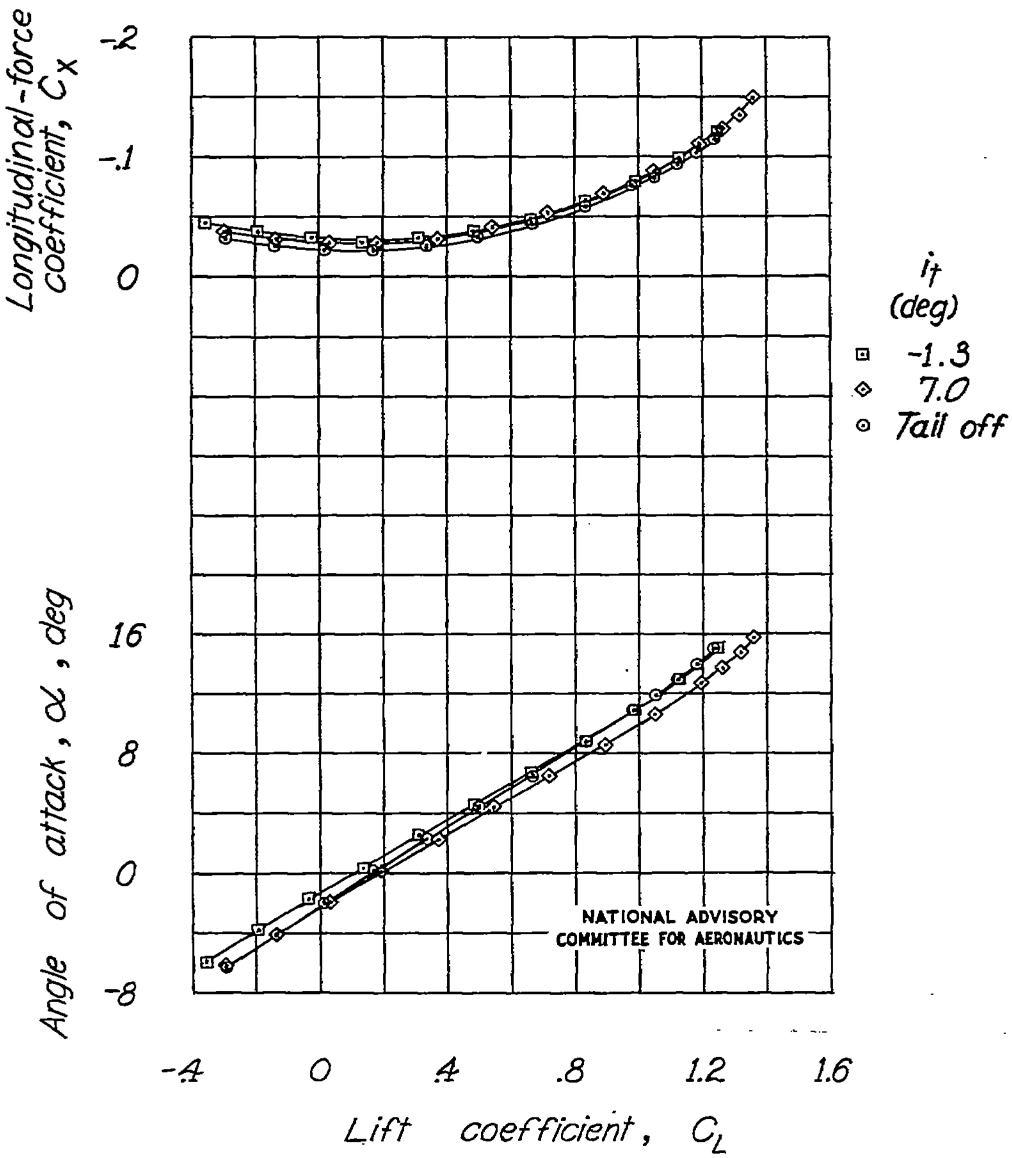

(a) Propeller off.

Figure 9.- Effect of stabilizer on the aerodynamic characteristics of the model as a single-engine high-wing airplane with flap neutral. Tail slot sealed.

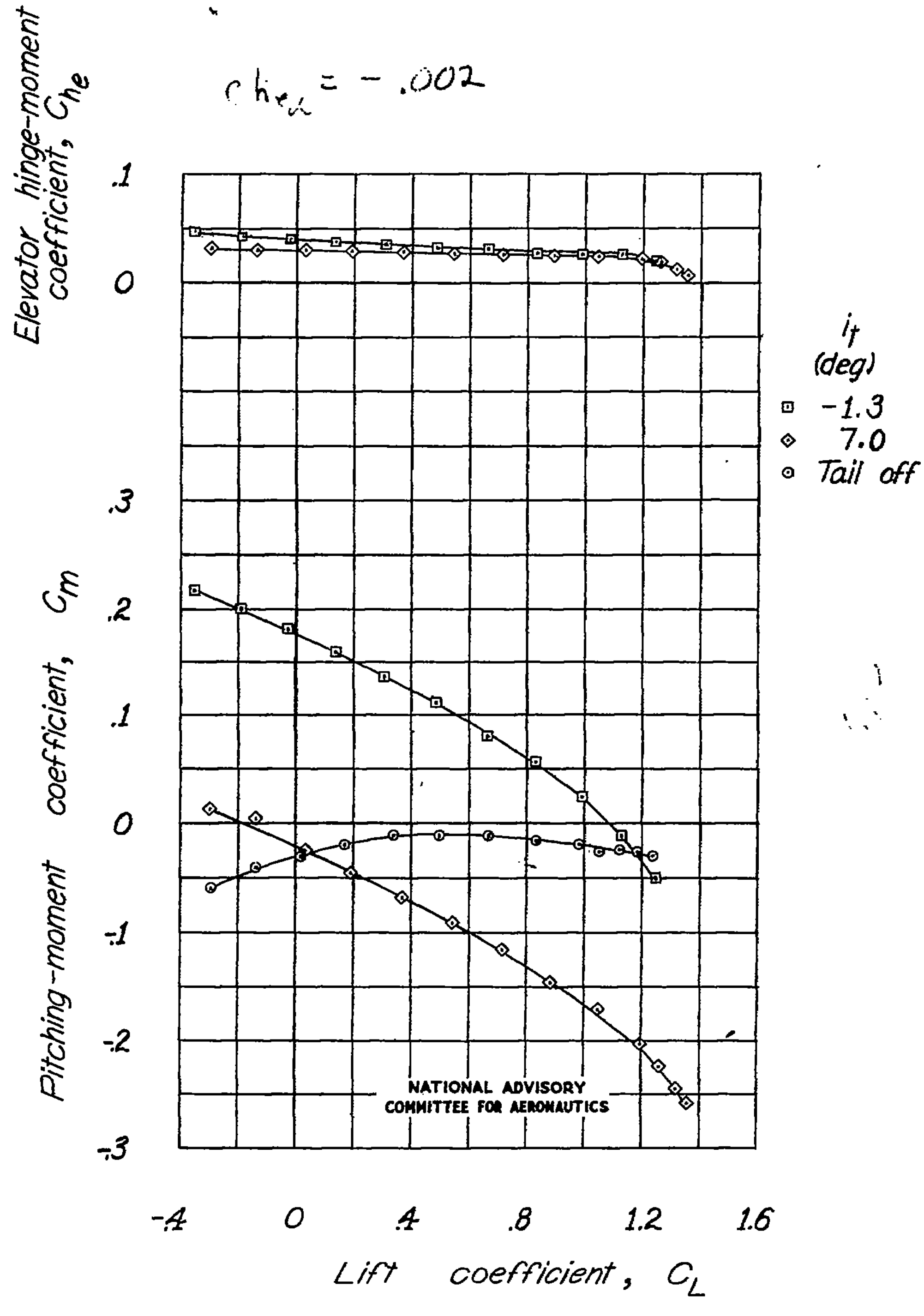

(a) Concluded.

Figure 9.- Continued.

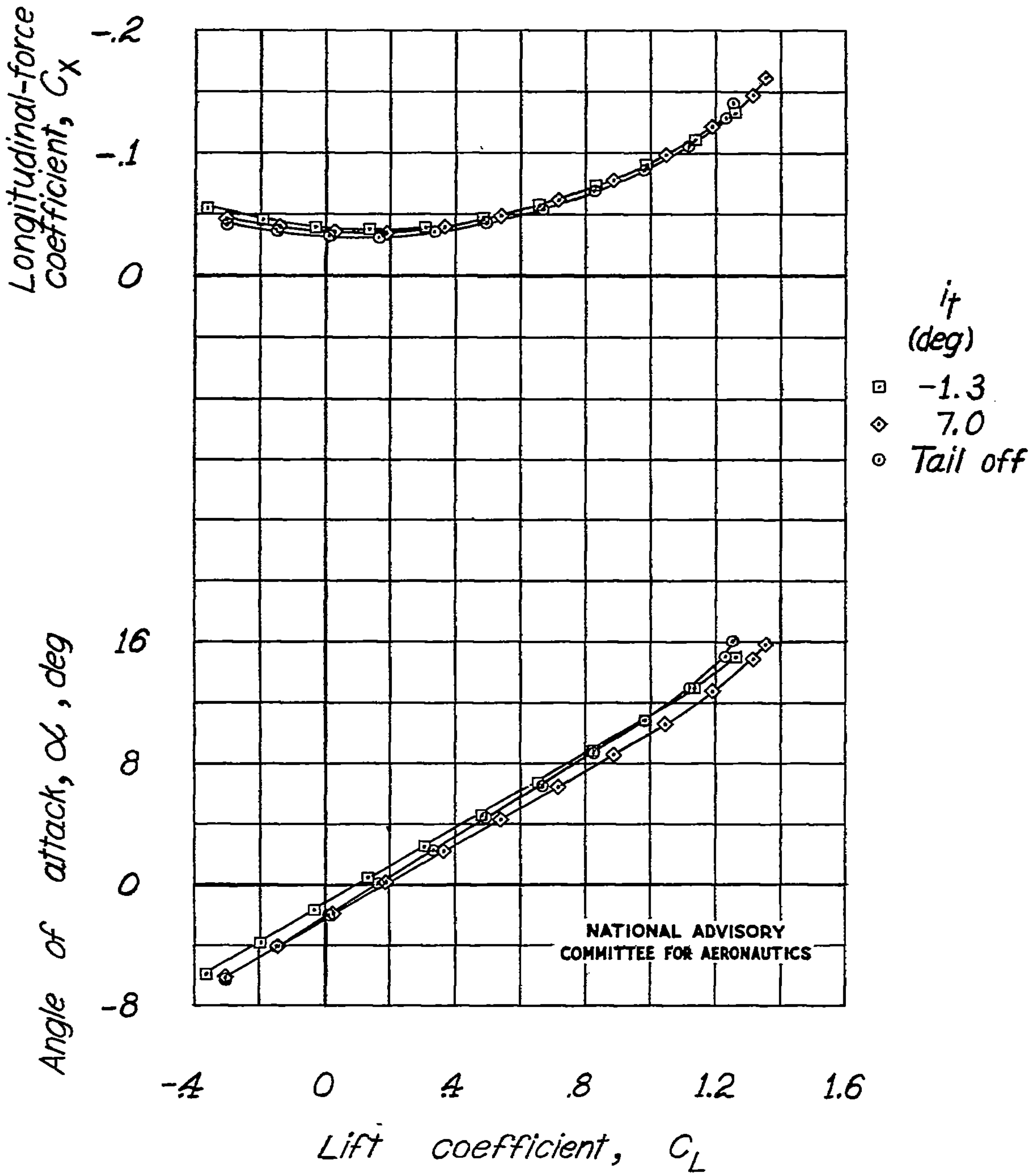

(b) Propeller windmilling.

Figure 9.-Continued.

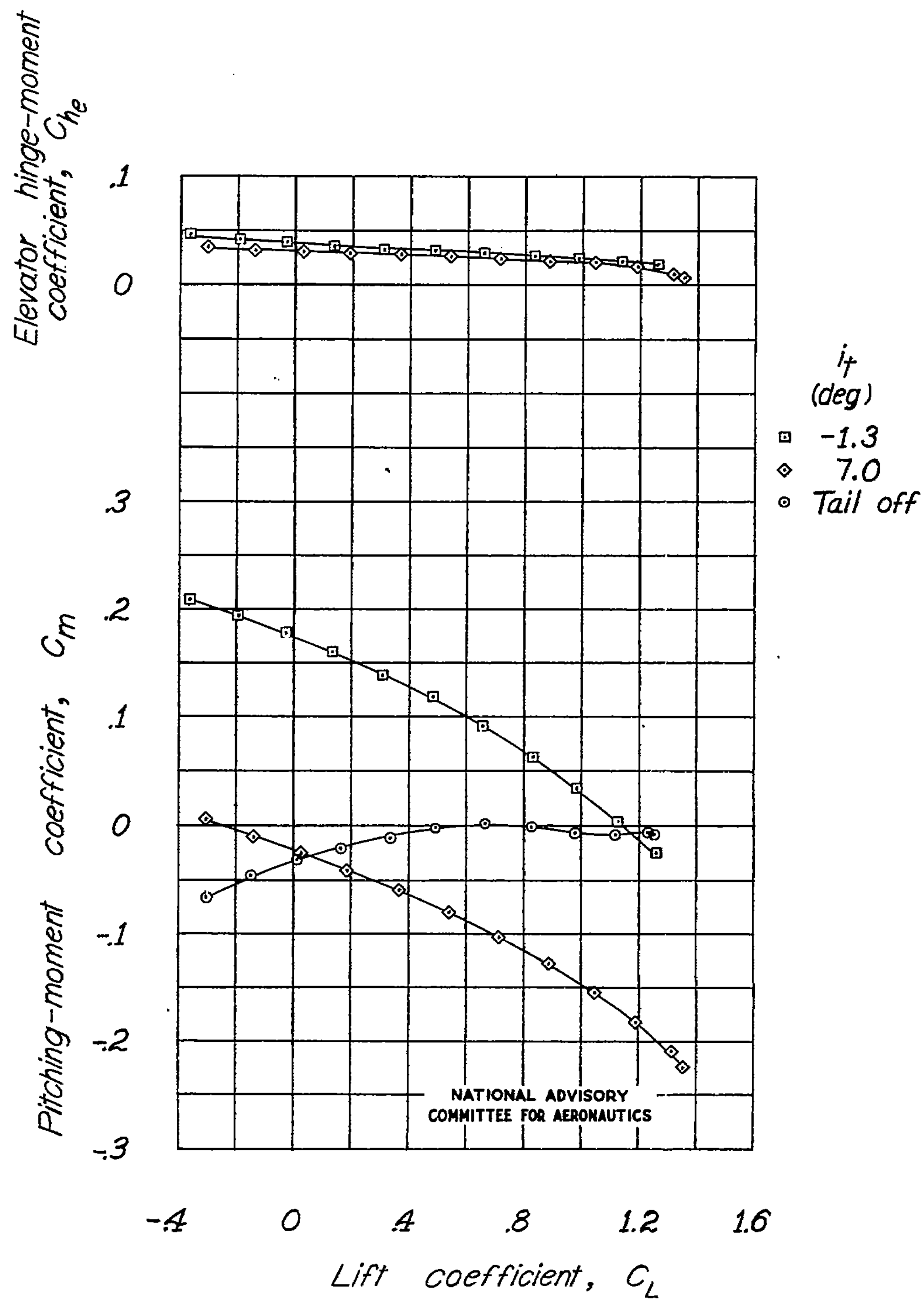

(b) Concluded.

Figure 9.- Continued.

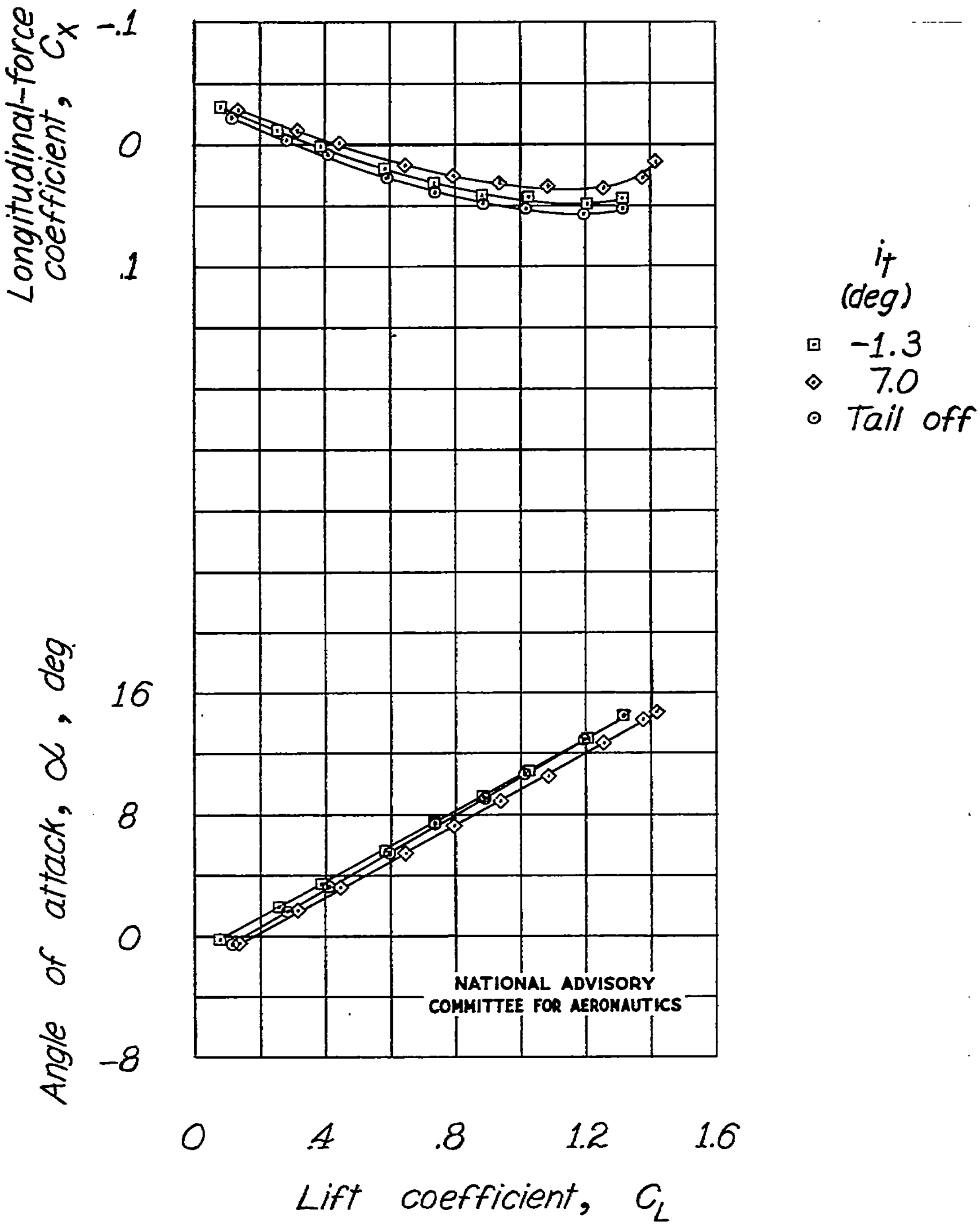

(c) Power on.

Figure 9.- Continued.

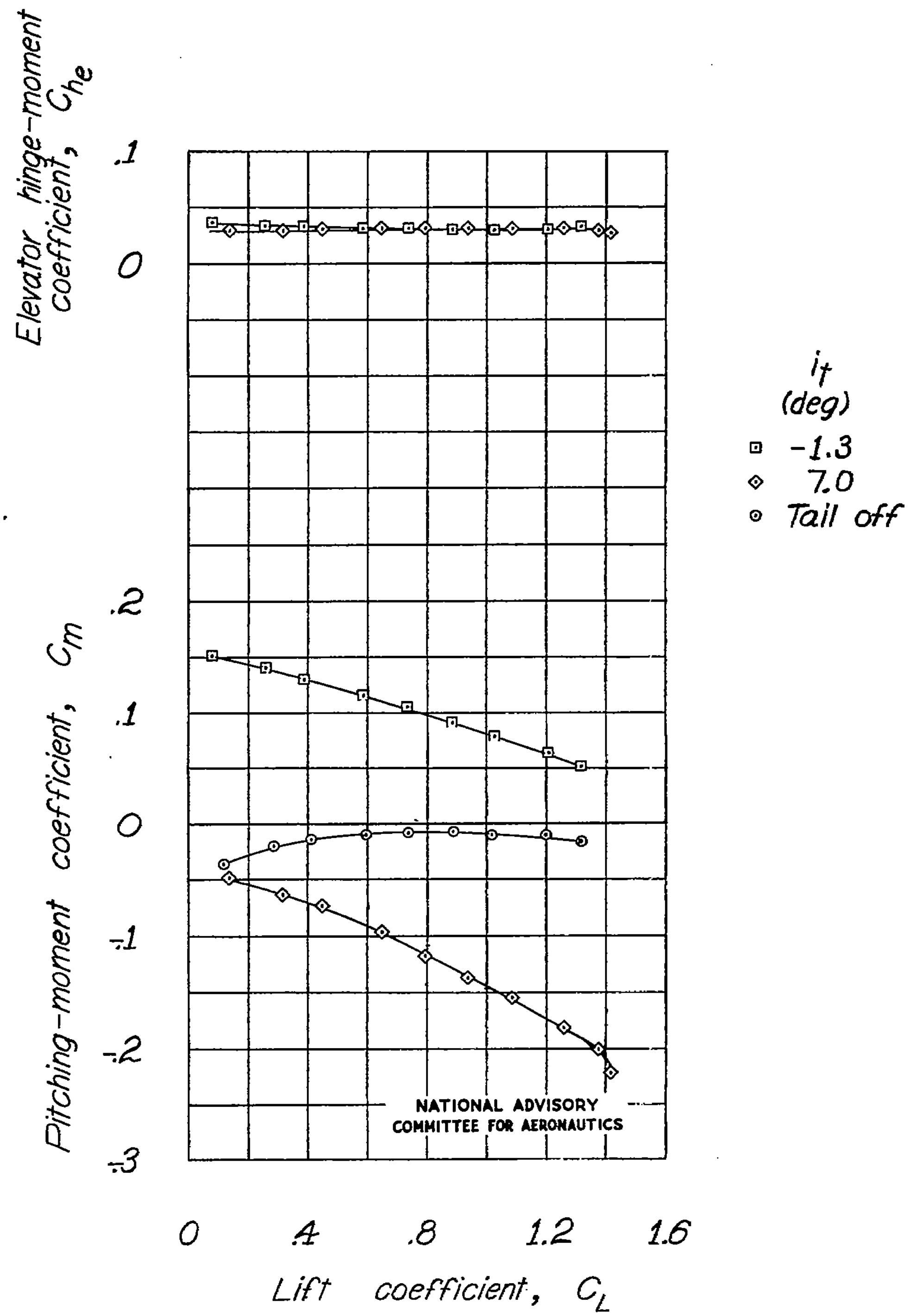

(c) Concluded.

Figure 9.- Concluded.

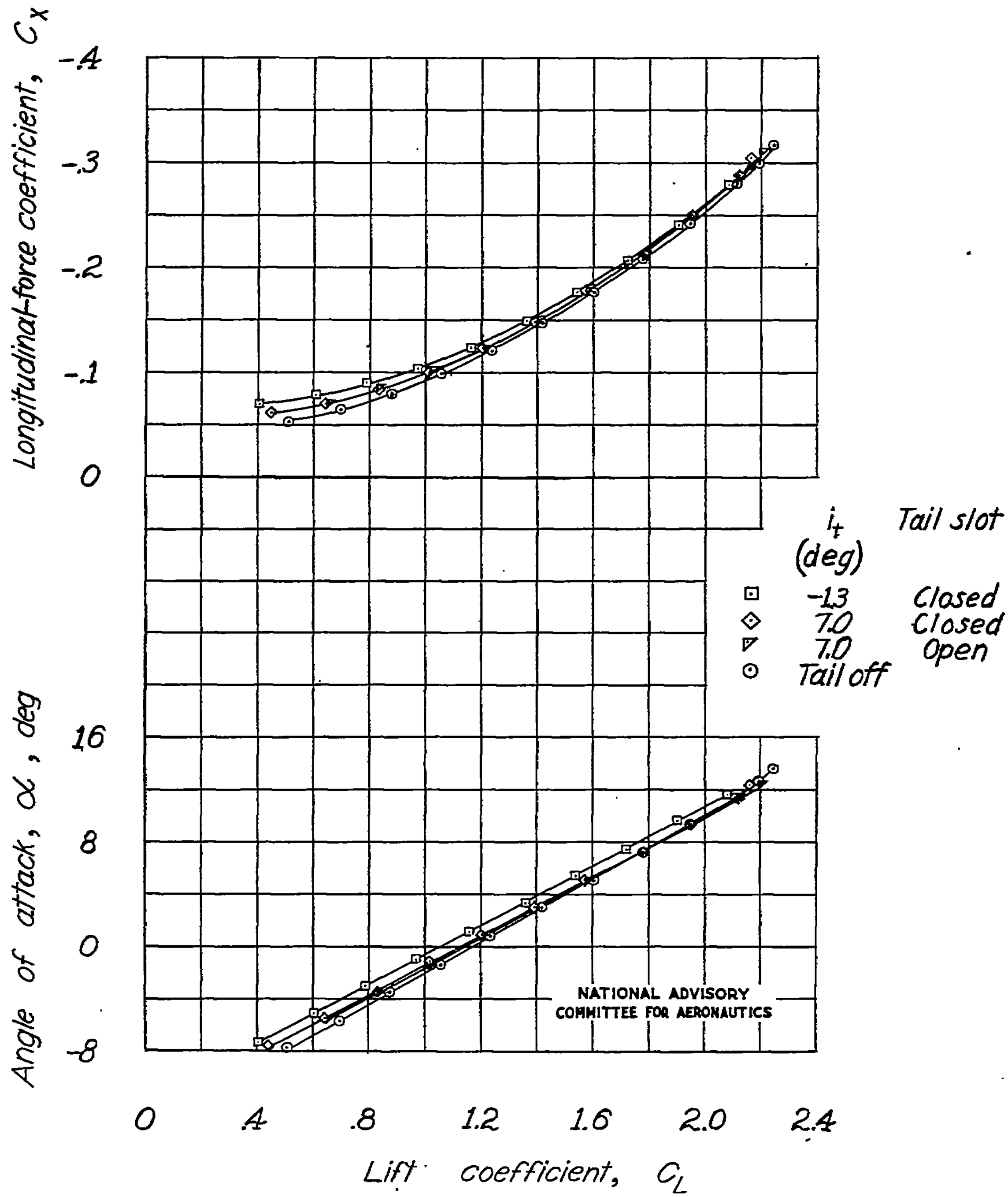

(a) Propeller off.

Figure 10.- Effect of stabilizer on the aerodynamic characteristics of the model as a single-engine high-wing airplane with a full-span single slotted flap.

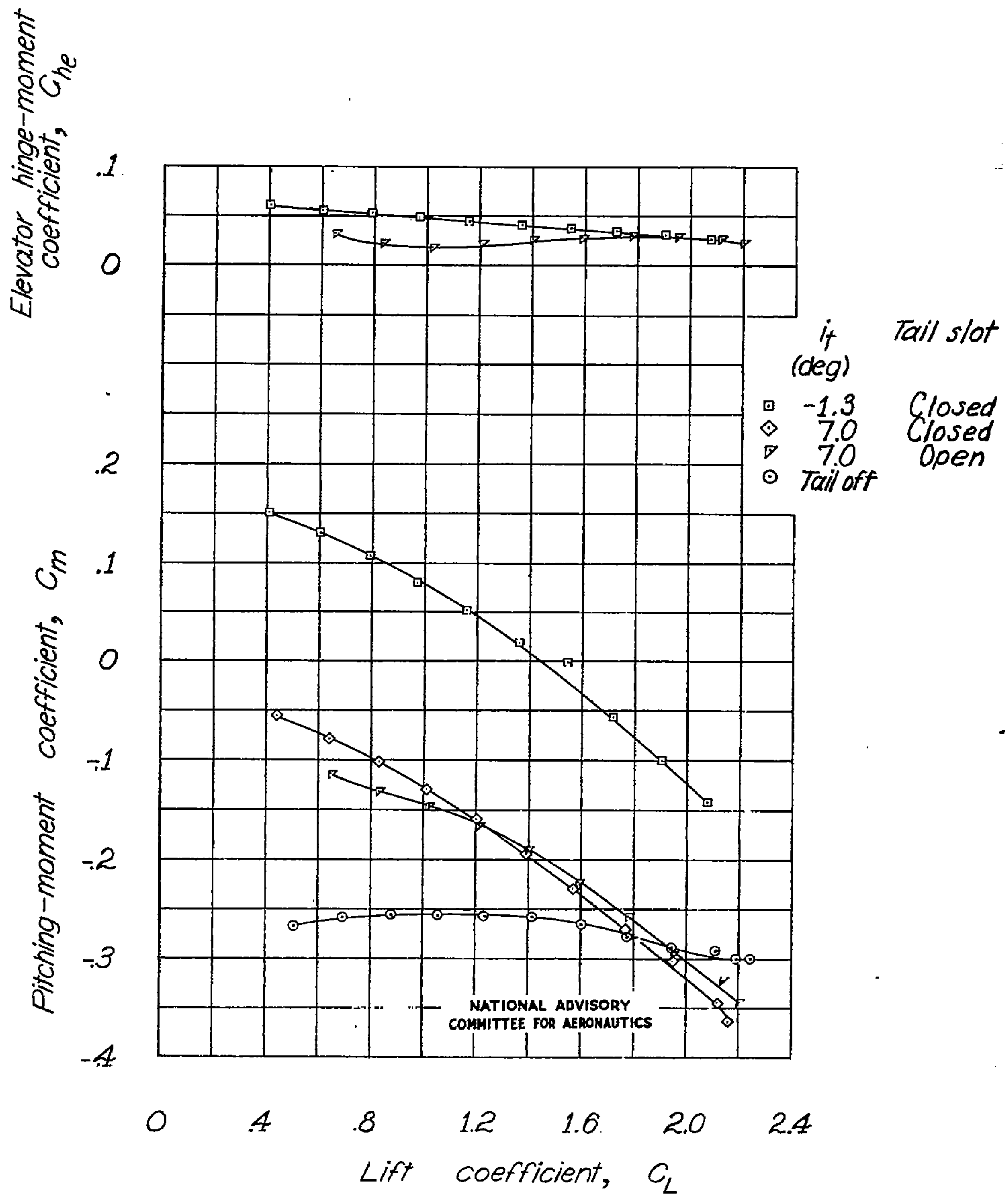

(a) Concluded.

Figure 10.-Continued.

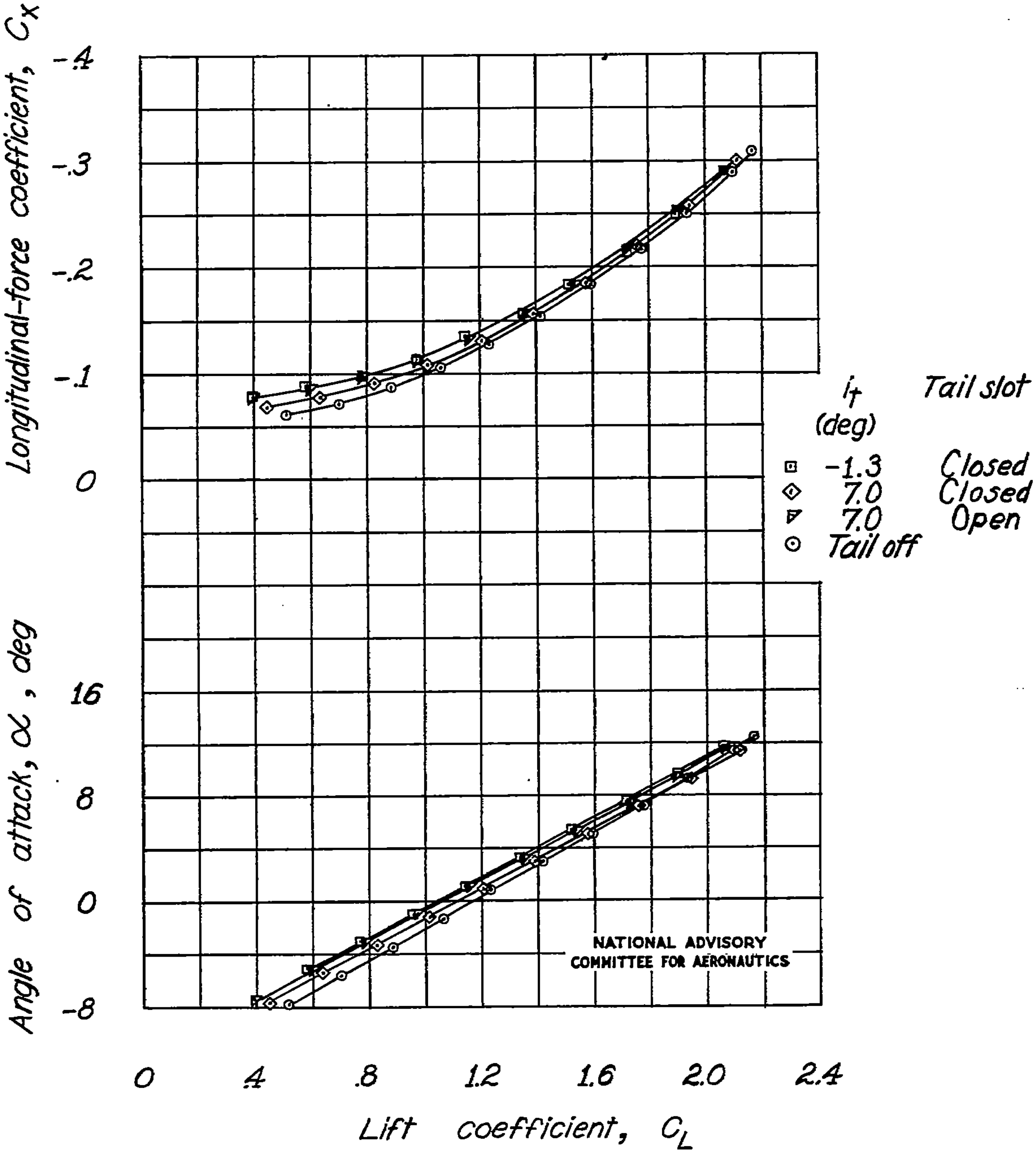

(b) Propeller windmilling.

Figure 10.–Continued.

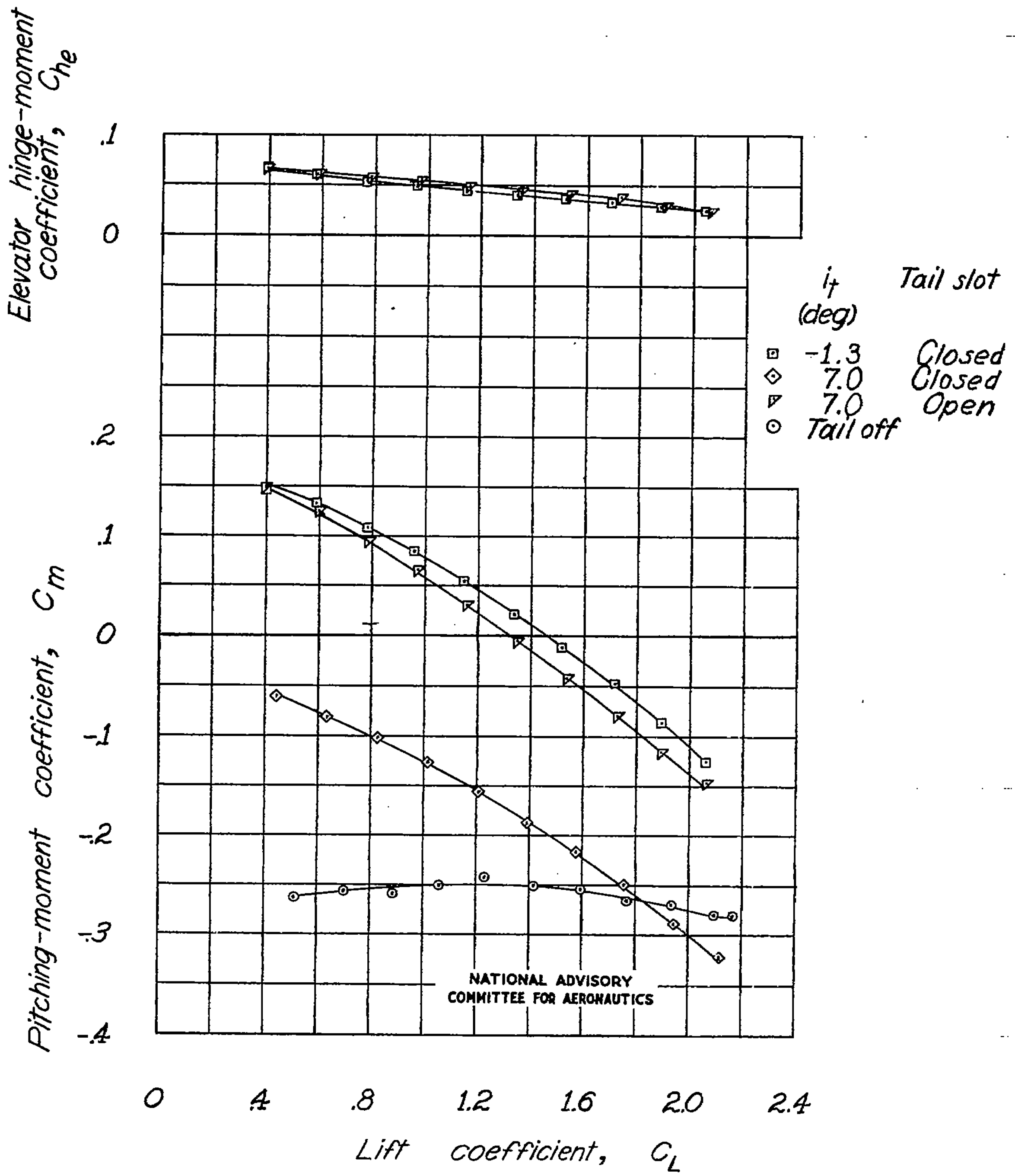

(b) Concluded.

Figure 10.-Continued.

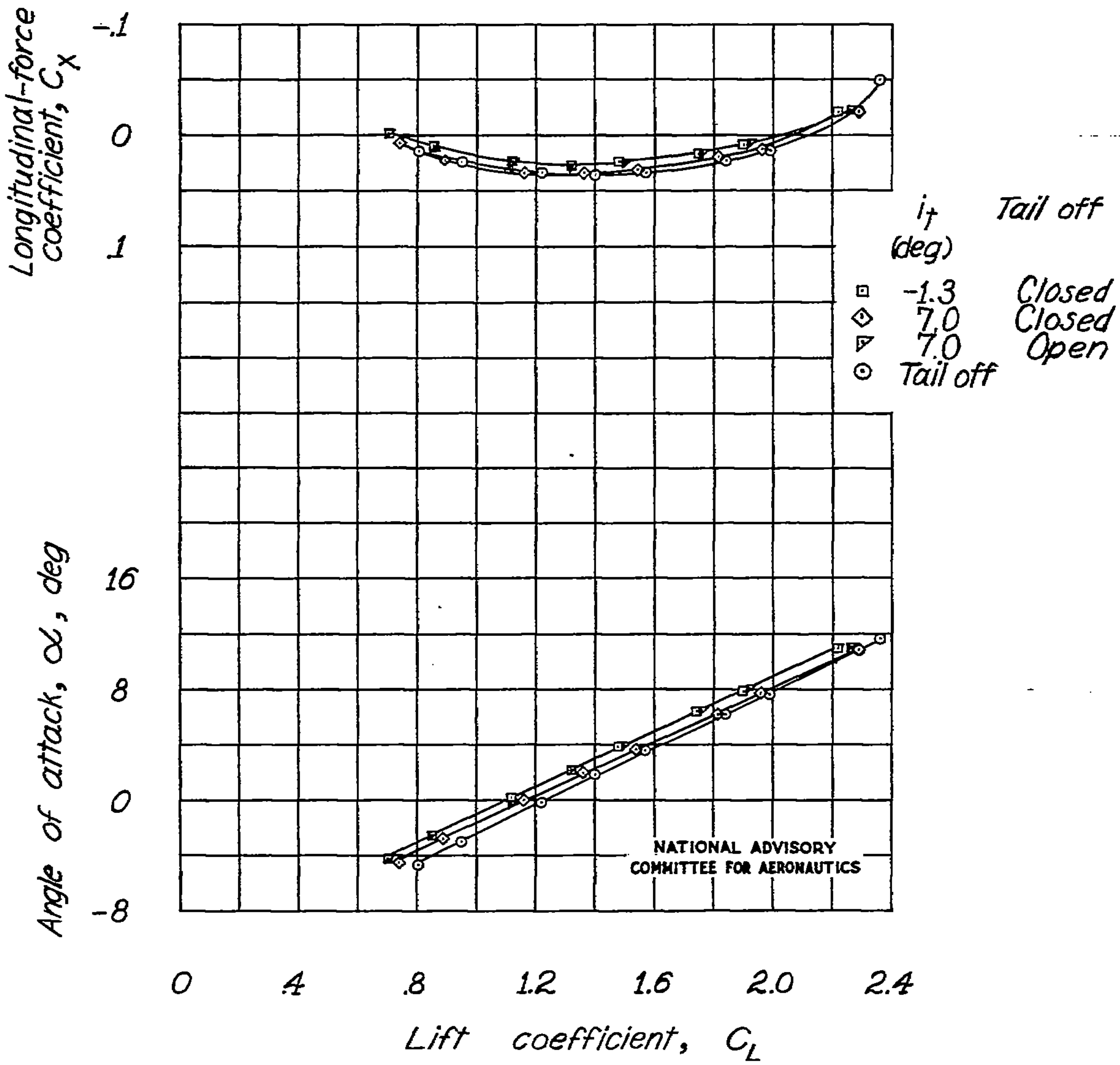

(c) Power on.

Figure 10.-Continued.

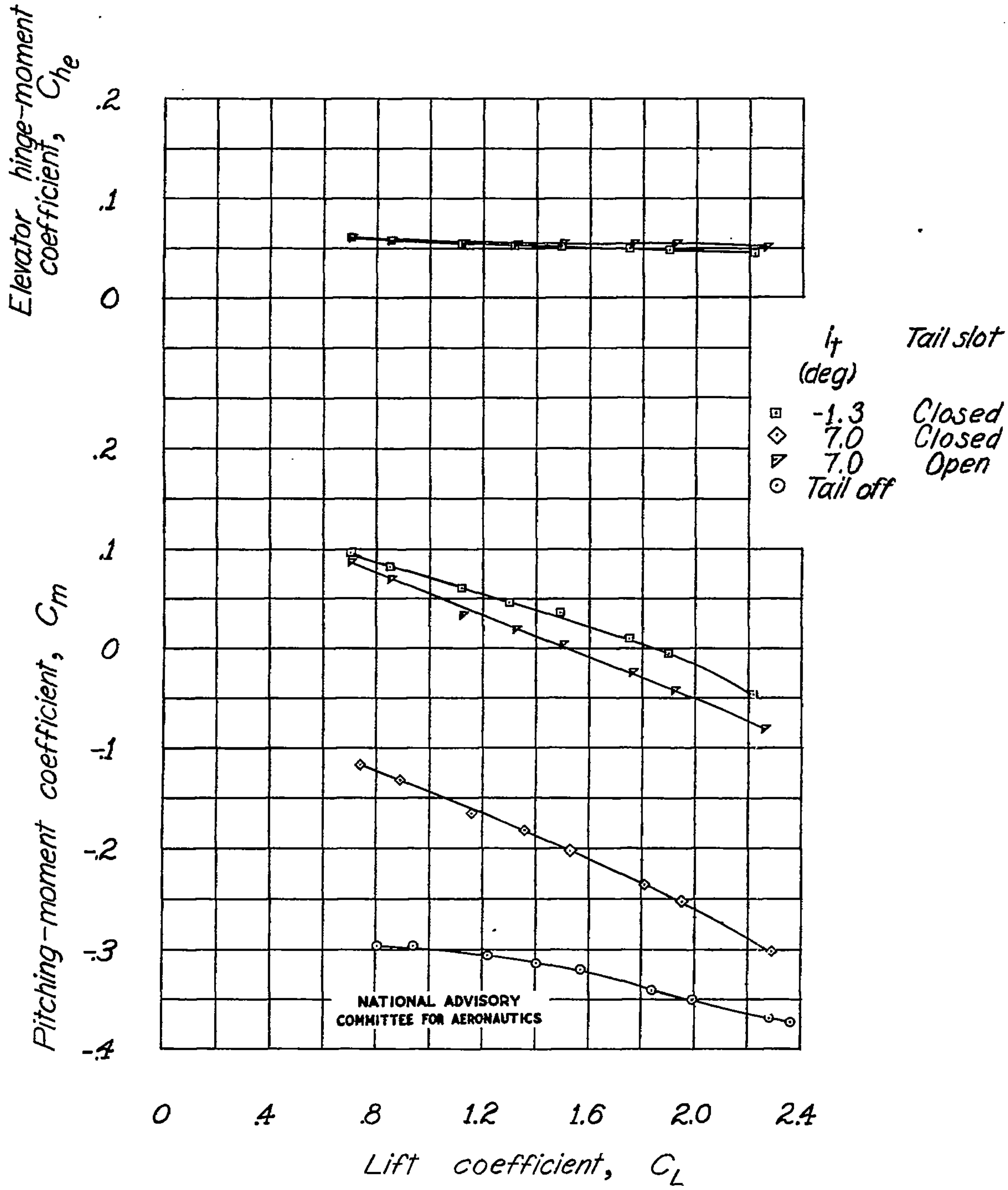

(c) Concluded.

Figure 10.-Concluded.

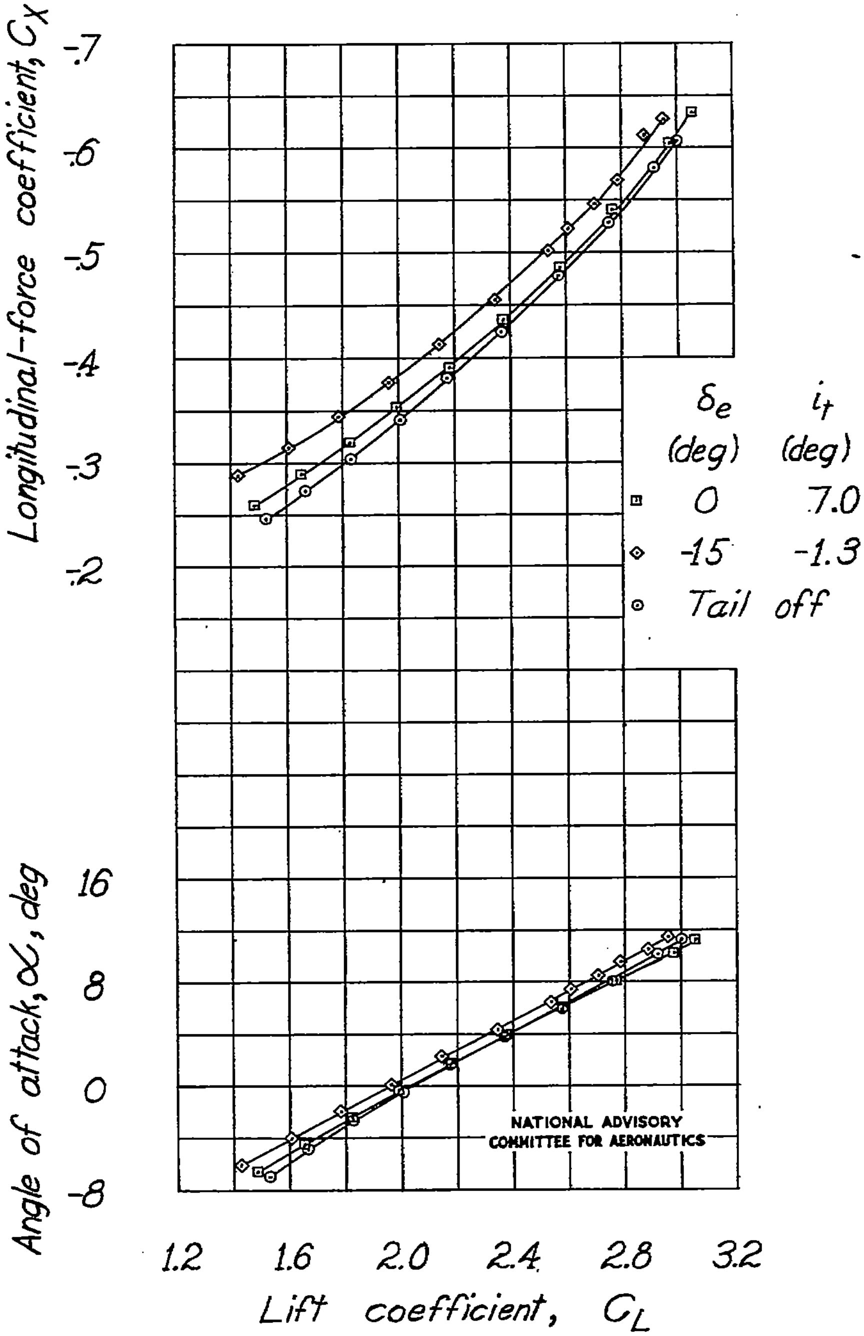

(a) Propeller off.

Figure 11.– Effect of stabilizer and elevator on the aerodynamic characteristics of the model as a single-engine high-wing airplane with a full-span double slotted flap.

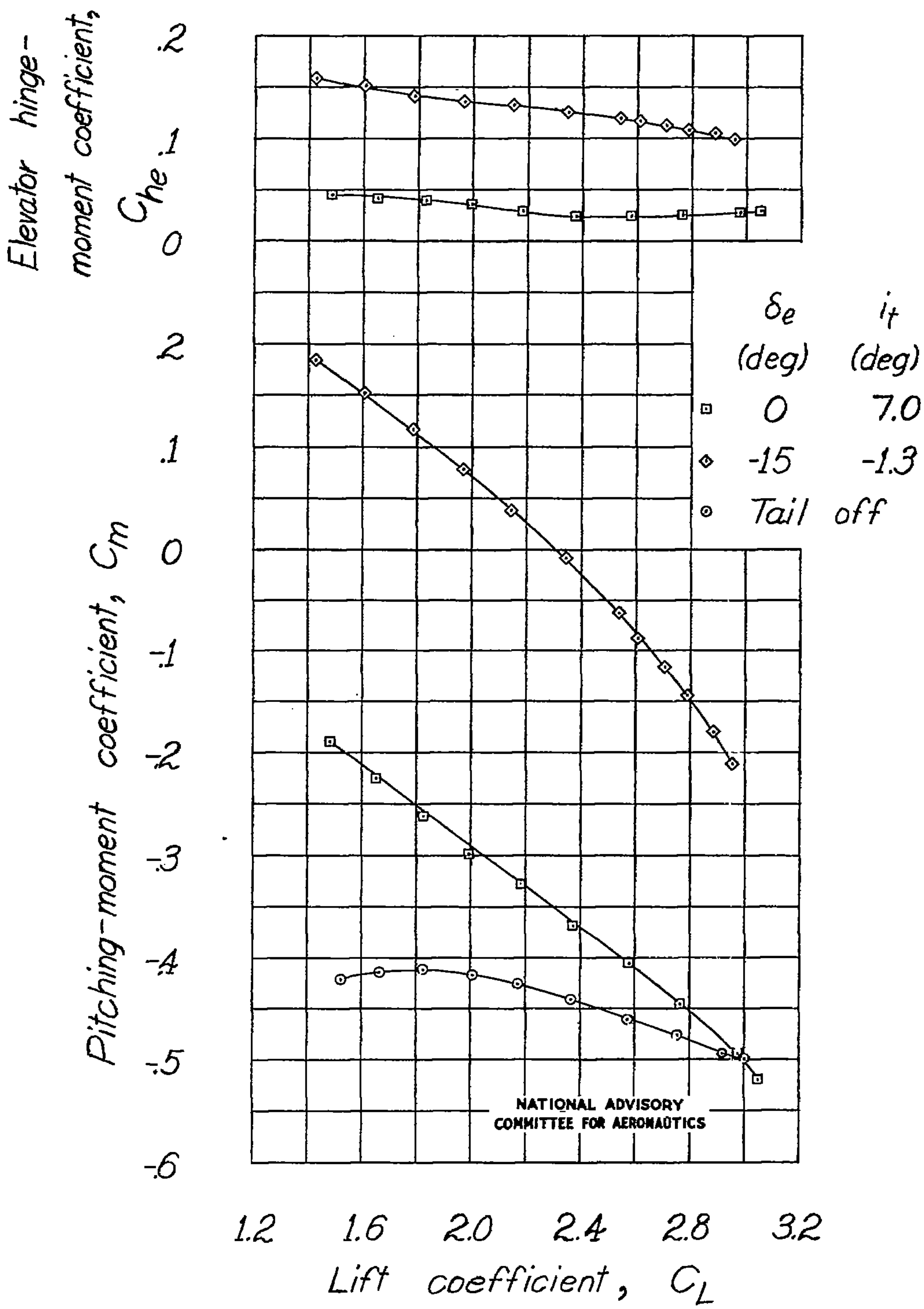

(a) Concluded.

Figure 11. - Continued.

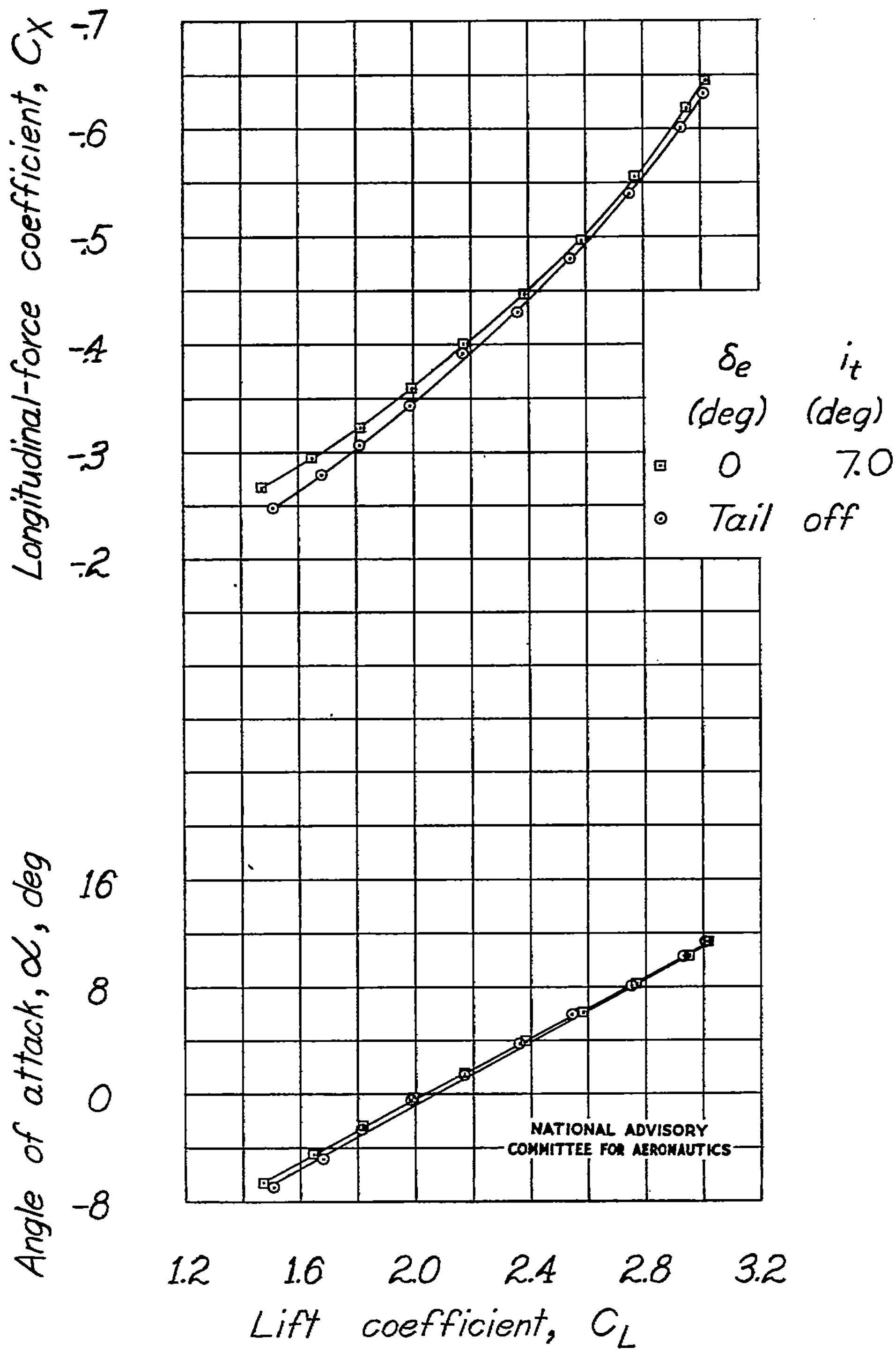

(b) Propeller windmilling.

Figure 11. – Continued.

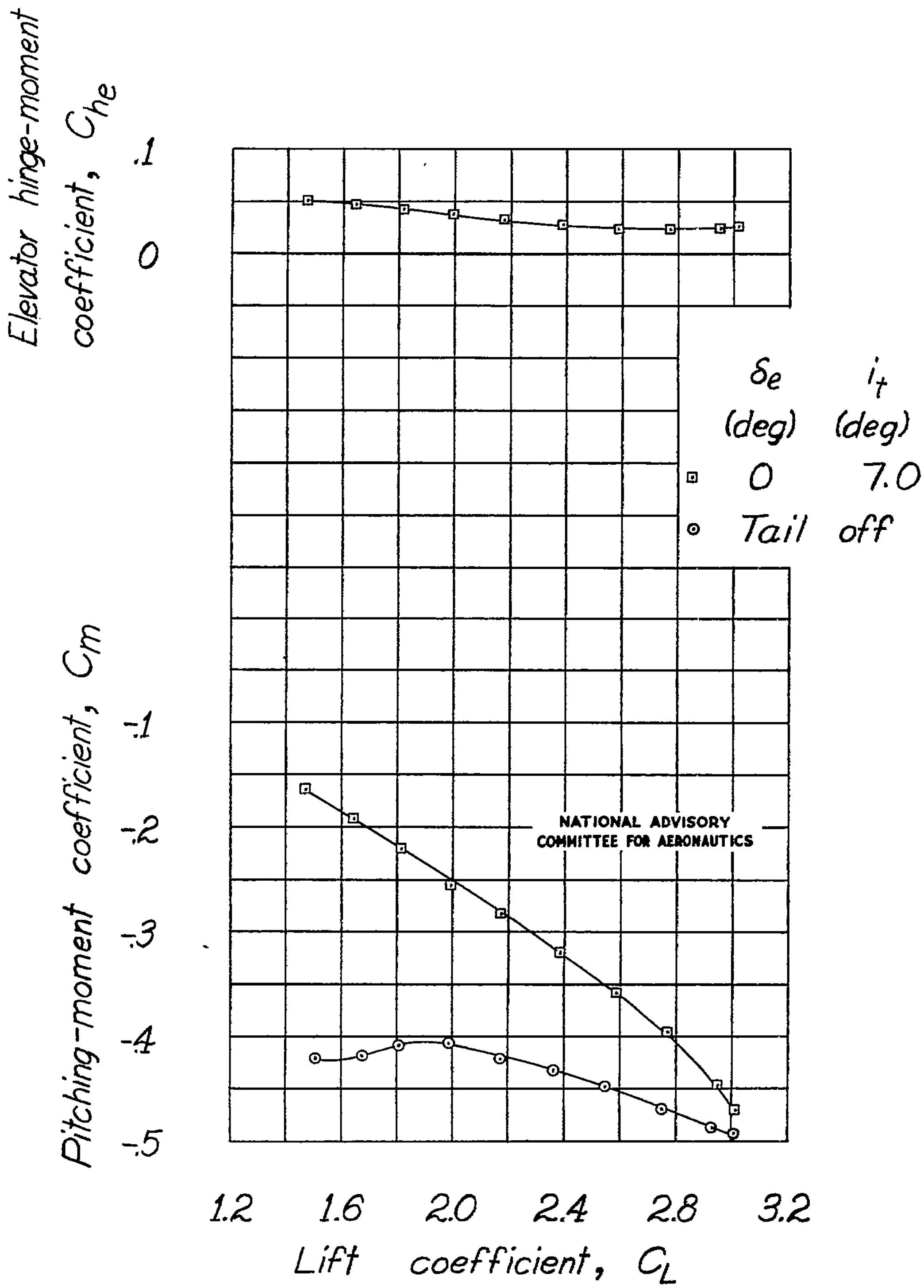

(b) Concluded.

Figure 11. –Continued.

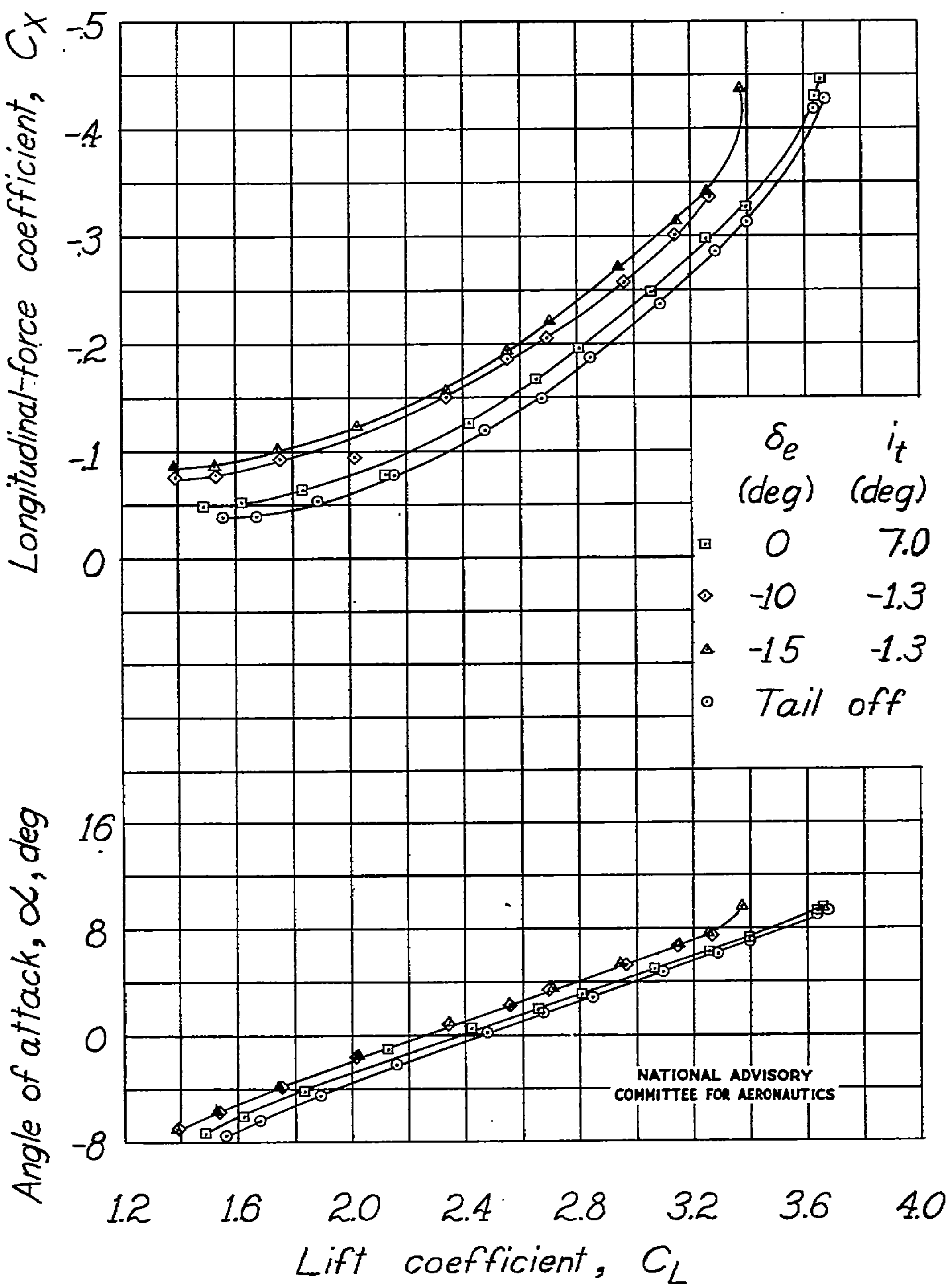

(c) Power on.

Figure 11.–Continued.

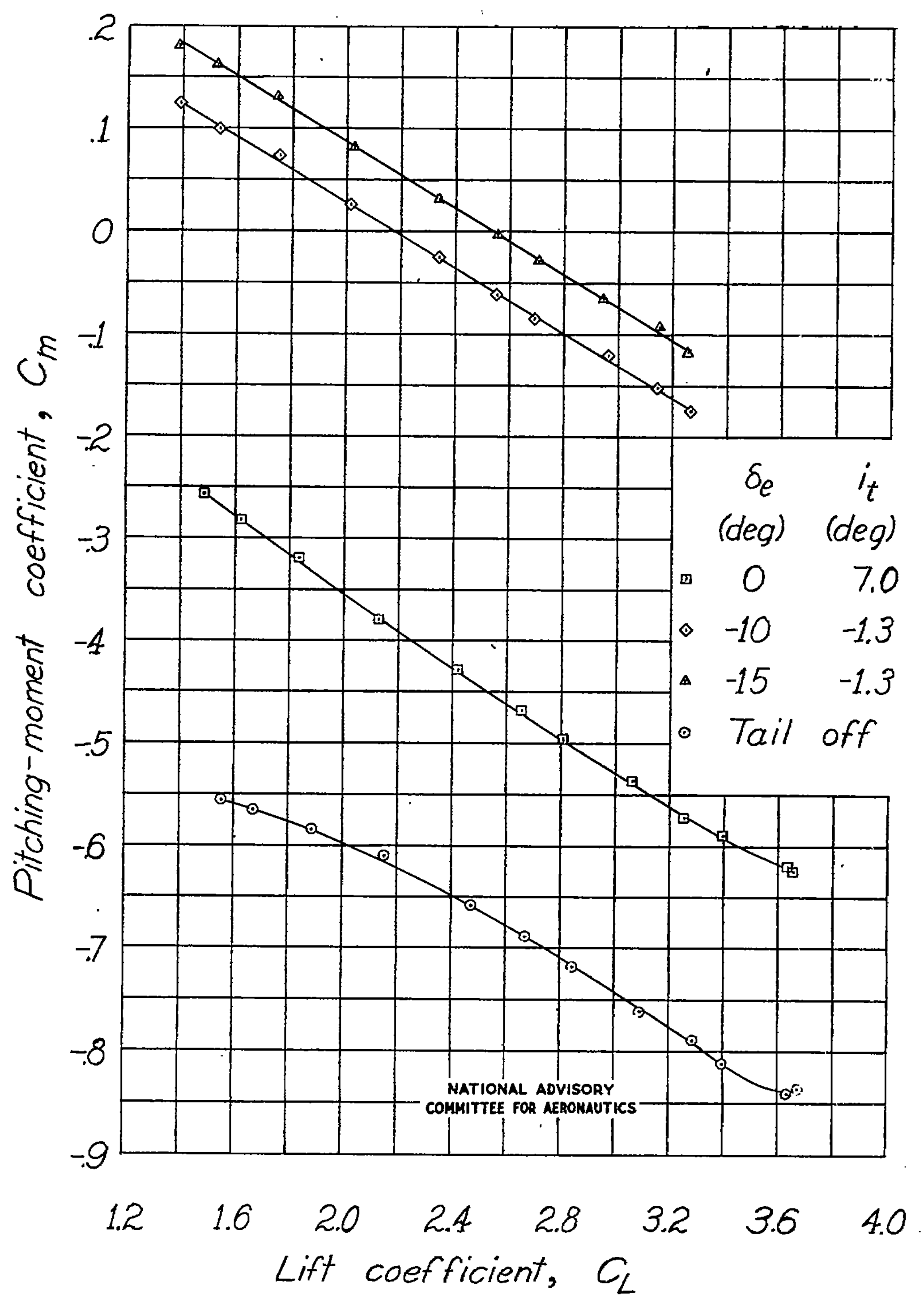

(c) Continued.

Figure 11. - Continued.

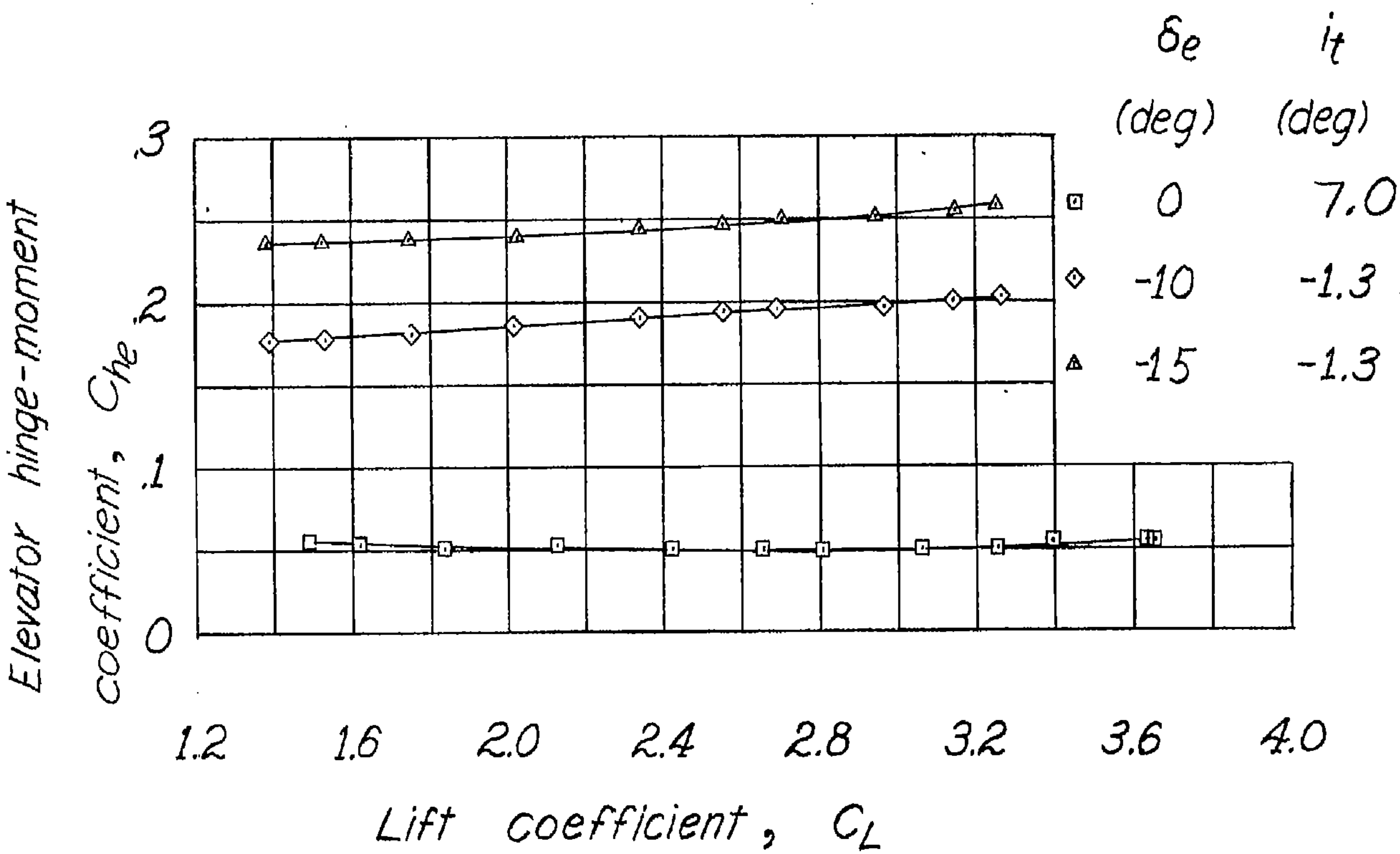

(c) Concluded.

NATIONAL ADVISORY
COMMITTEE FOR AERONAUTICS

Figure 11.- Concluded.

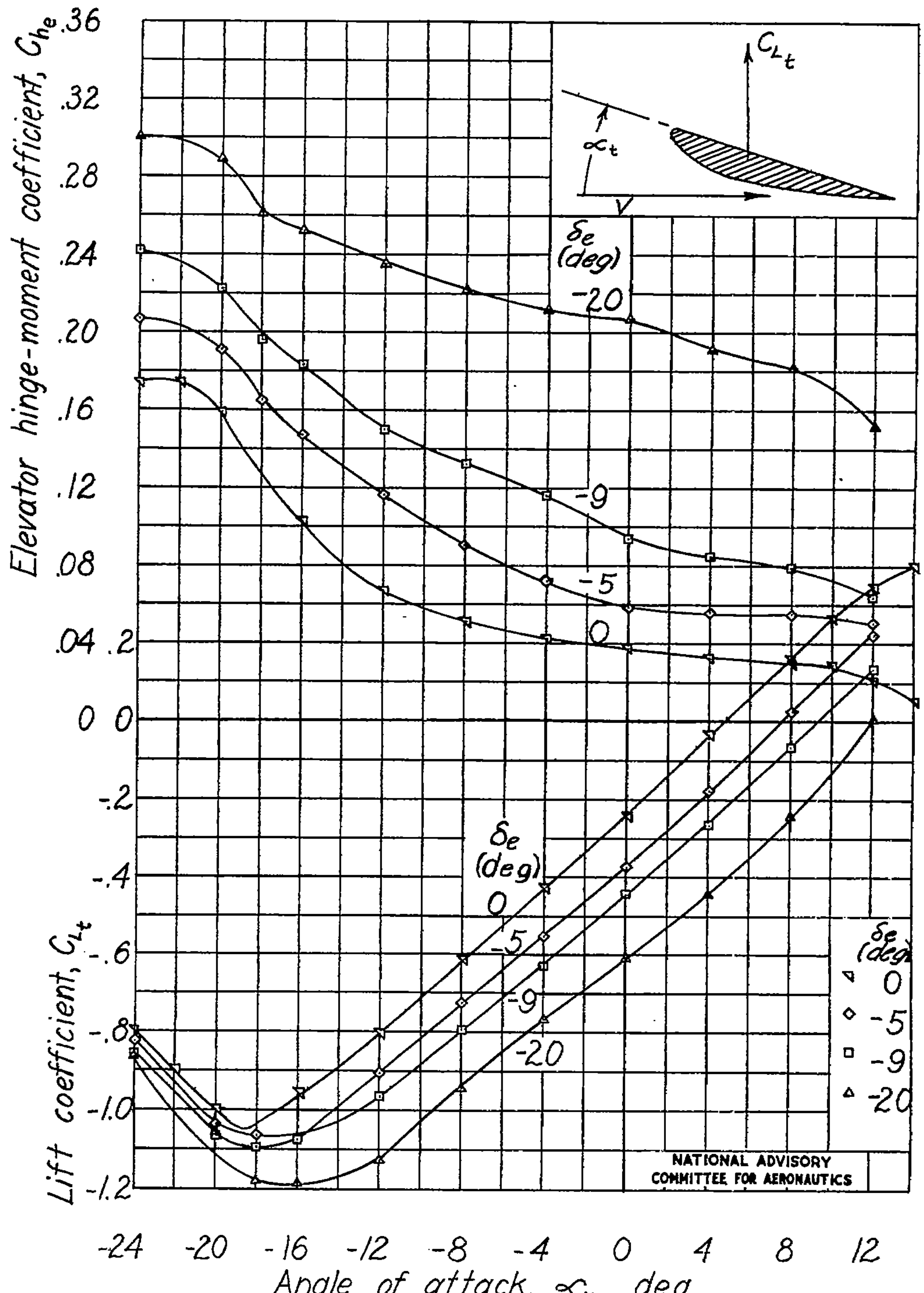

(a) Slot closed.

Figure 12.- Aerodynamic characteristics of the isolated horizontal tail.

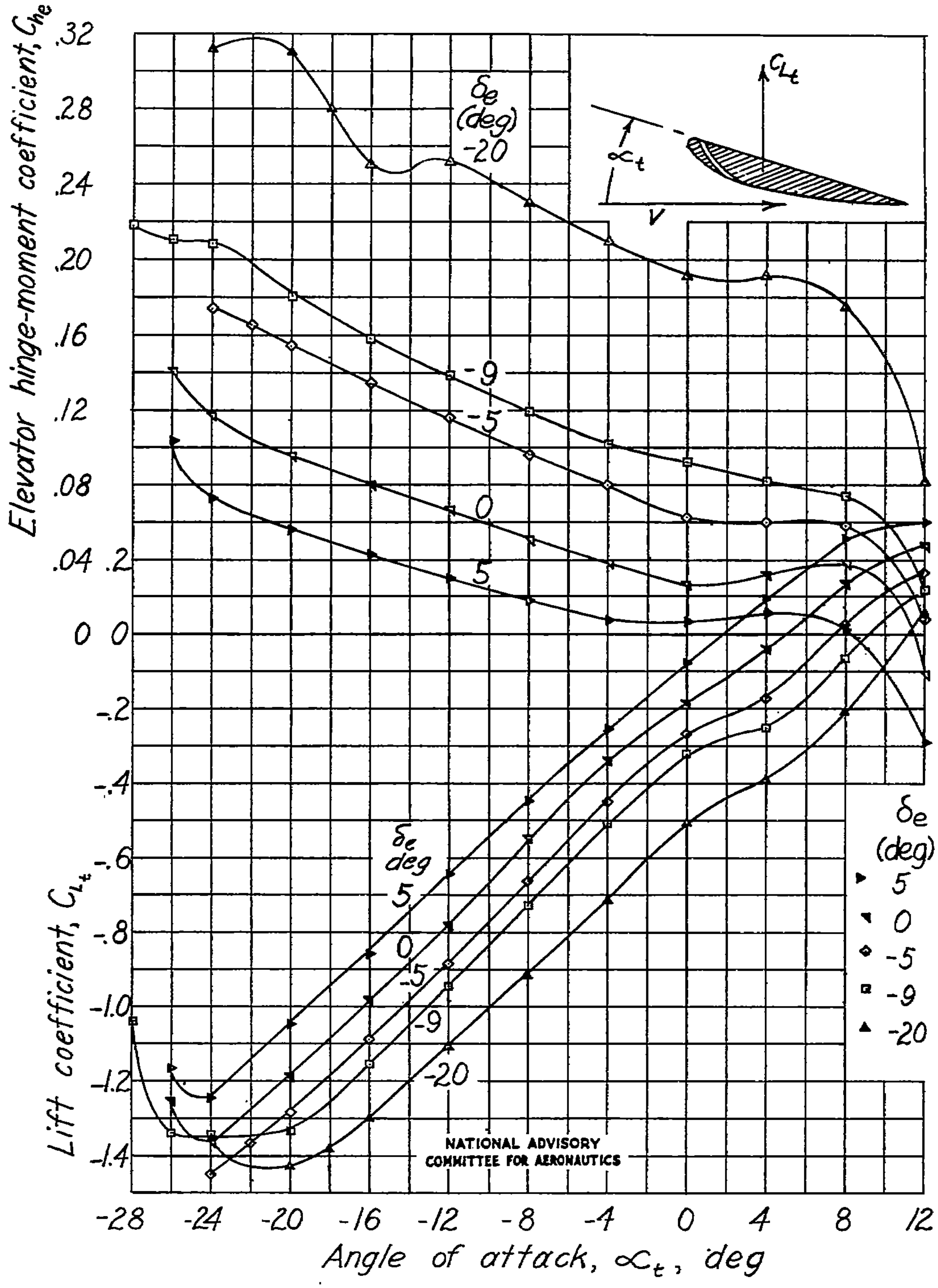

(b) Slot open.

Figure 12.- Concluded.

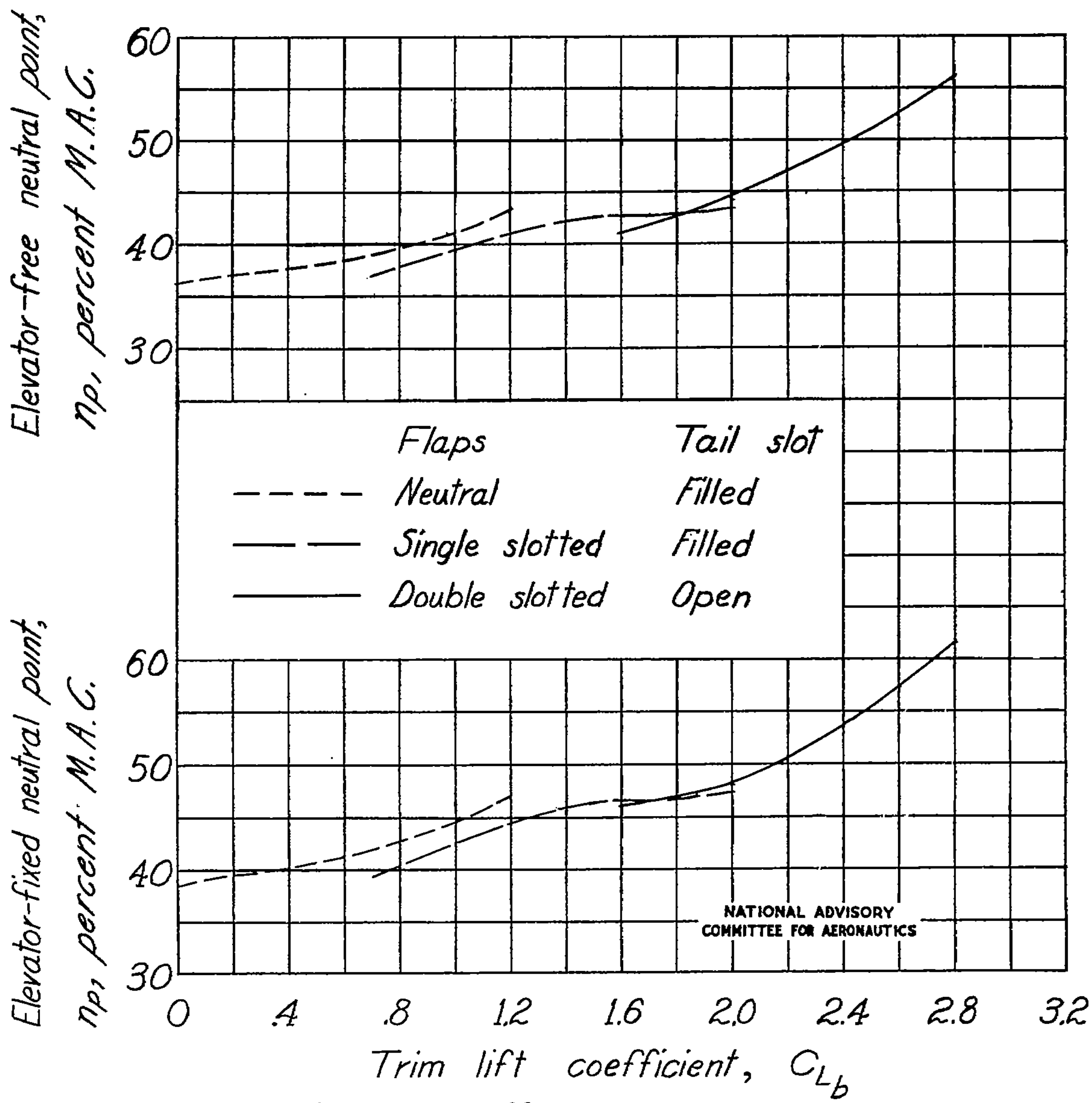

(a) Propeller off.

Figure 13.- Effect of flap deflection on the neutral points of the model as a single-engine high-wing airplane.

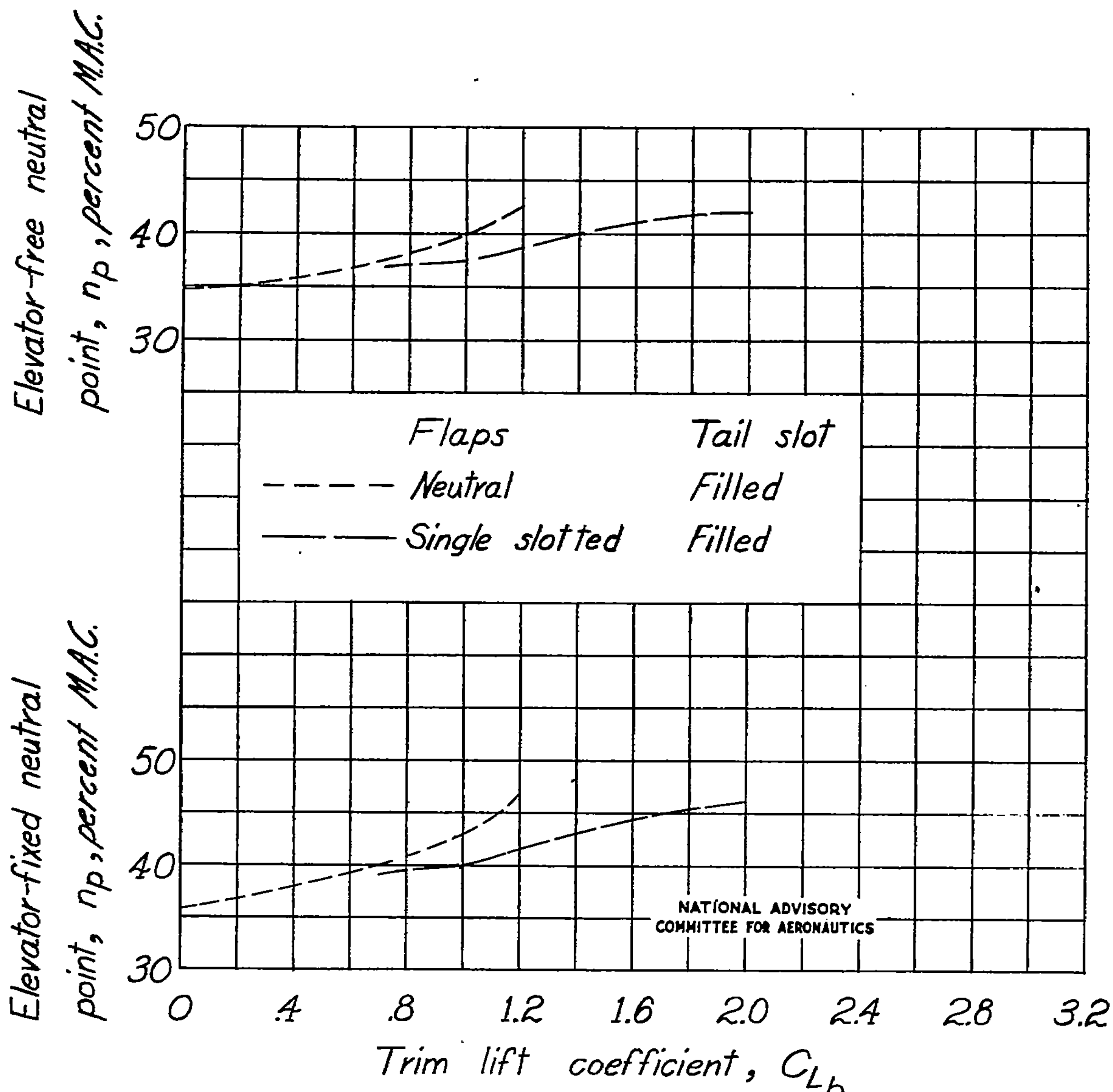

(b) Propeller windmilling.

Figure 13.– Continued.

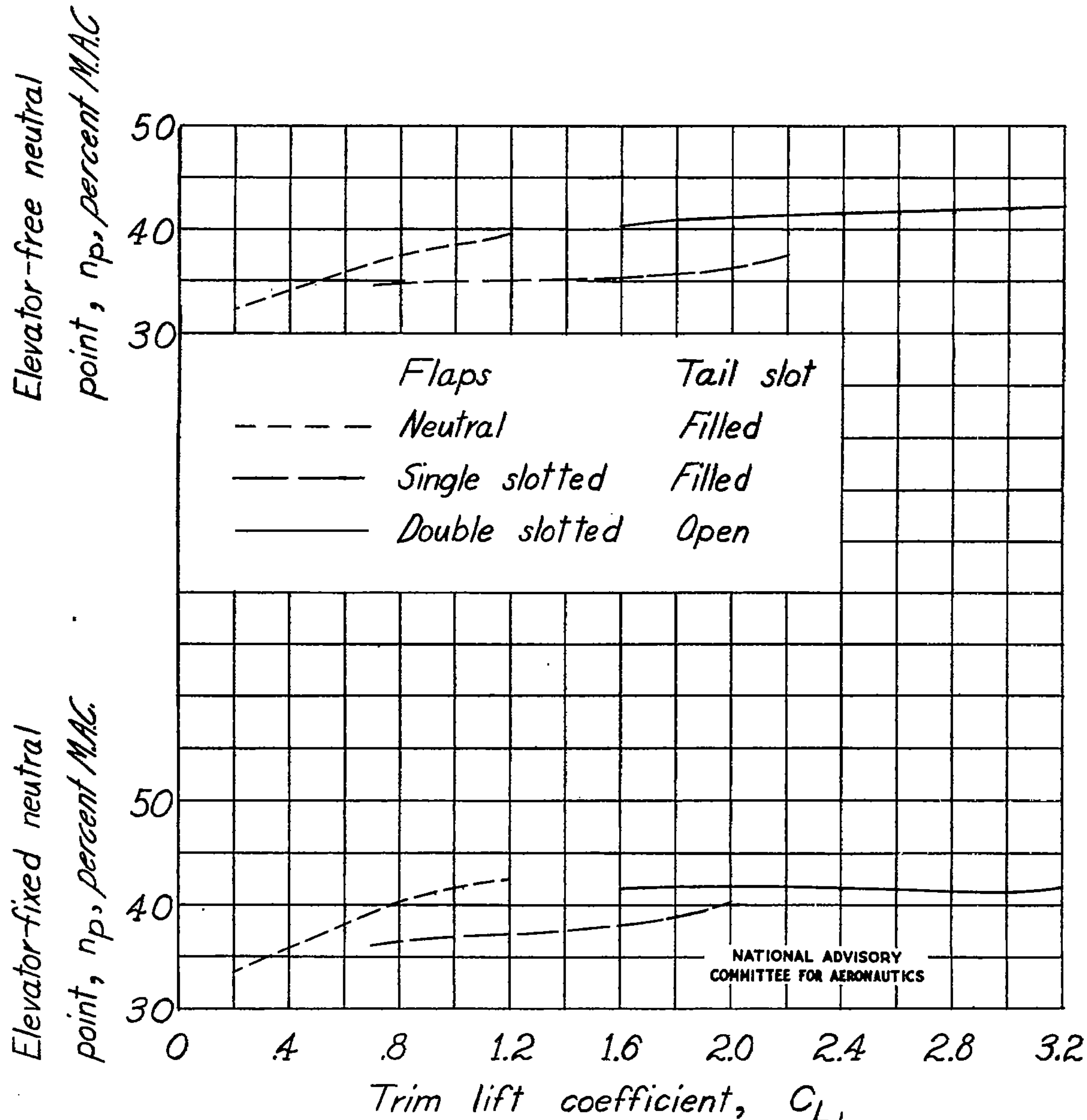

(c) Power on.

Figure 13.- Concluded.

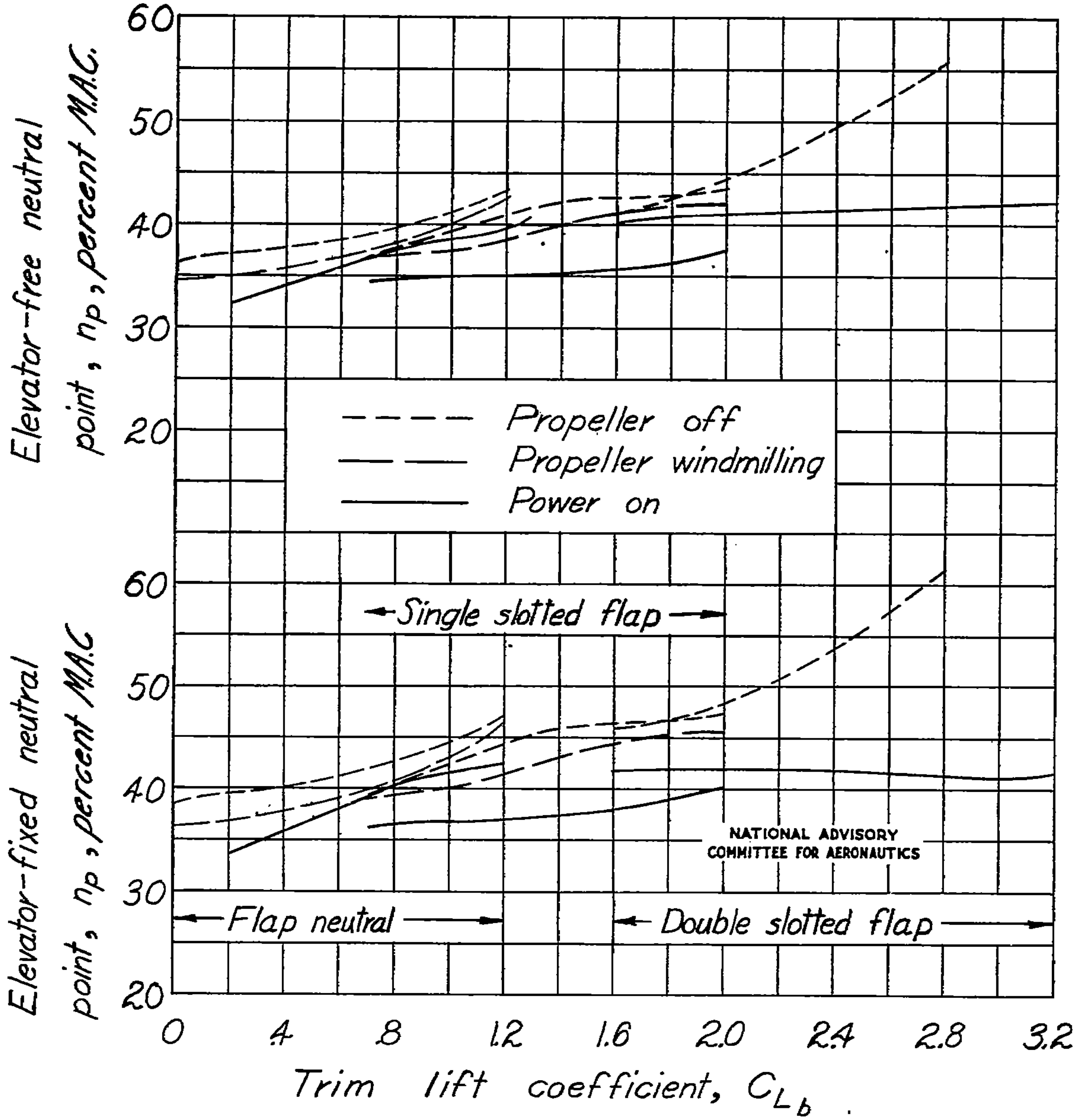

Figure 14.– Effect of power on the neutral points of the model as a single-engine high-wing airplane.

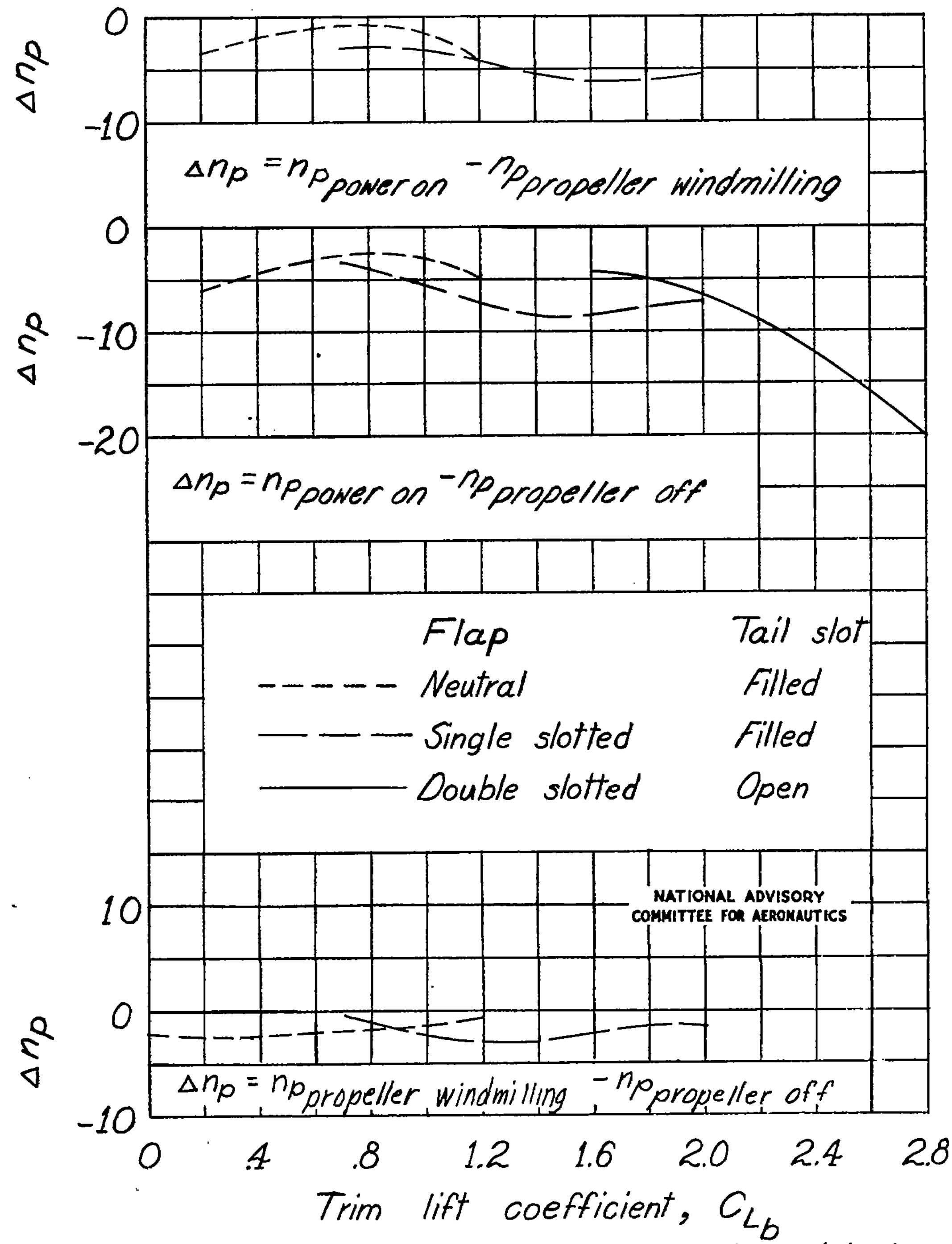

Figure 15.- Increments of neutral-point location due to power for the model as a single-engine high-wing airplane.

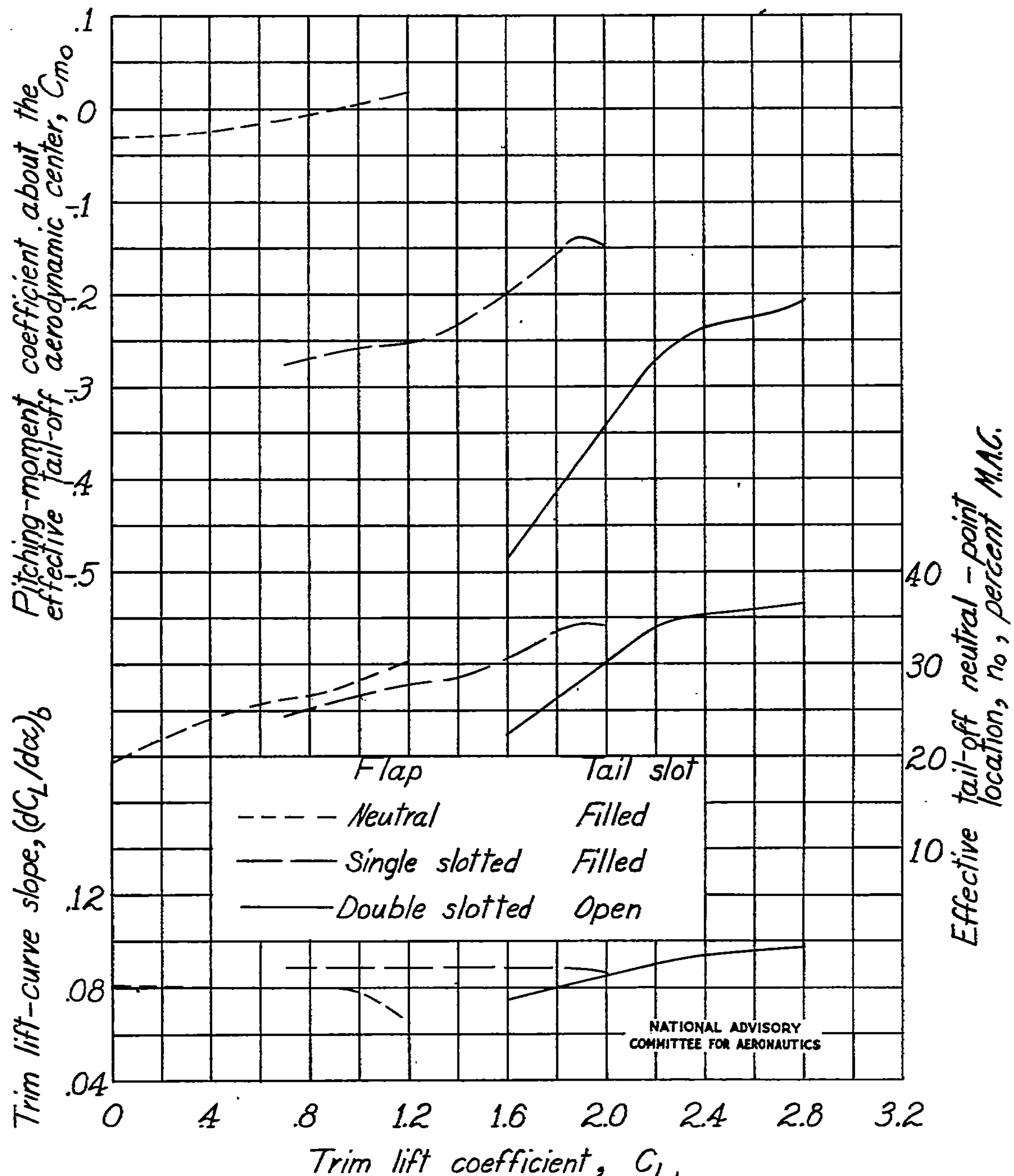

(a) Propeller off.

Figure 16.- Effect of flap on the various longitudinal-stability parameters of the model as a single-engine high-wing airplane.

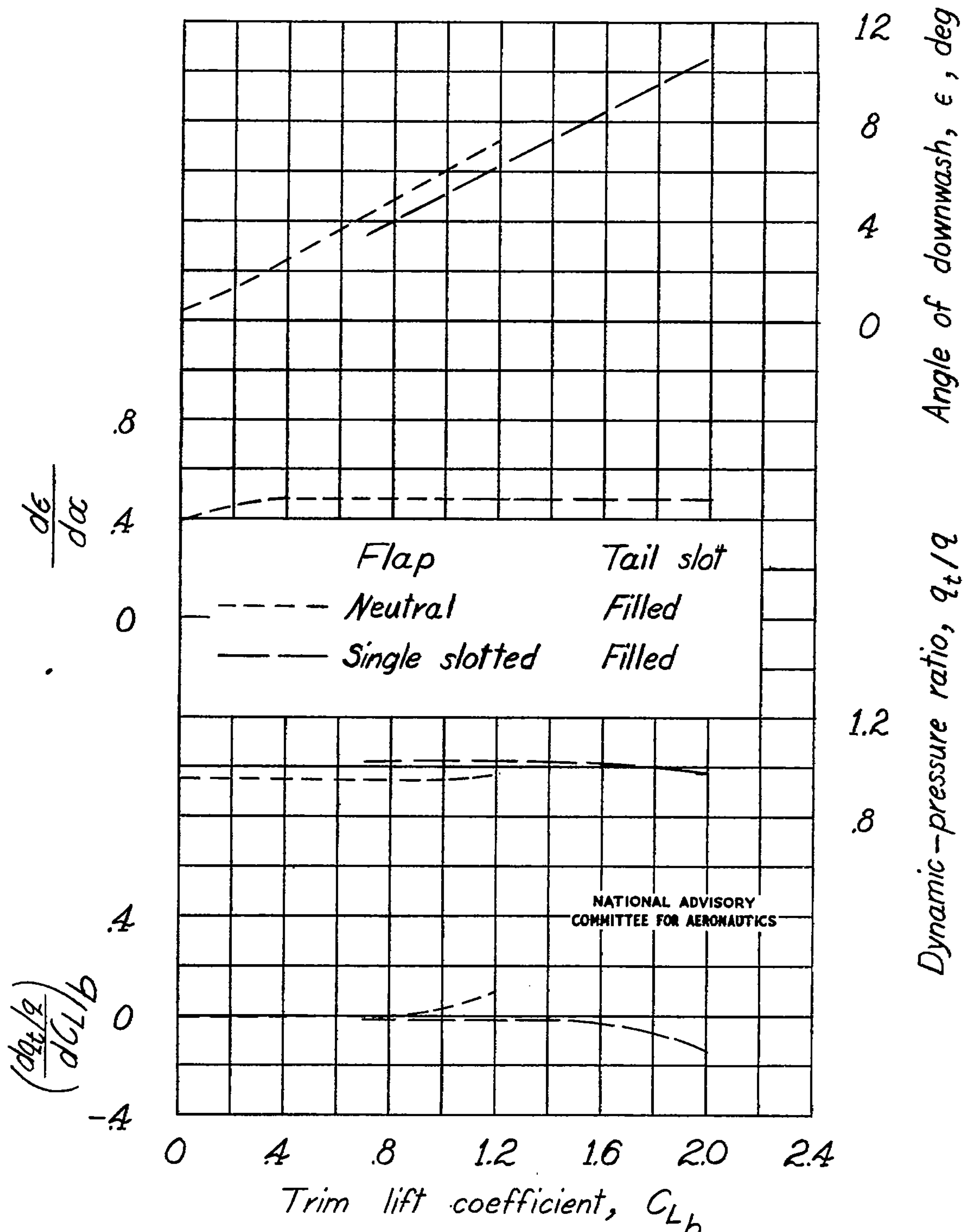

(a) Concluded.

Figure 16 .- Continued.

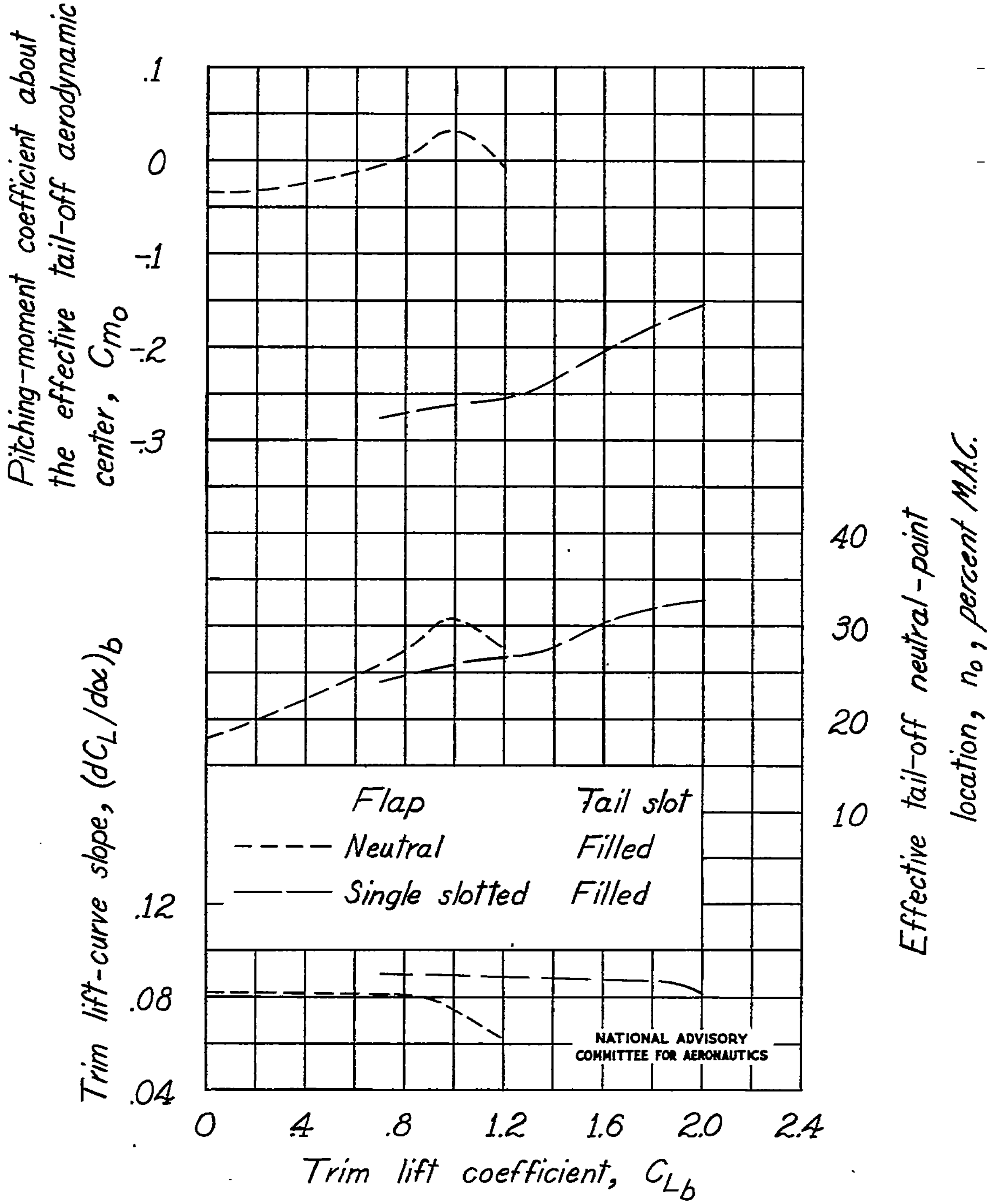

(b) Windmilling.

Figure 16.- Continued.

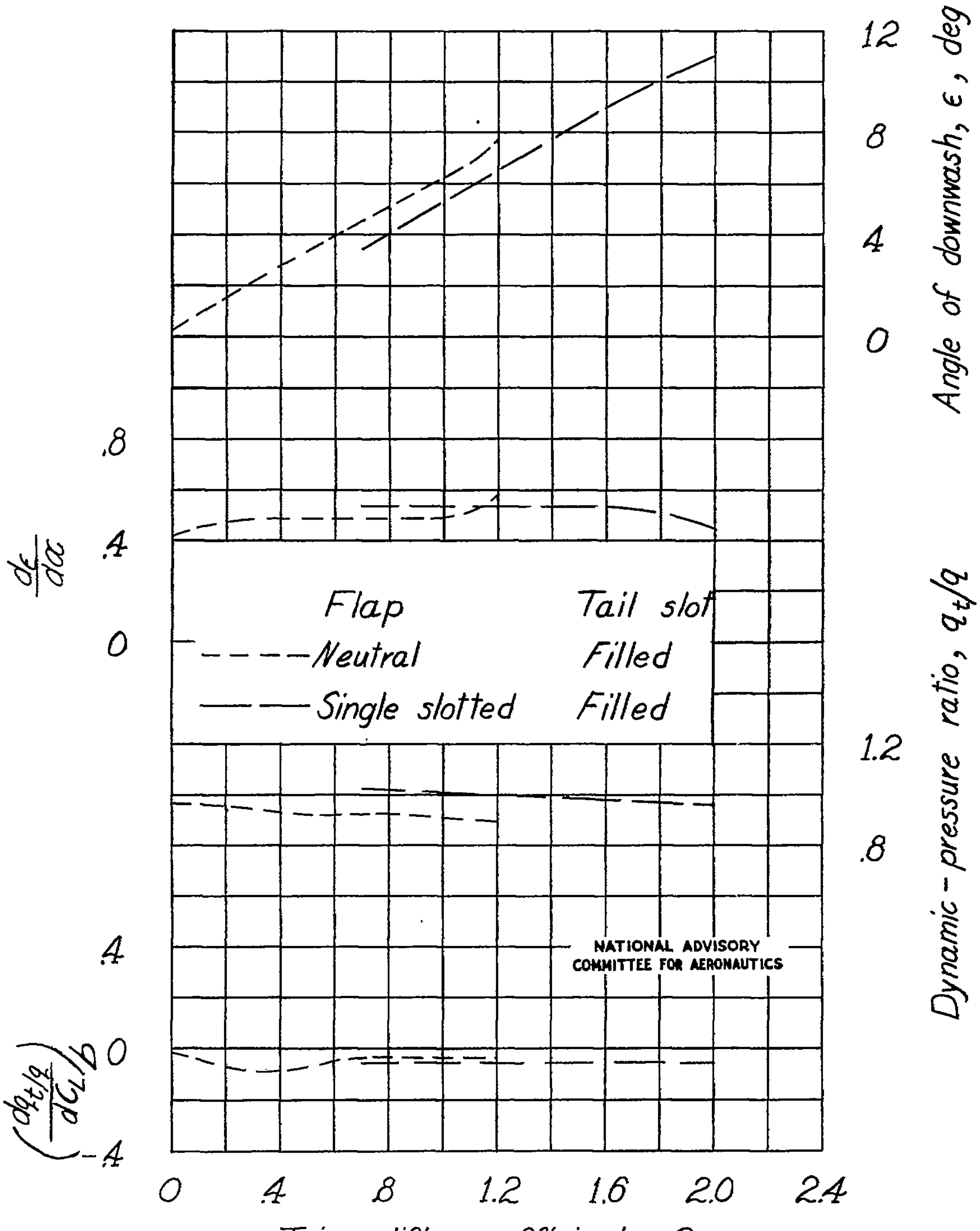

Trim lift coefficient, C_{L_b}

(b) Concluded.

Figure 16.– Continued.

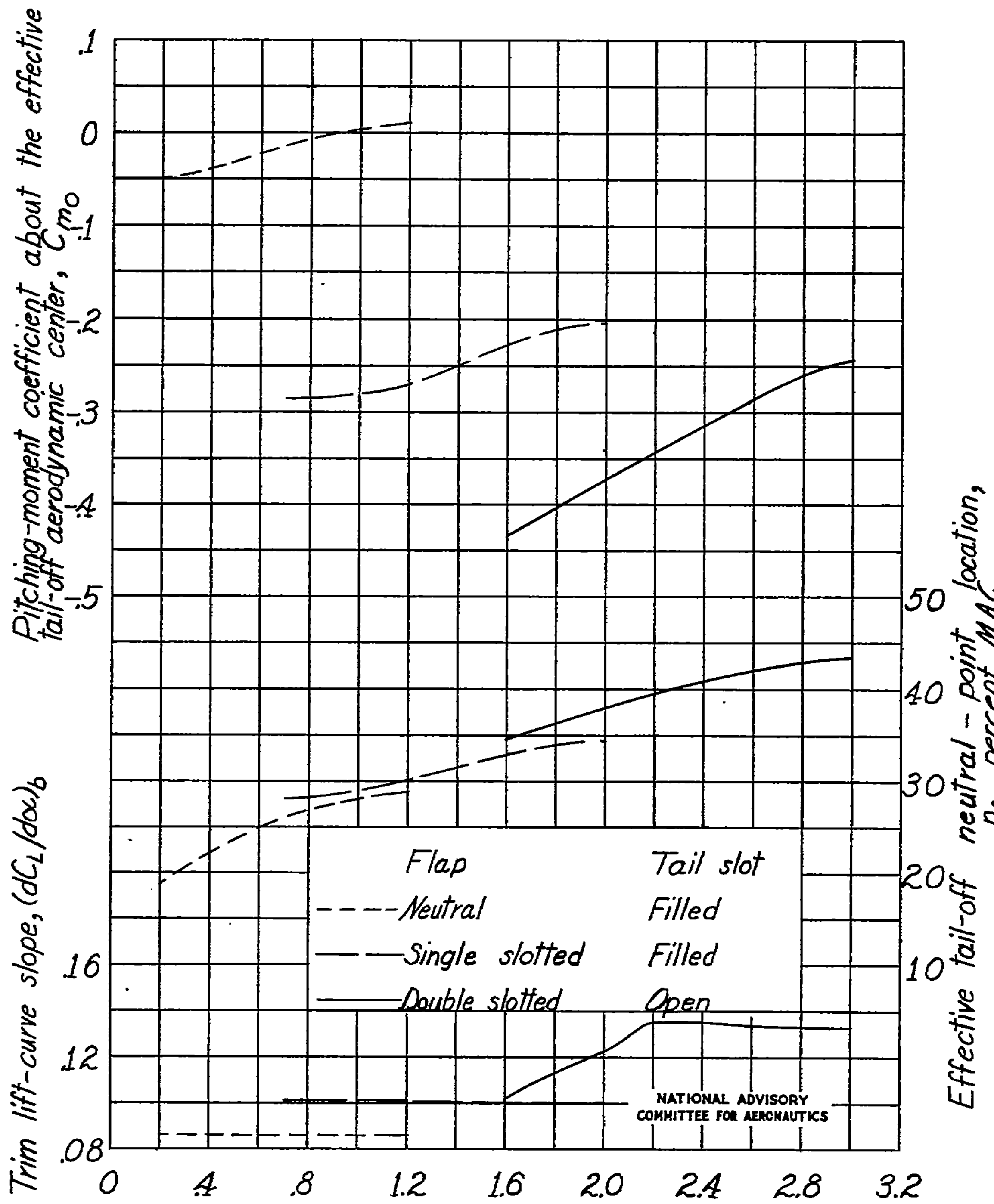

(c) Power on.

Figure 16.—Continued.

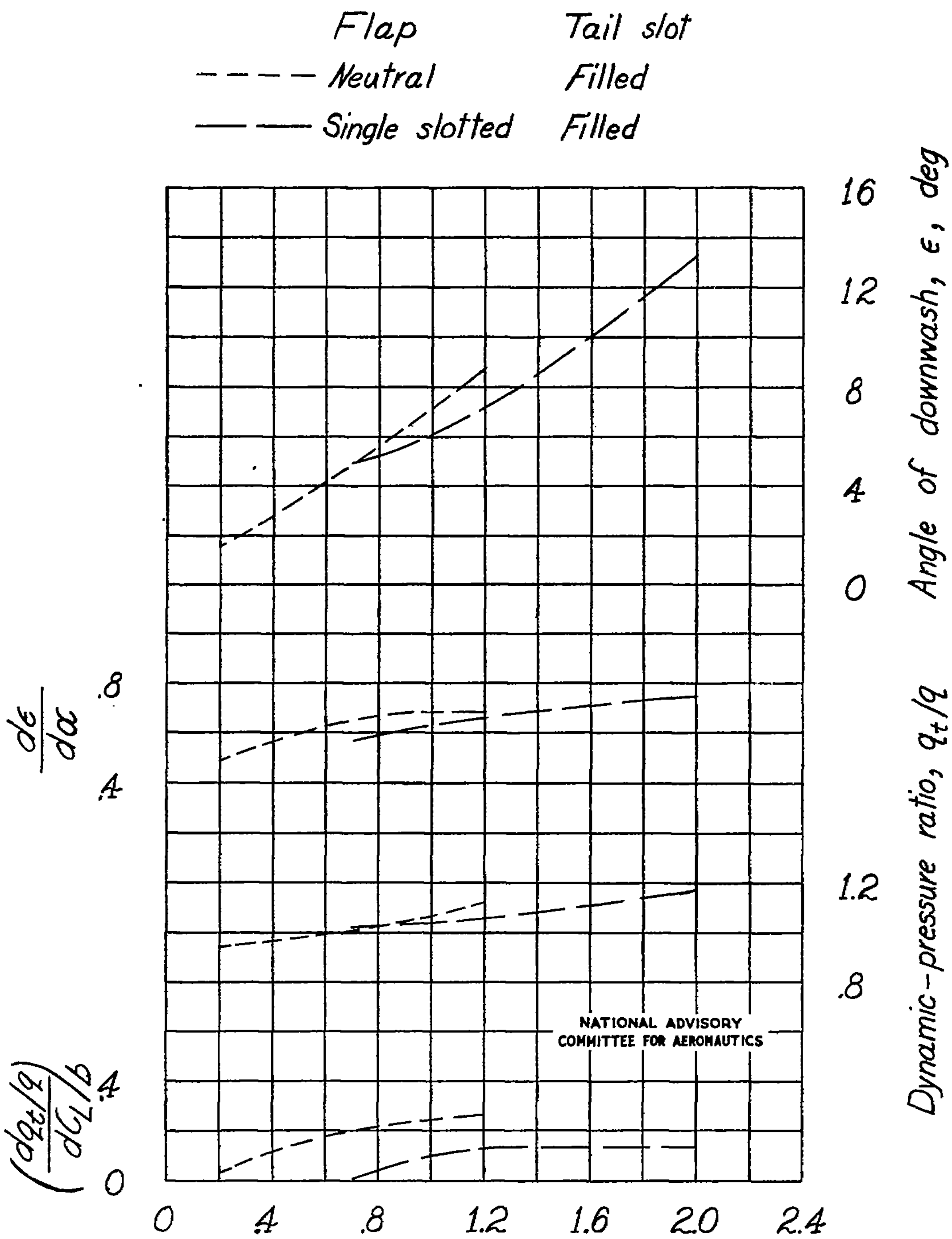

Trim lift coefficient, C_{L_b}

(c) Concluded.

Figure 16.- Concluded.

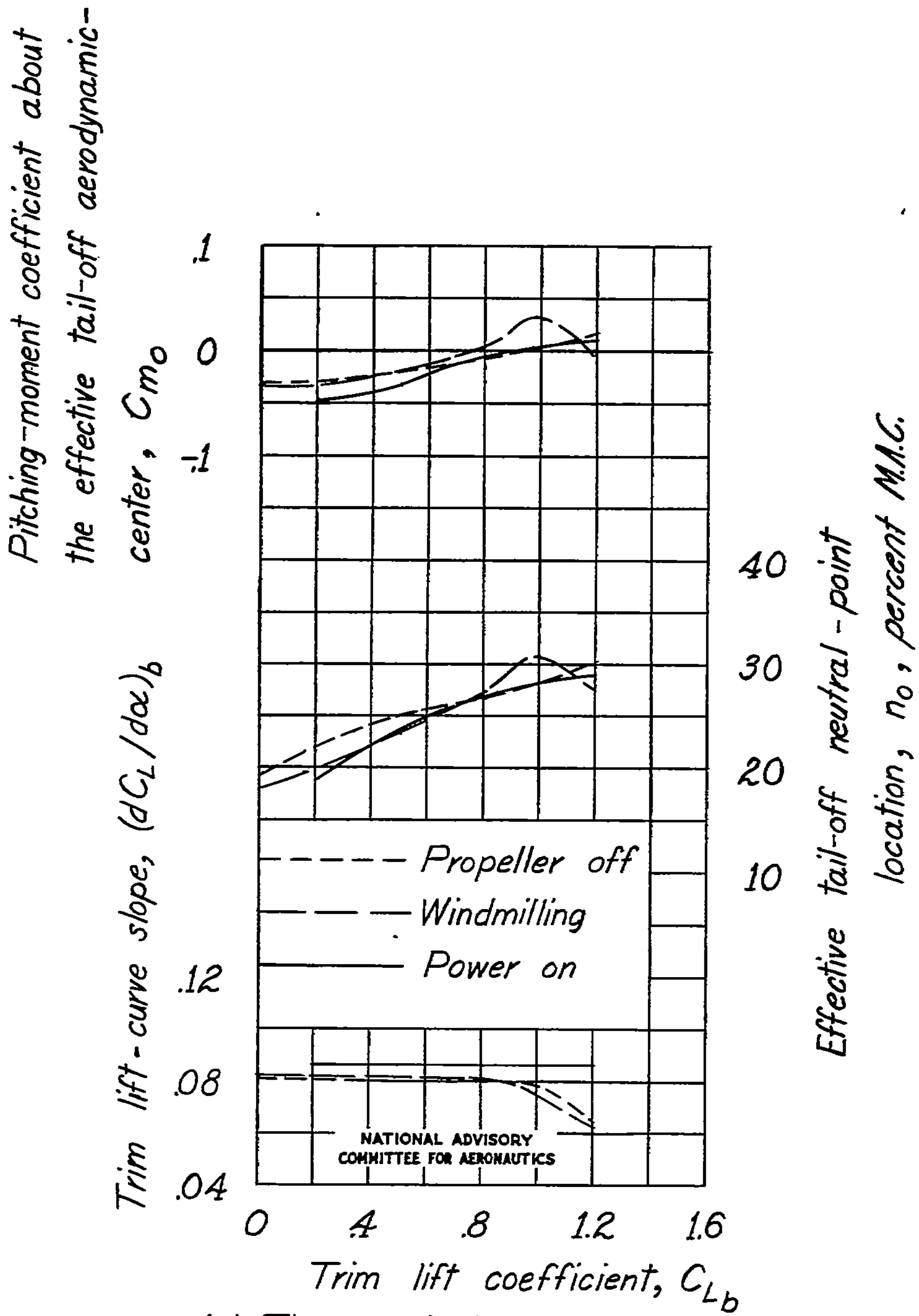

(a) Flap neutral.

Figure 17.- Effect of power on the various longitudinal-stability parameters of the model as a single-engine high-wing airplane.

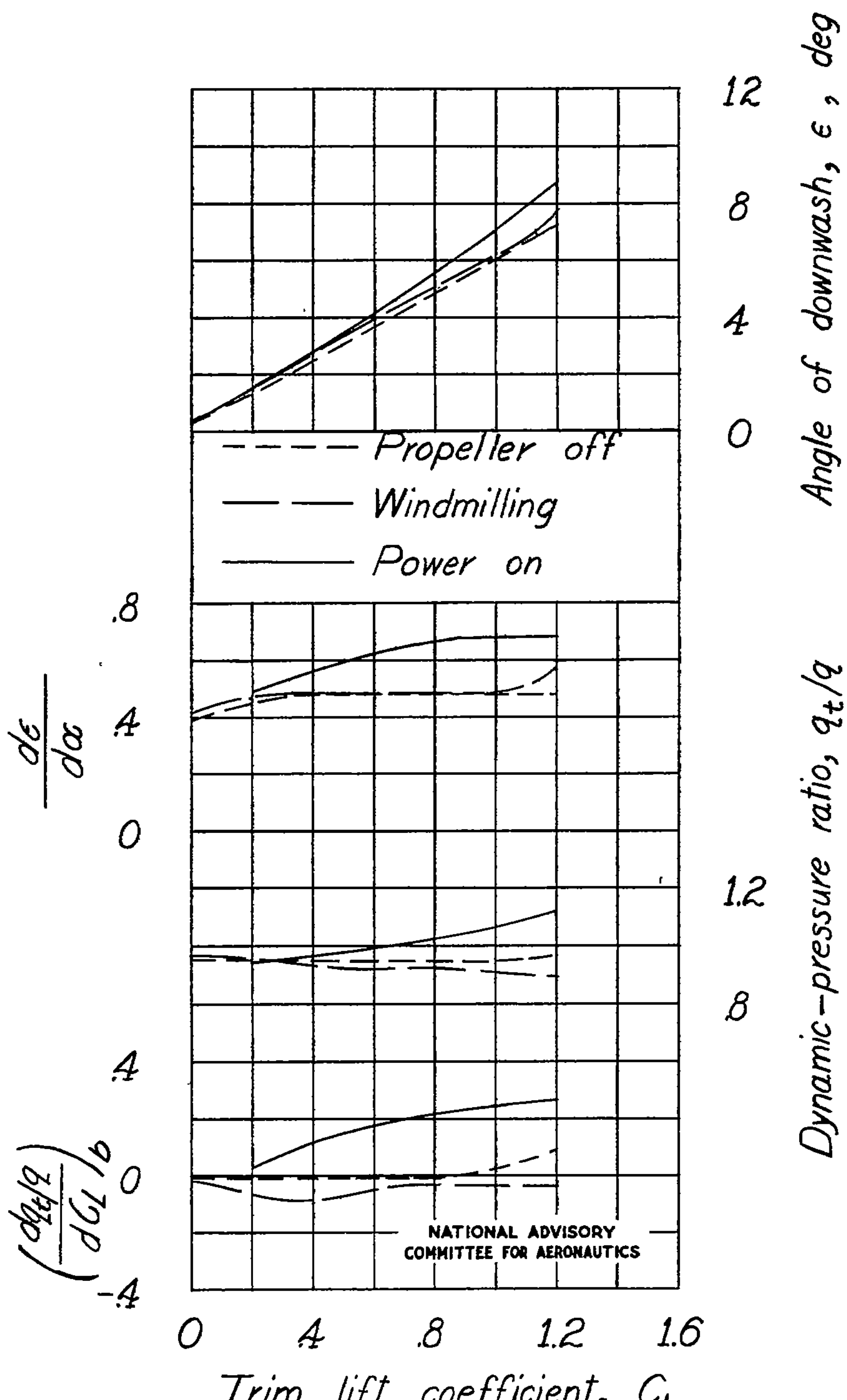

(a) Concluded.

Figure 17.– Continued.

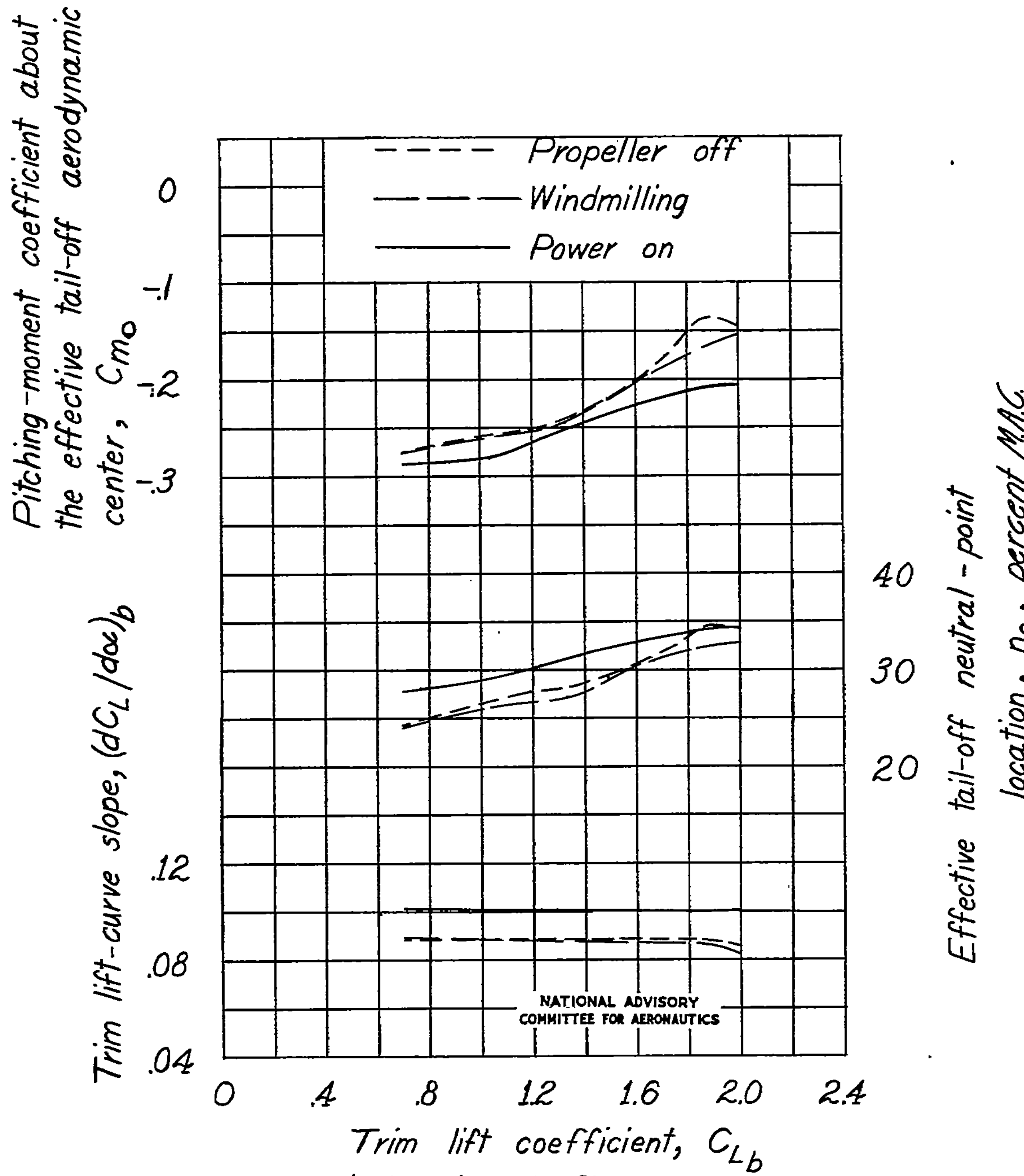

(b) Single slotted flap.

Figure 17.– Continued.

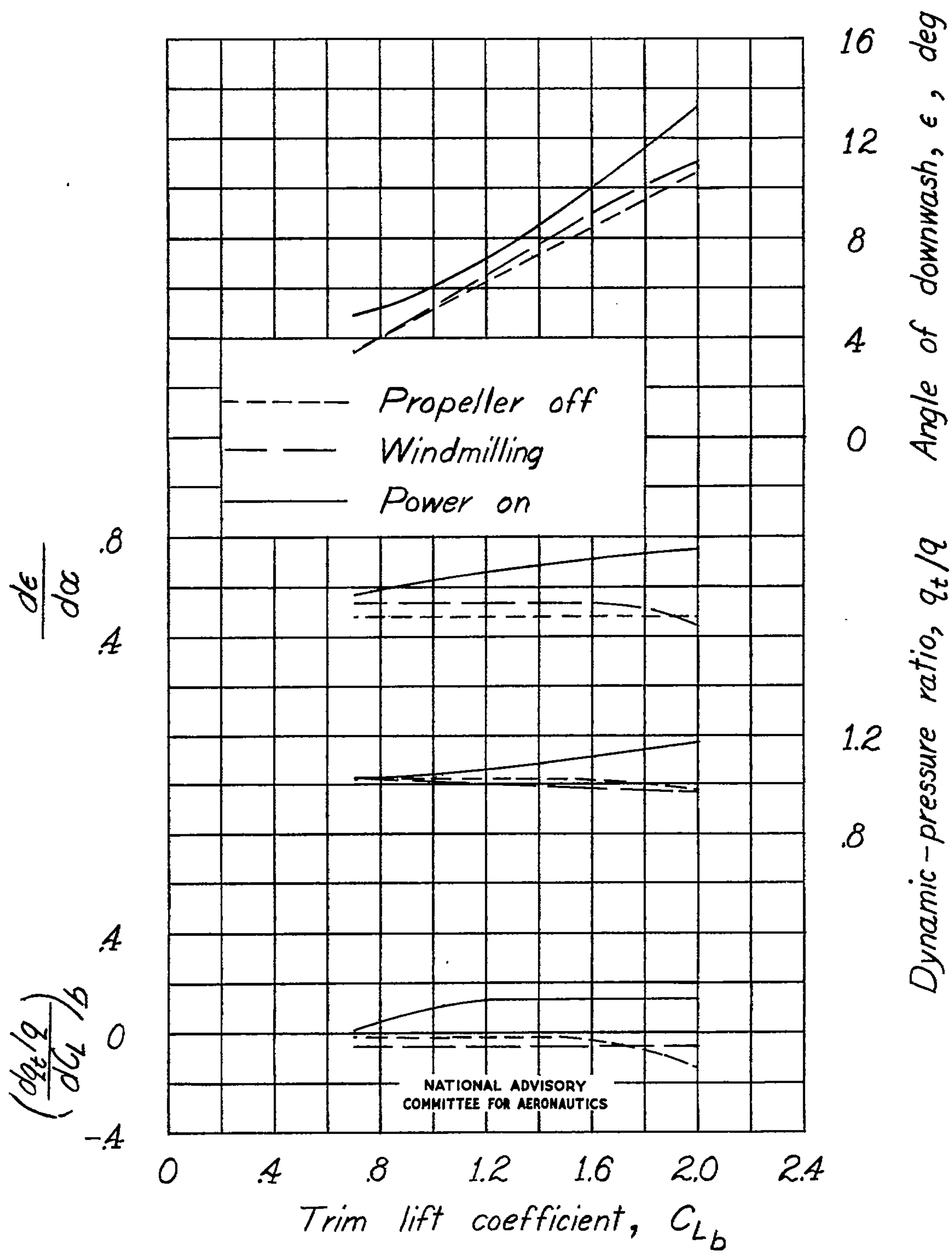

(b) Concluded.

Figure 17.- Continued.

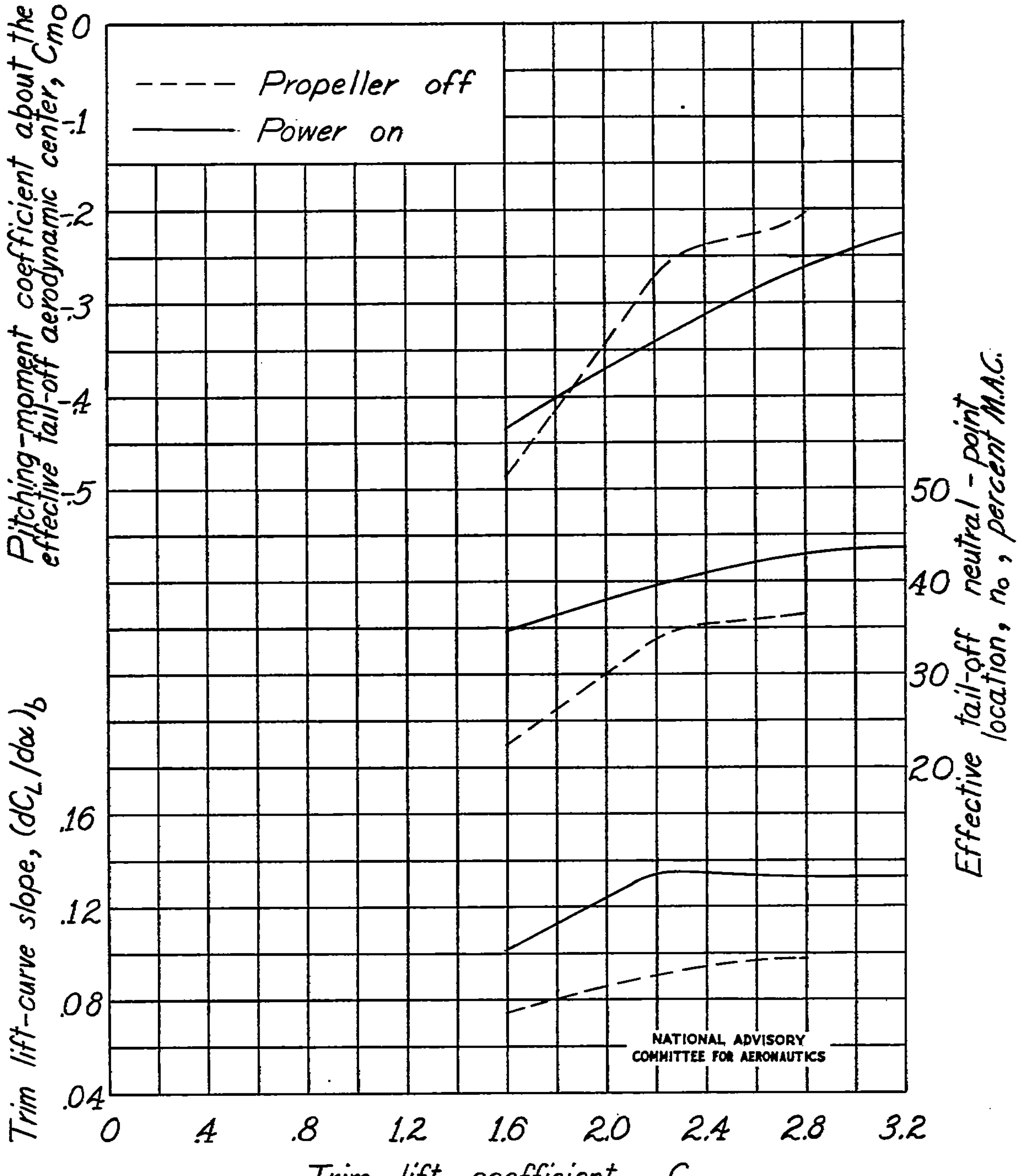

(c) Double slotted flap.

Figure 17.- Concluded.

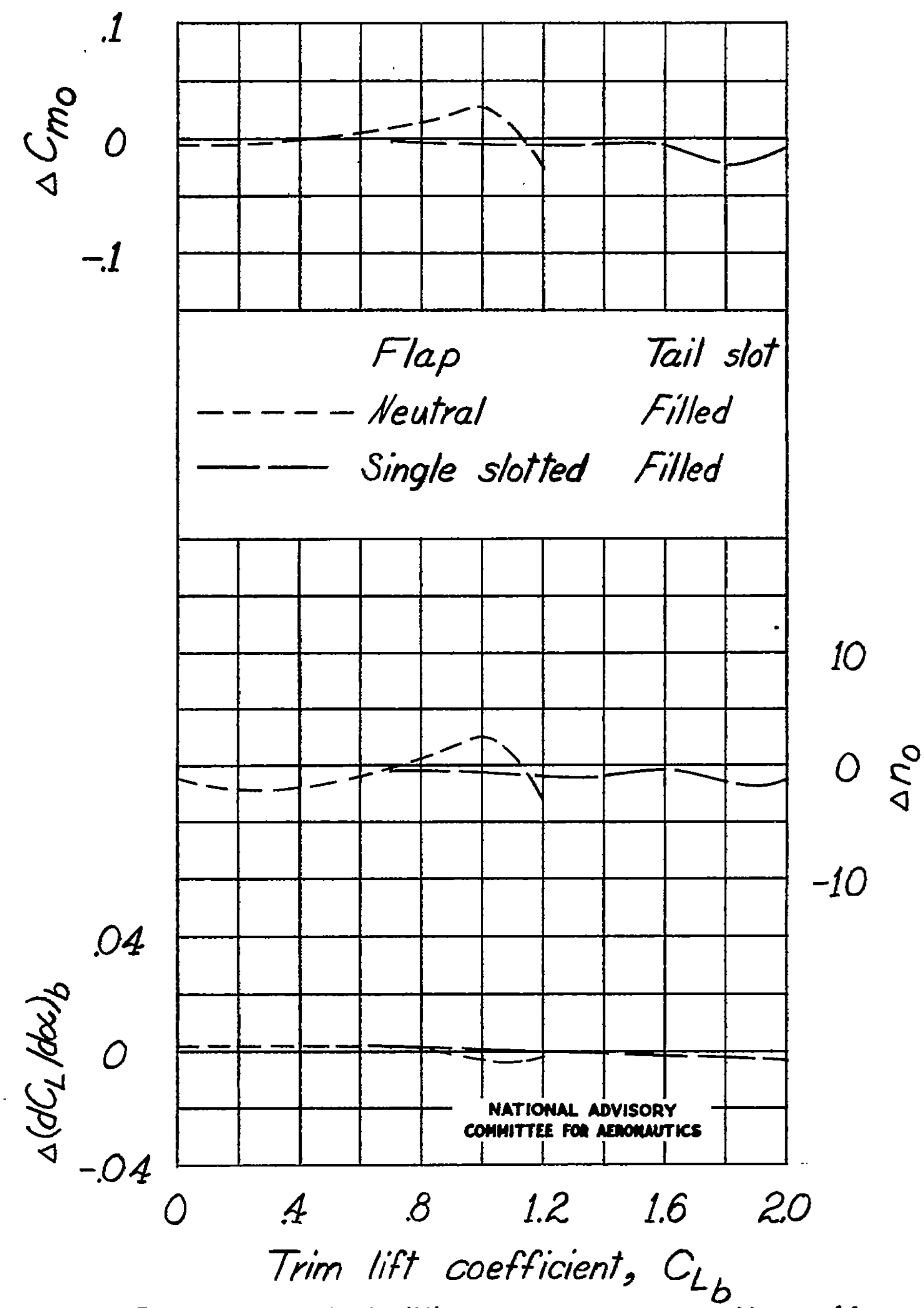

(a) Propeller windmilling minus propeller off.

Figure 18.– Increments of the longitudinal-stability parameters due to power for the model as a single-engine high-wing airplane.

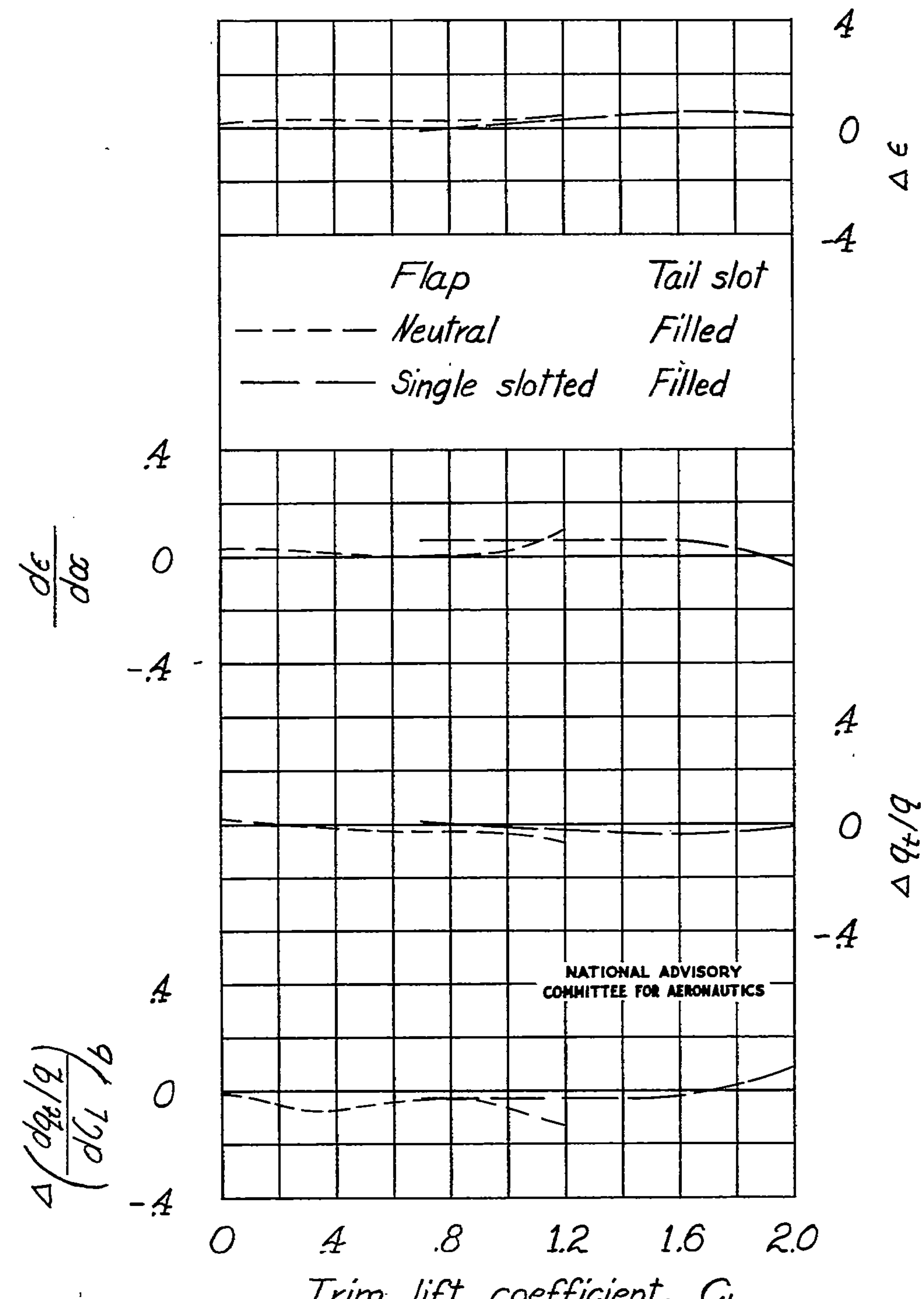

(a) Concluded.

Figure 18.- Continued.

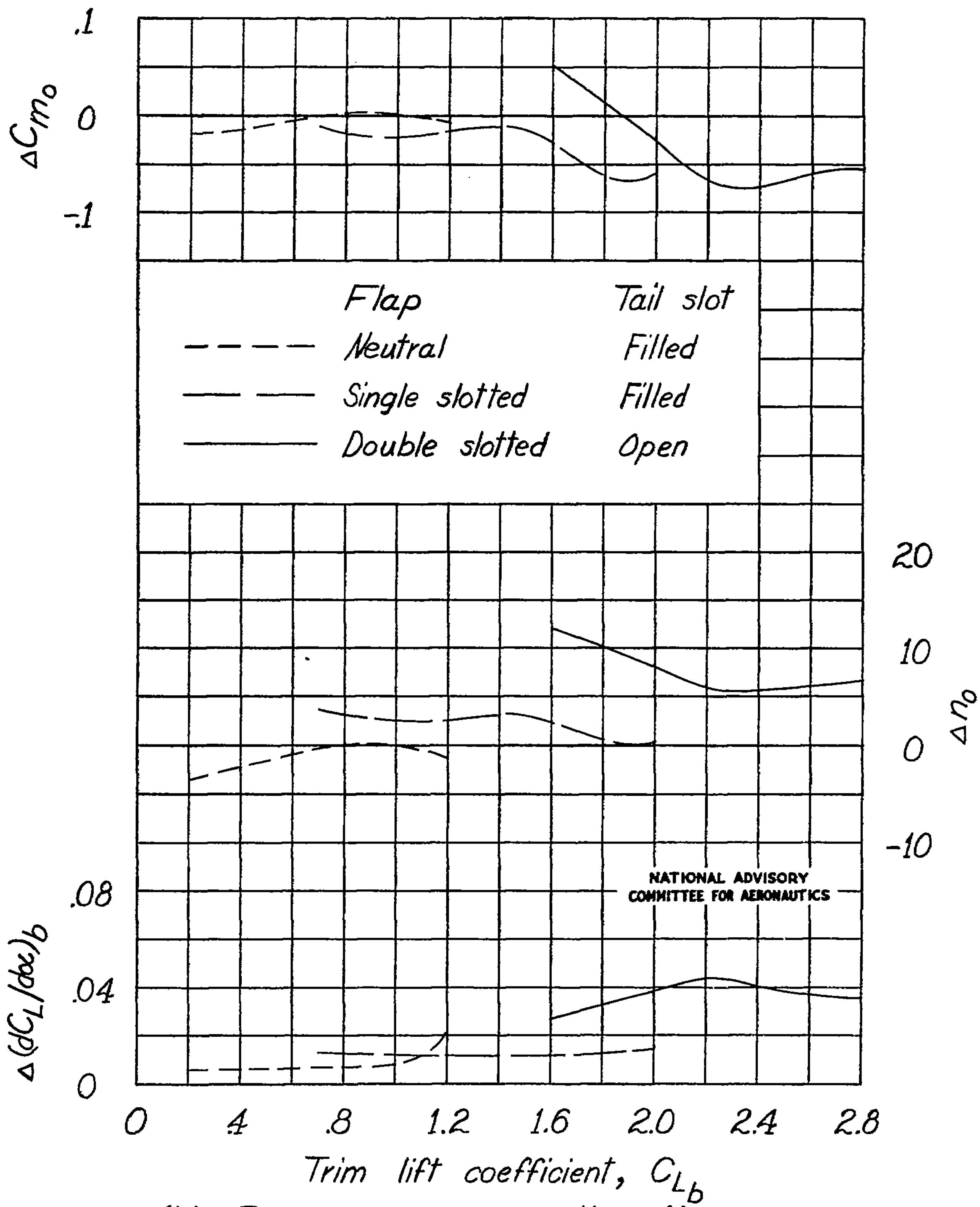

(b) Power on minus propeller off.

Figure 18.- Continued.

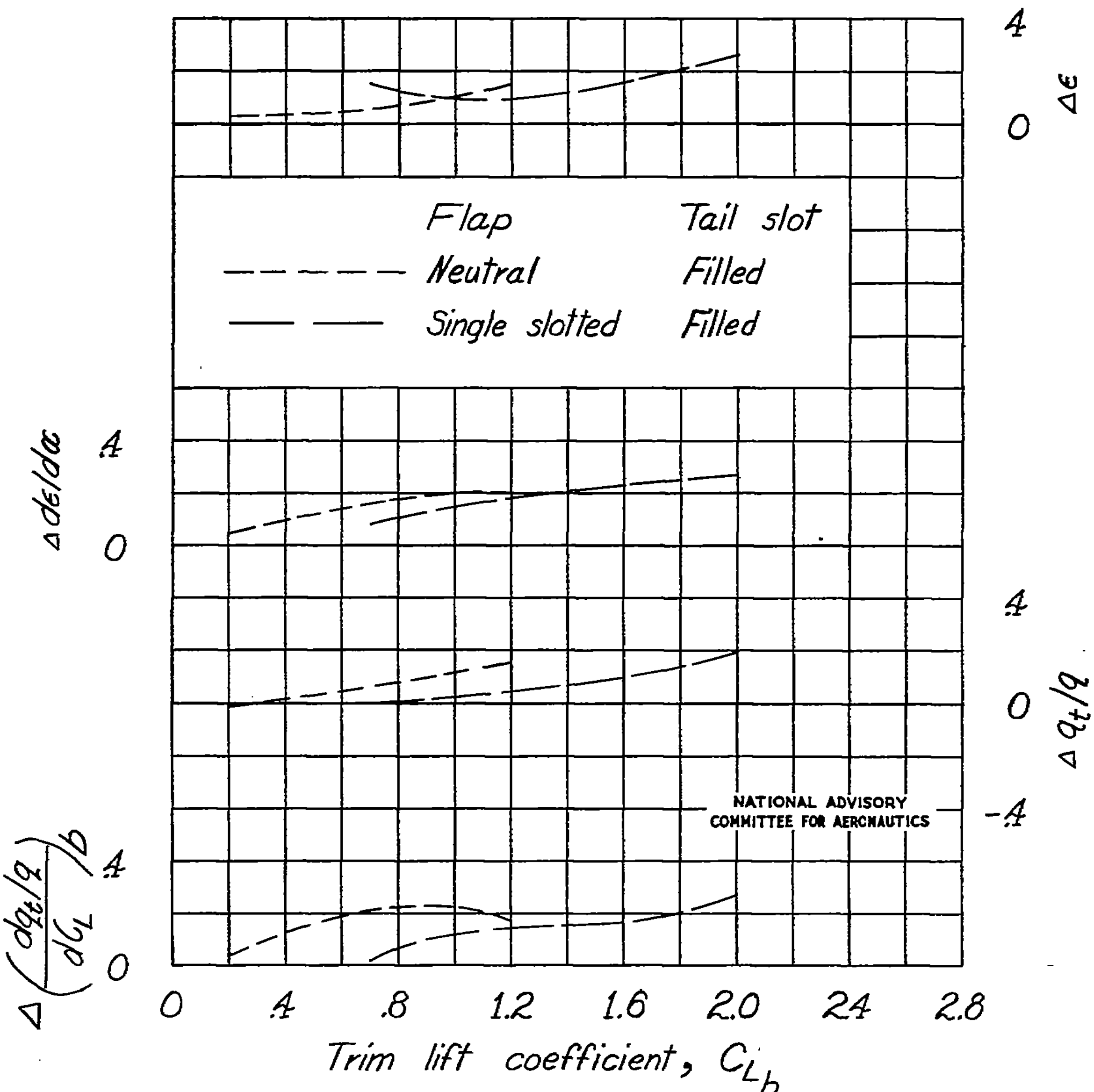

(b) Concluded.

Figure 18.- Concluded.

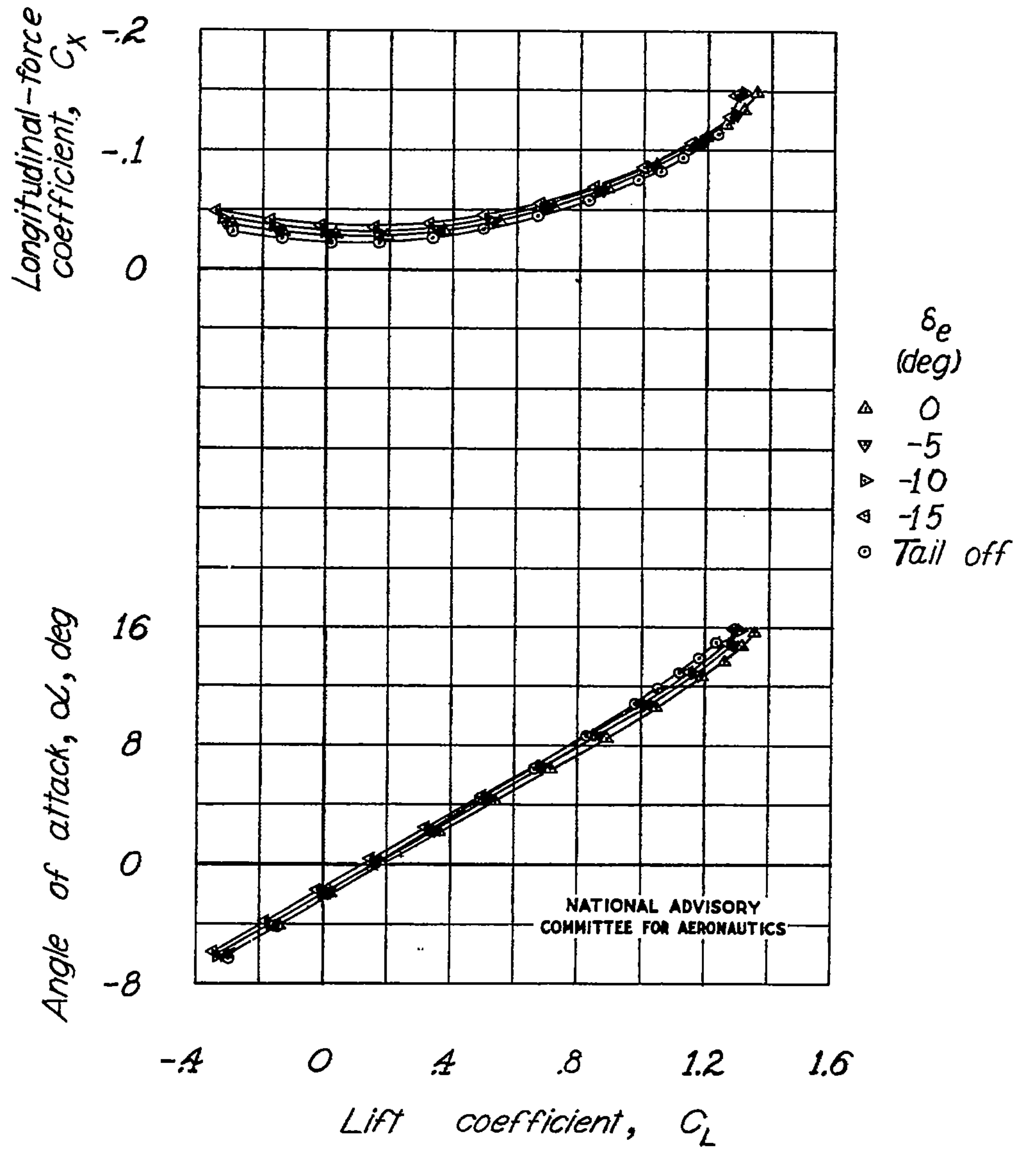

(a) Propeller off.

Figure 19.- Effect of elevator on the aerodynamic characteristics of the model as a single-engine high-wing airplane with flaps neutral. $i_t = 7°$; tail slot closed.

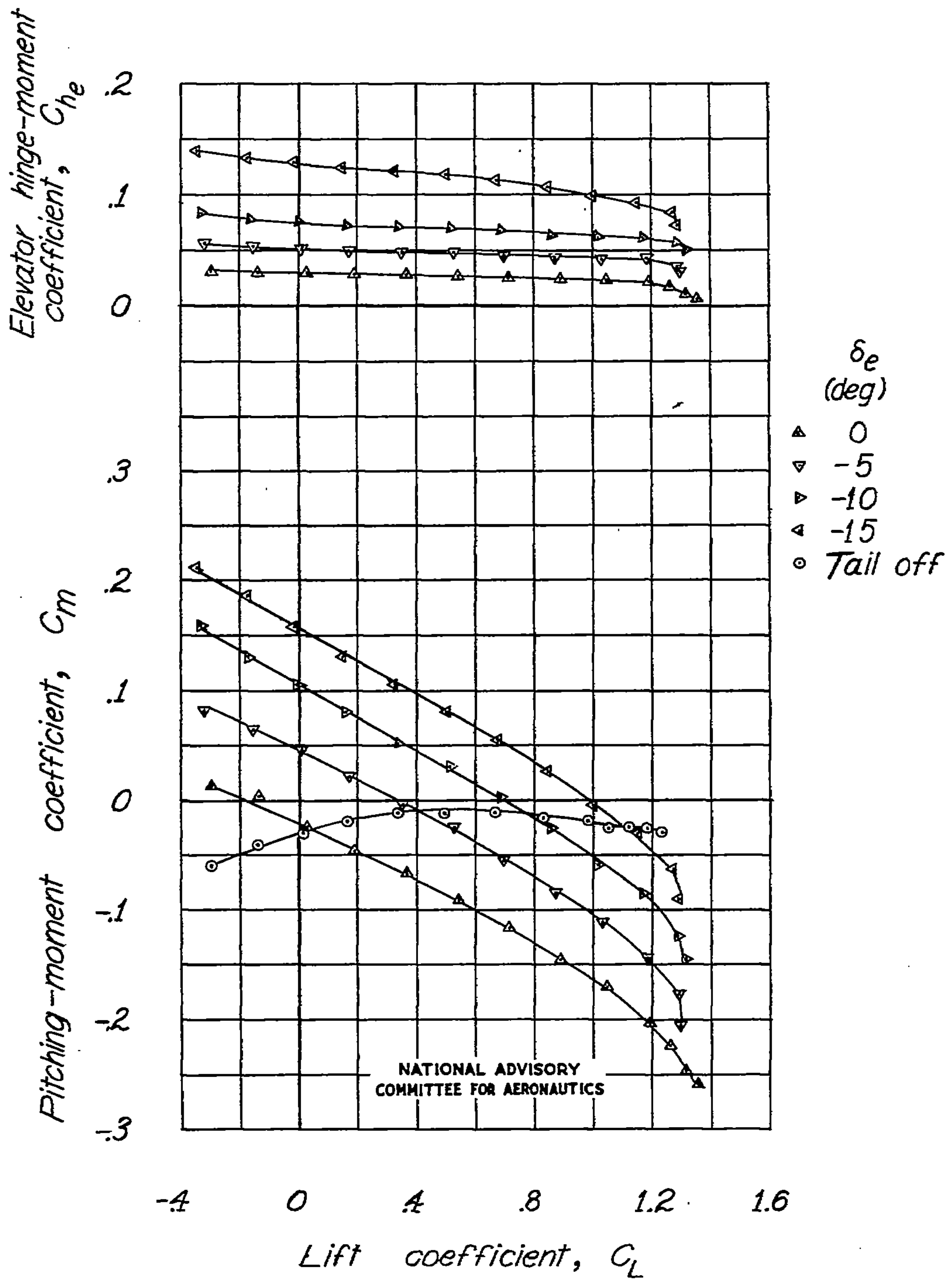

(a) Concluded.

Figure 19.-Continued.

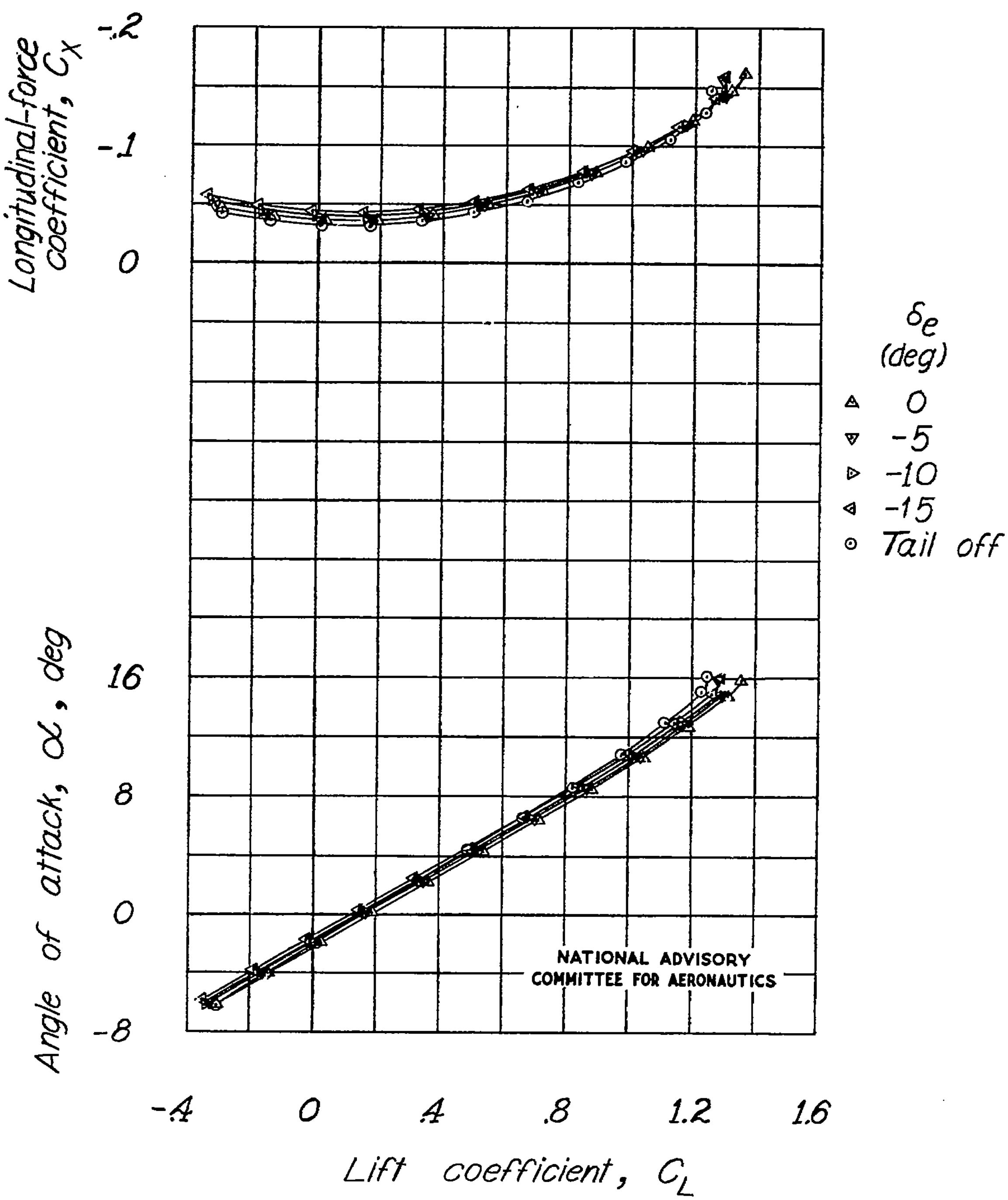

(b) Propeller windmilling.

Figure 19.-Continued.

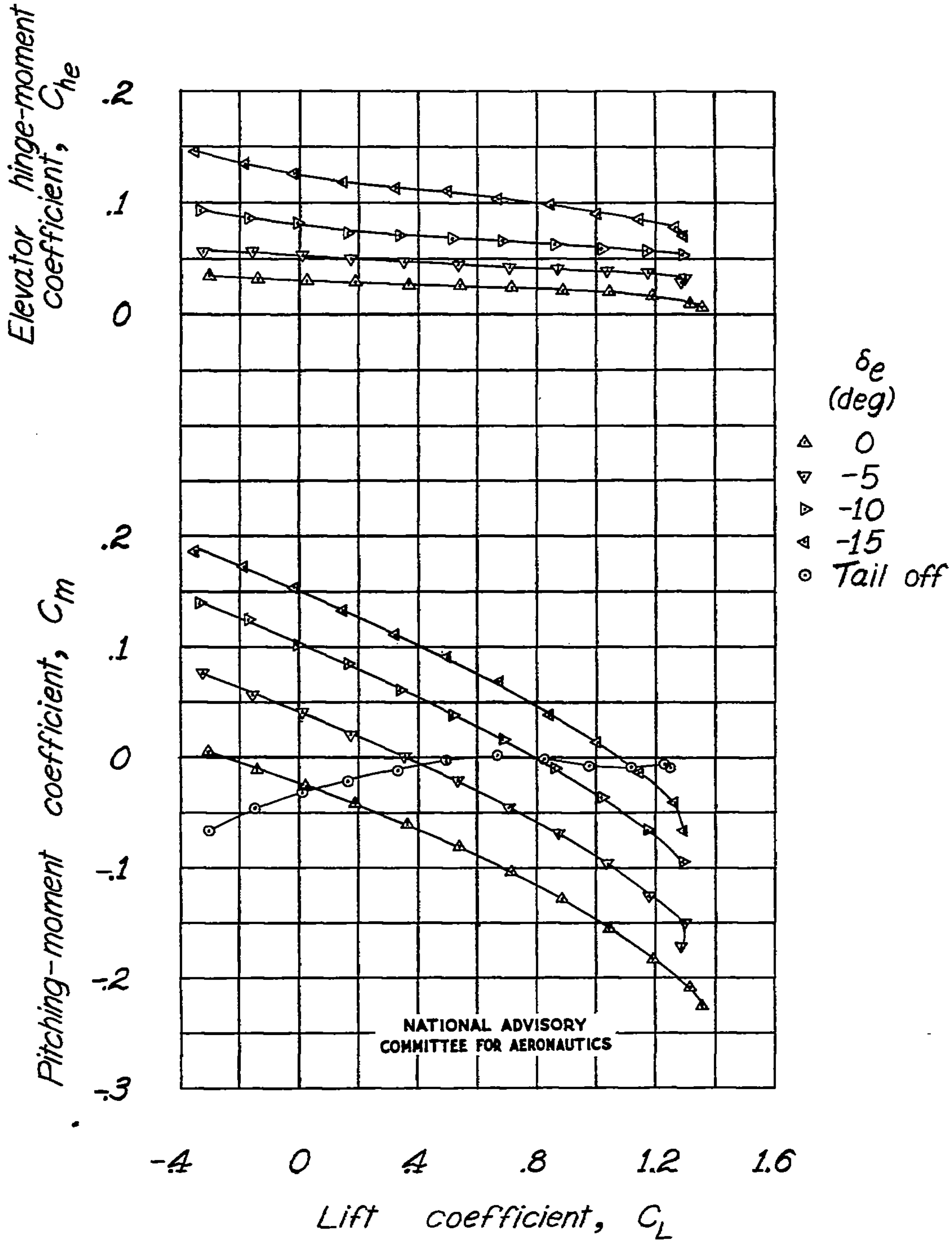

(b) Concluded.

Figure 19.-Continued.

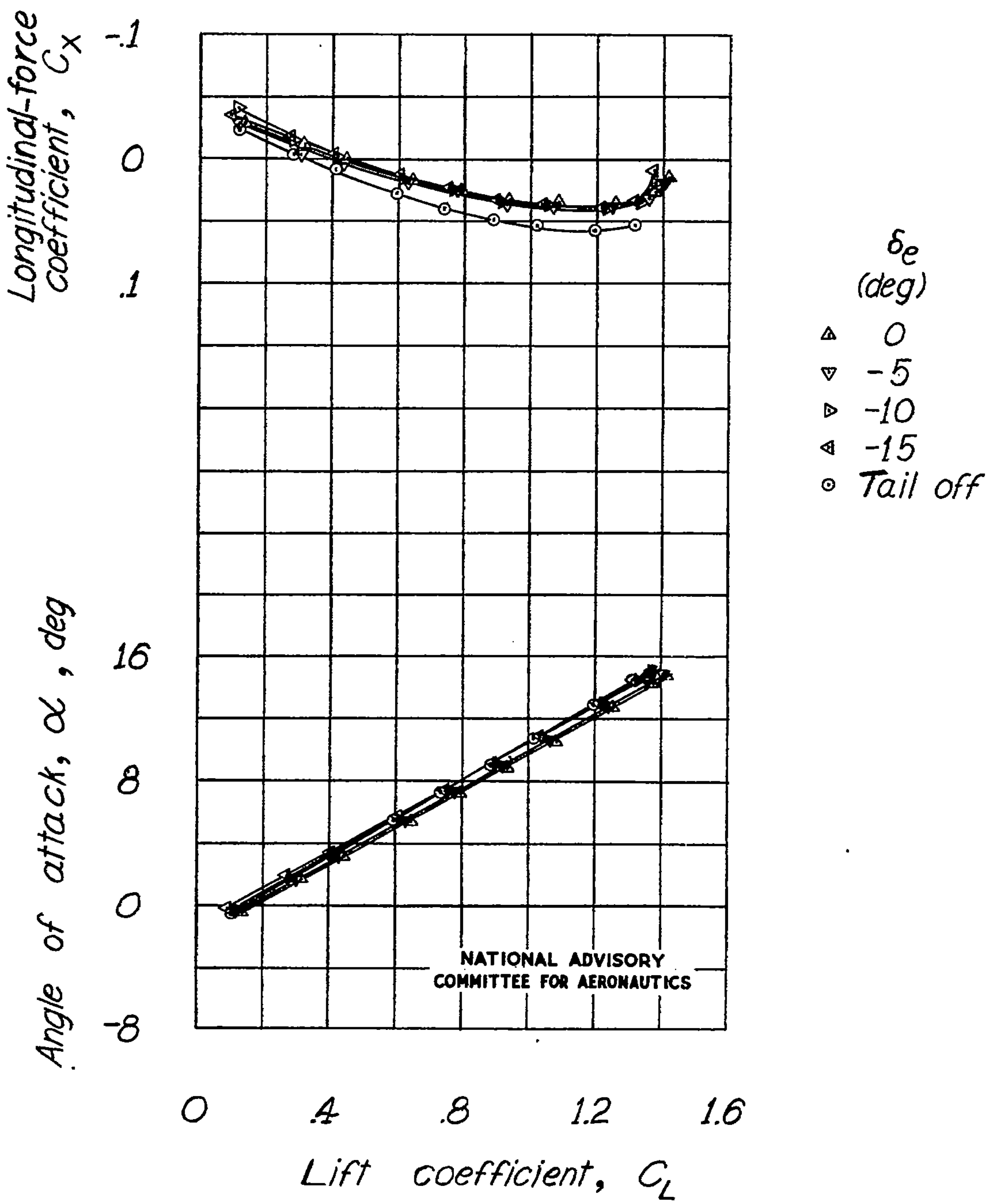

(c) Power on.

Figure 19.-Continued.

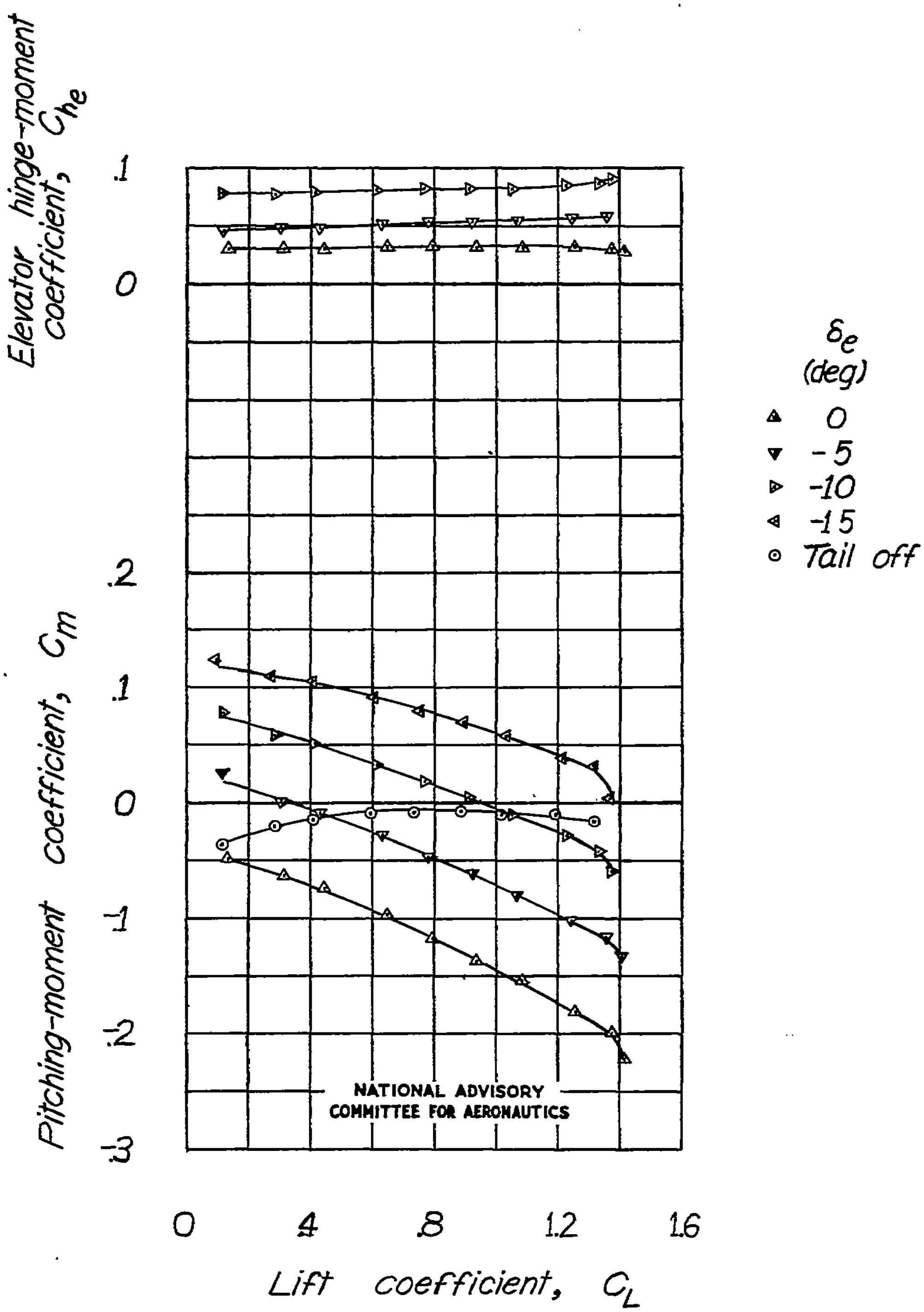

(c) Concluded.

Figure 19.-Concluded.

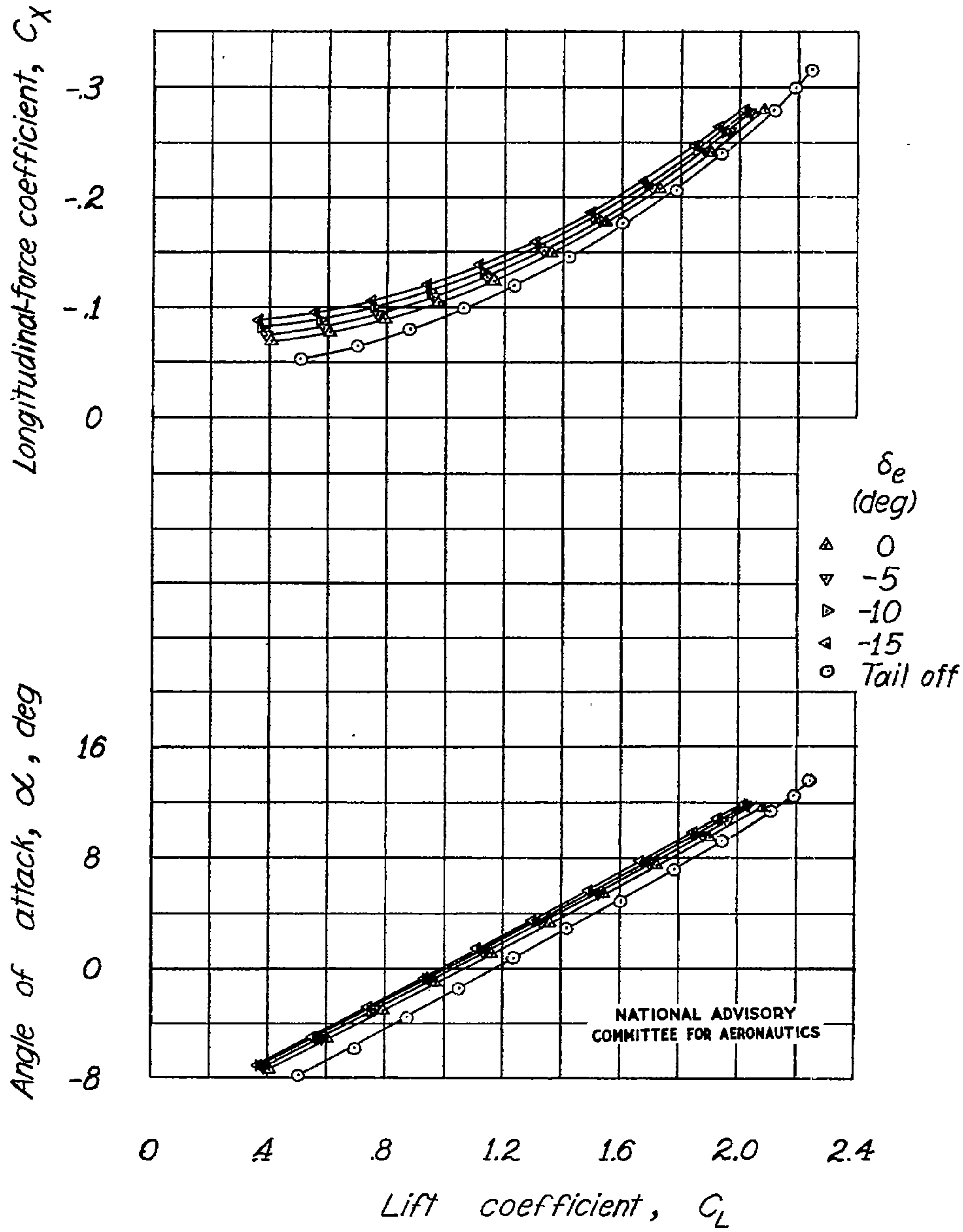

(a) Propeller off.

Figure 20.- Effect of elevator on the aerodynamic characteristics of the model as a single-engine high-wing airplane with a full-span single slotted flap. $i_t = -1.3°$; tail slot closed.

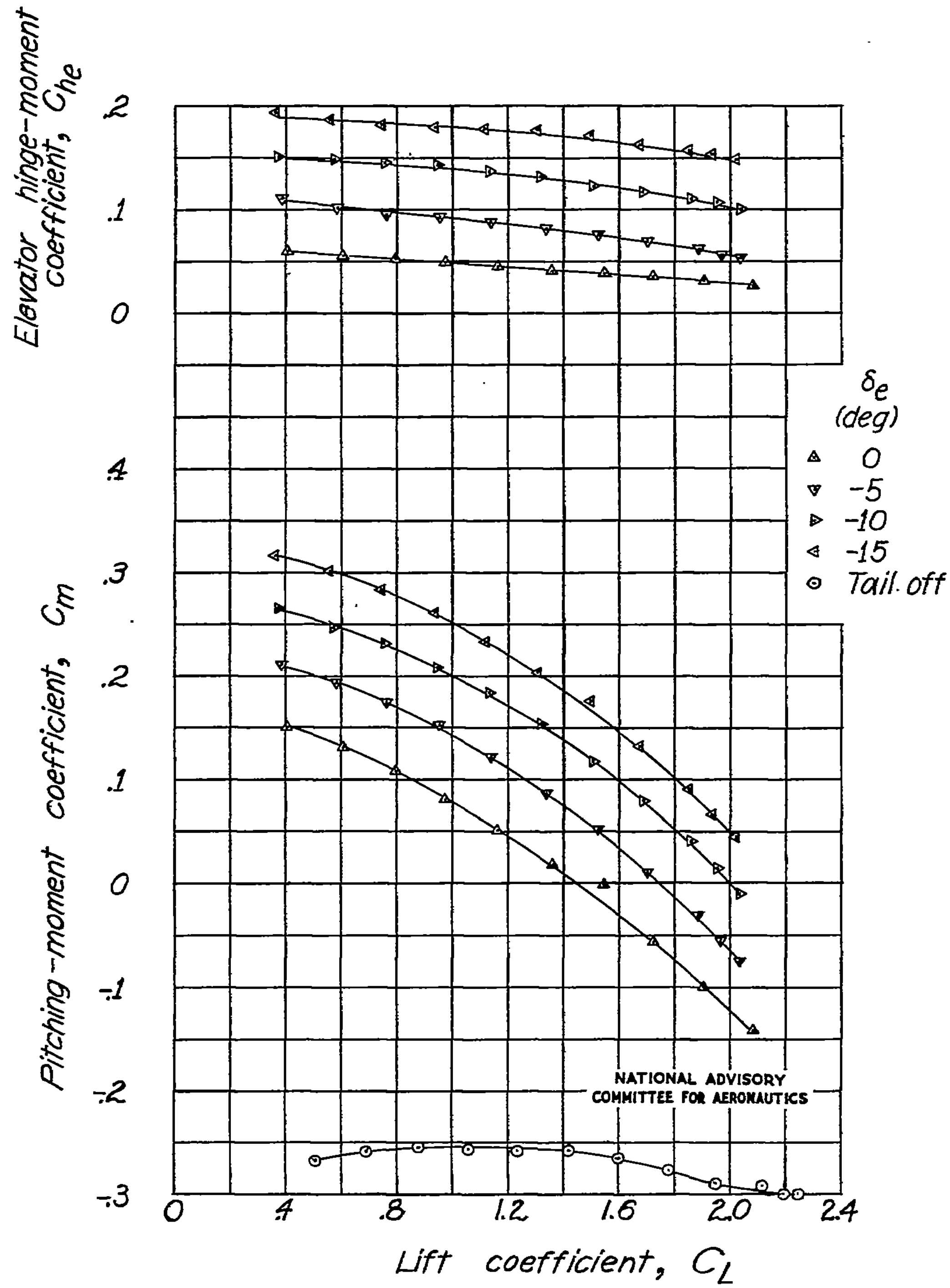

(a) Concluded.

Figure 20.- Continued.

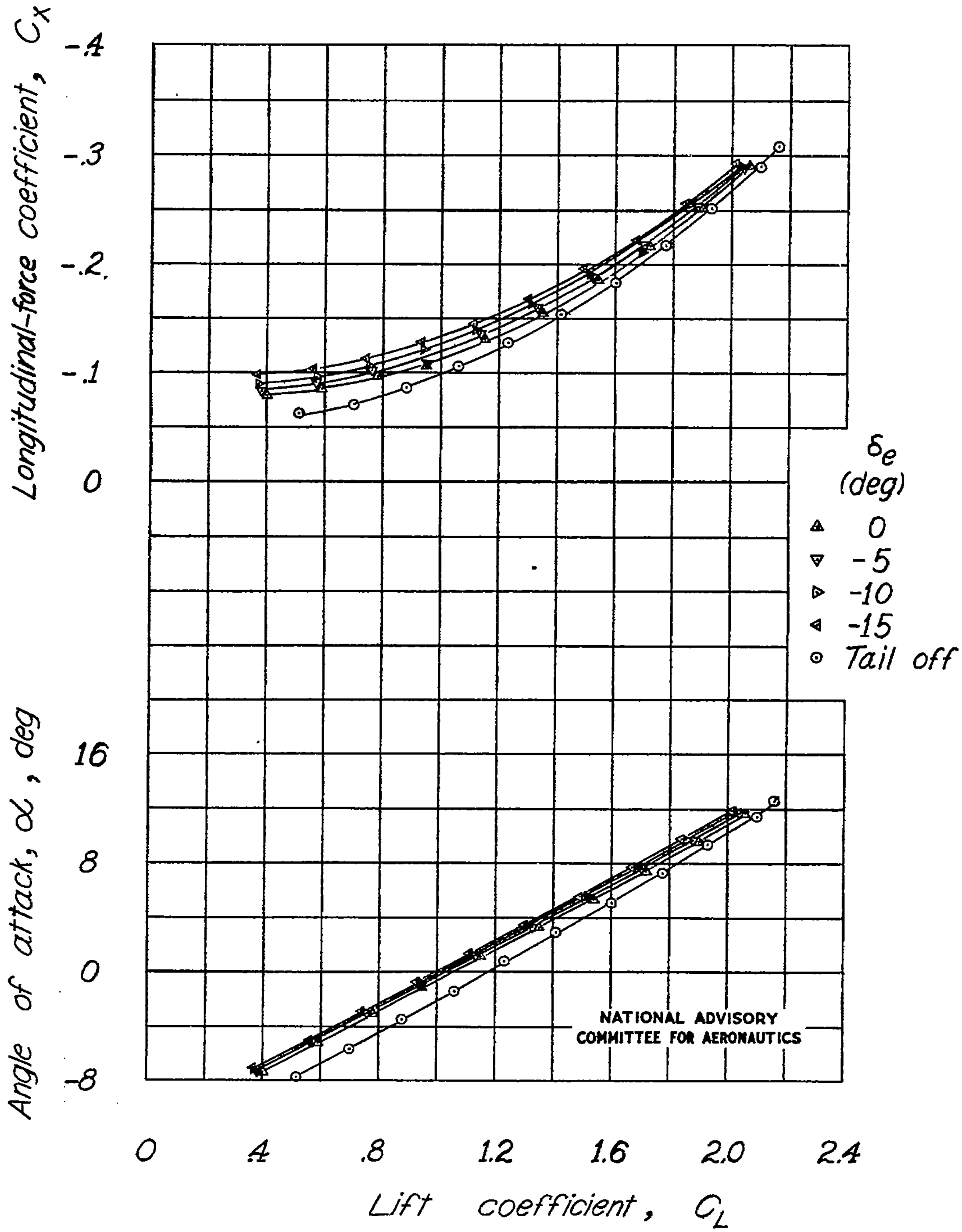

(b) Propeller windmilling.

Figure 20.-Continued.

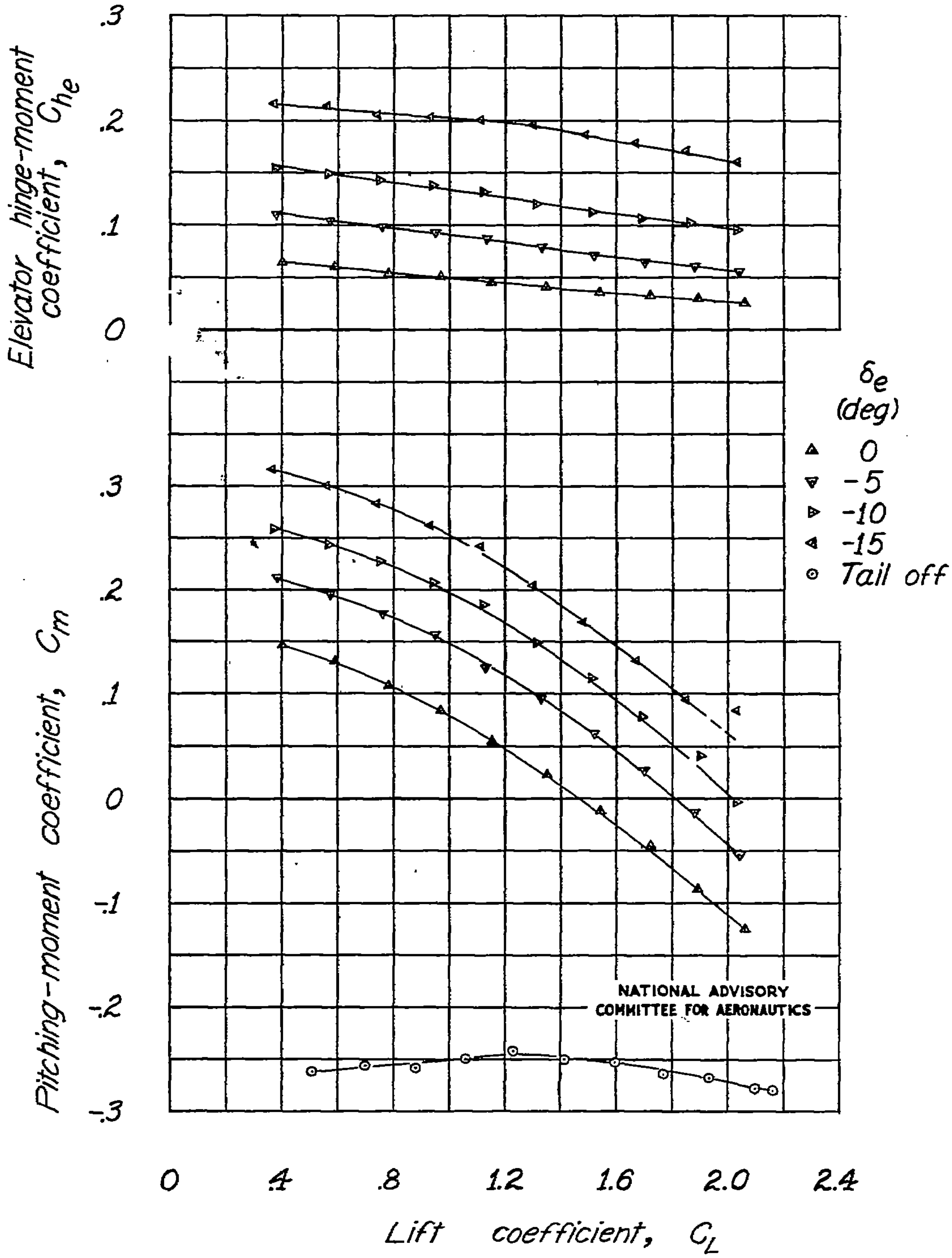

(b) Concluded.

Figure 20.-Continued.

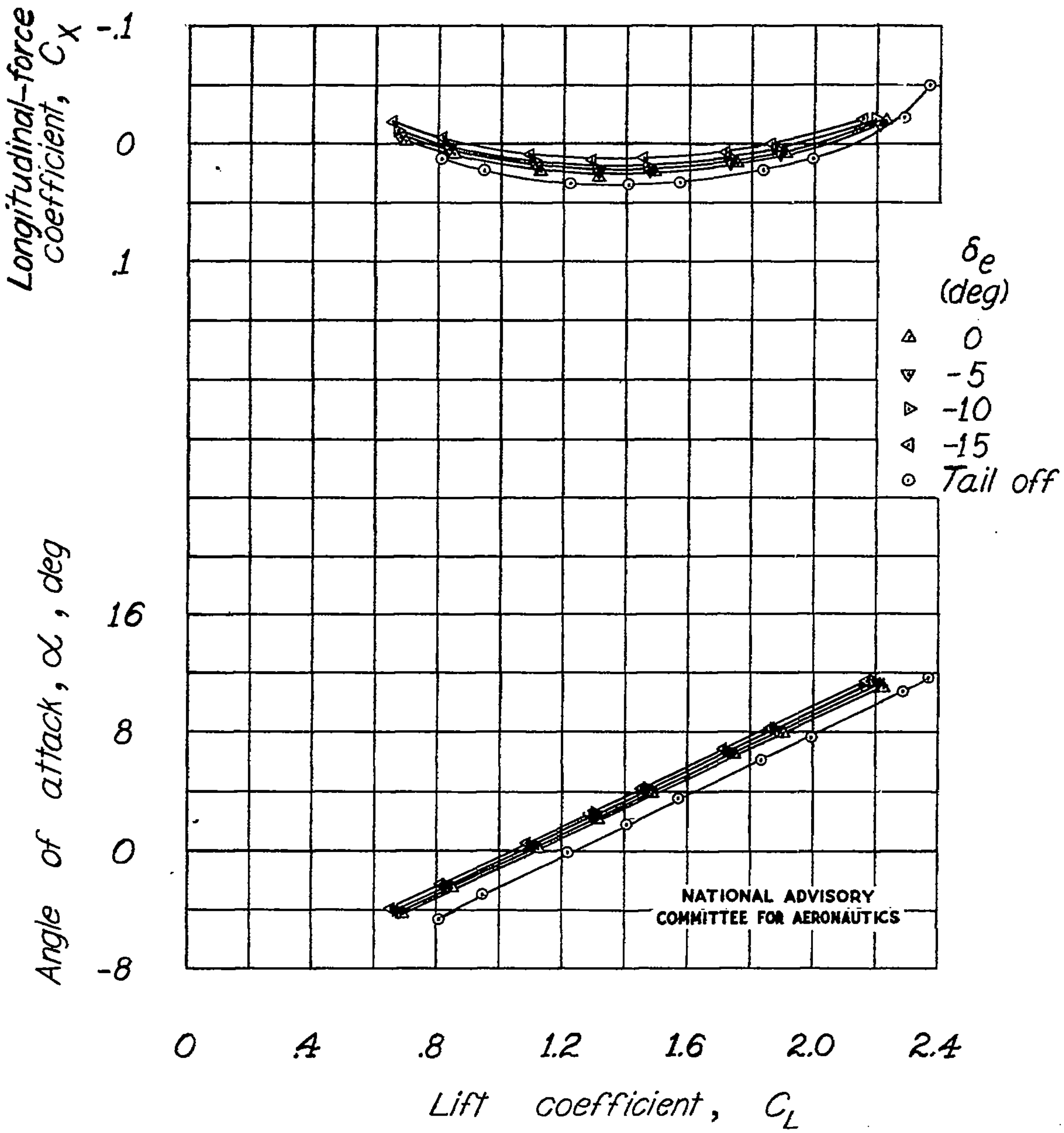

(c) Power on.

Figure 20.-Continued.

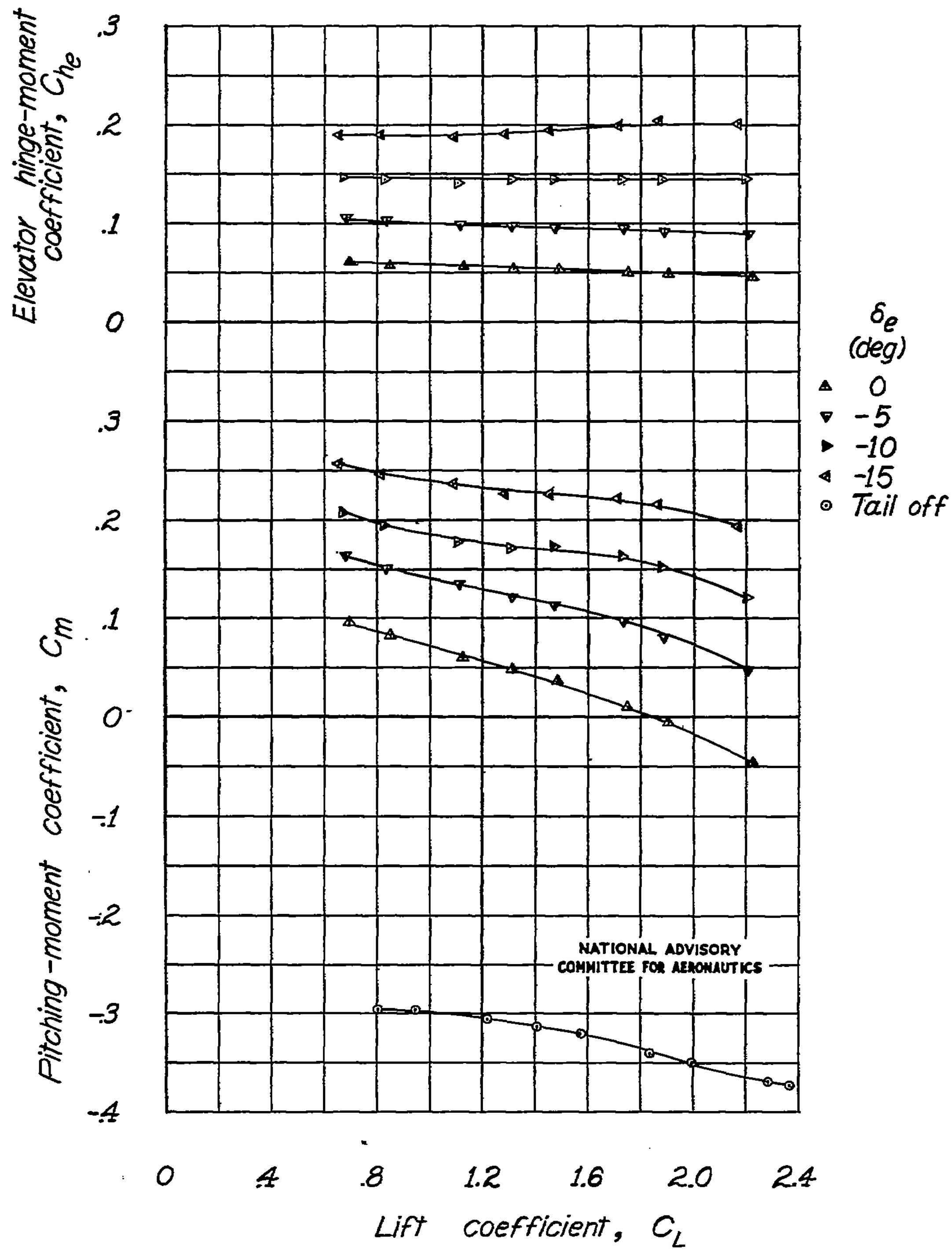

(c) Concluded.

Figure 20.-Concluded.

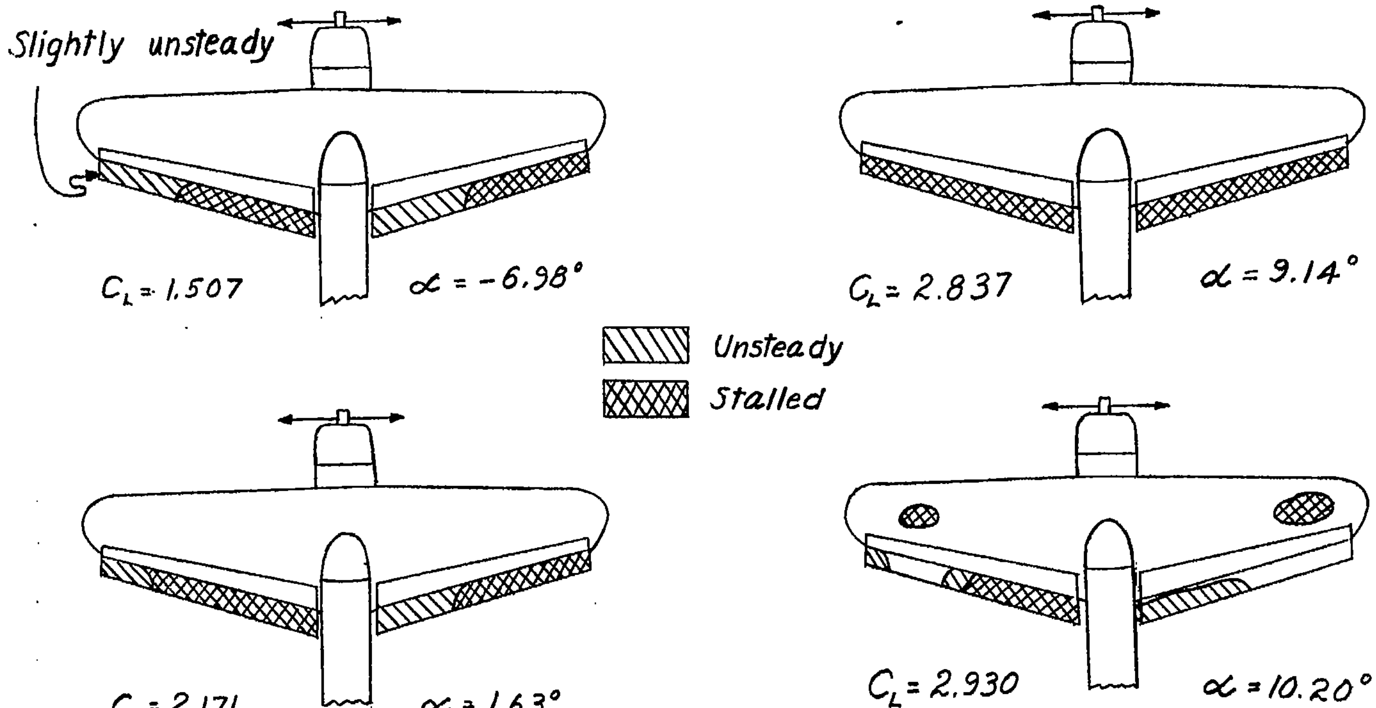

(a) Propeller windmilling. $q = 16.37$ pounds per square foot.

Figure 21.- Tuft studies of the model as a single-engine high-wing airplane with full-span double slotted flap.

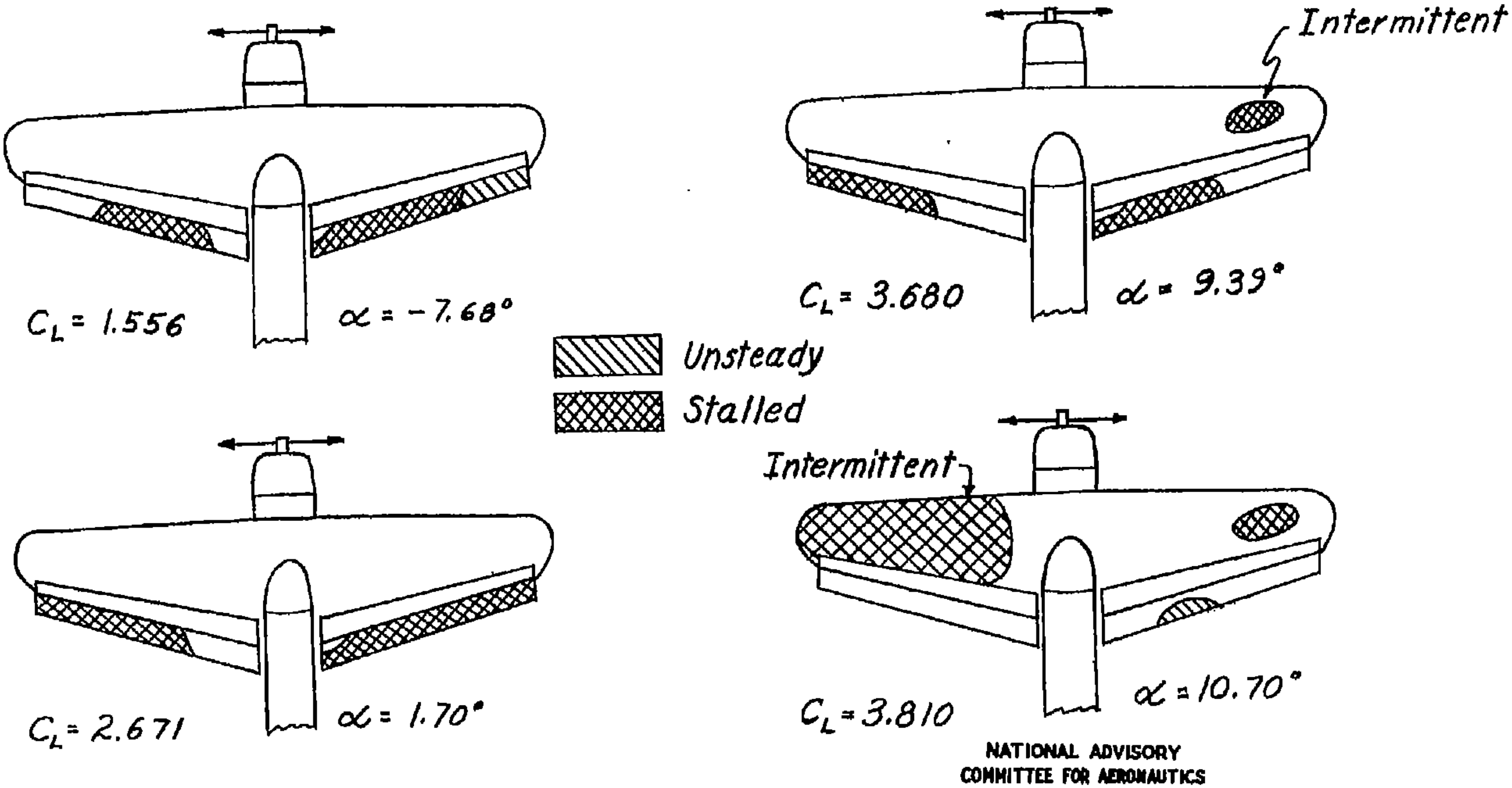

(b) Power on. $q = 12.53$ pounds per square foot; $T_c' = 0.161C_L$.

Figure 21.- Concluded.

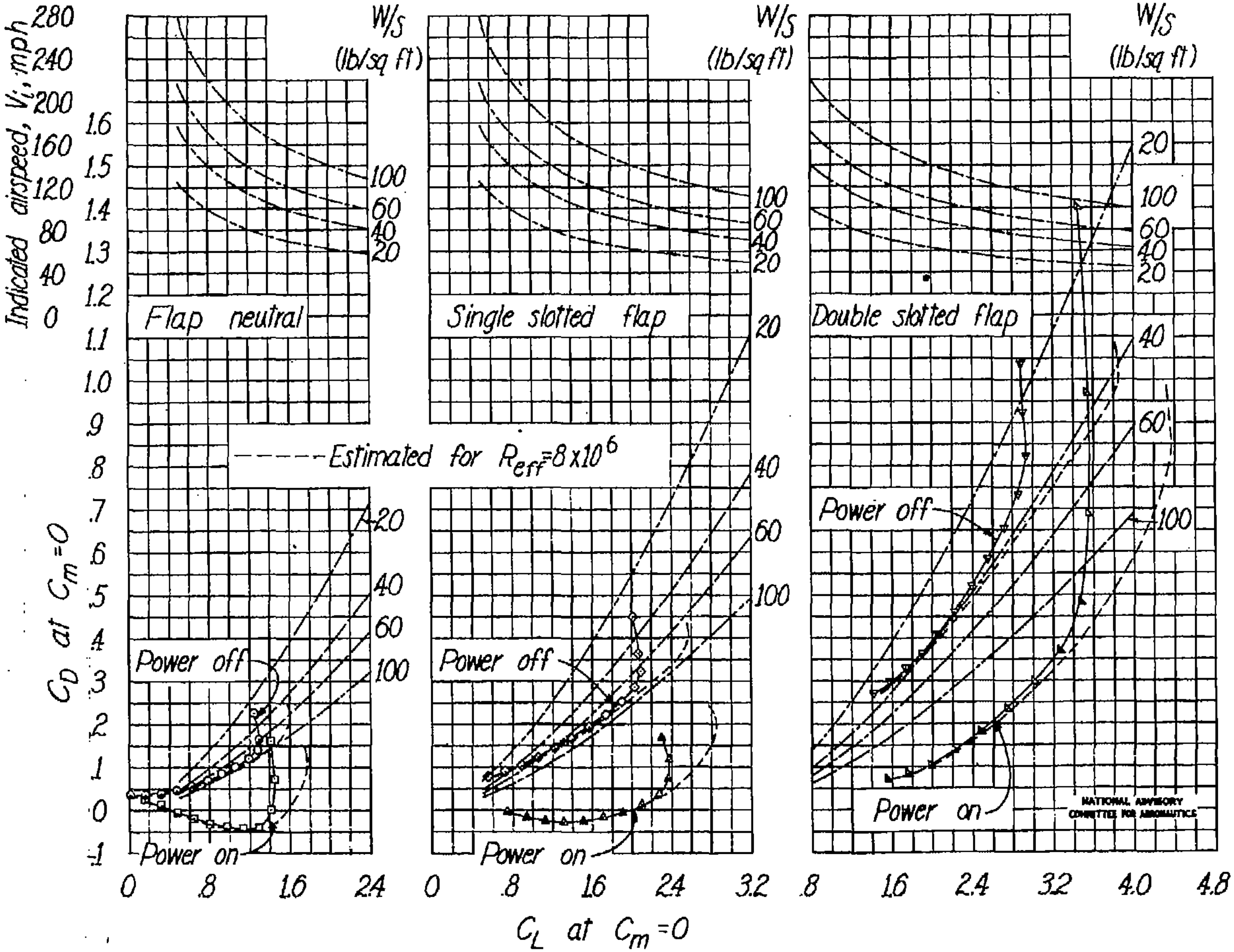

Figure 22.-Data for the effect of power and flap deflection on the landing characteristics of the model as a single-engine high-wing airplane. Curves for C_D at $C_m=0$ are for $V_S = 25$ feet per second.

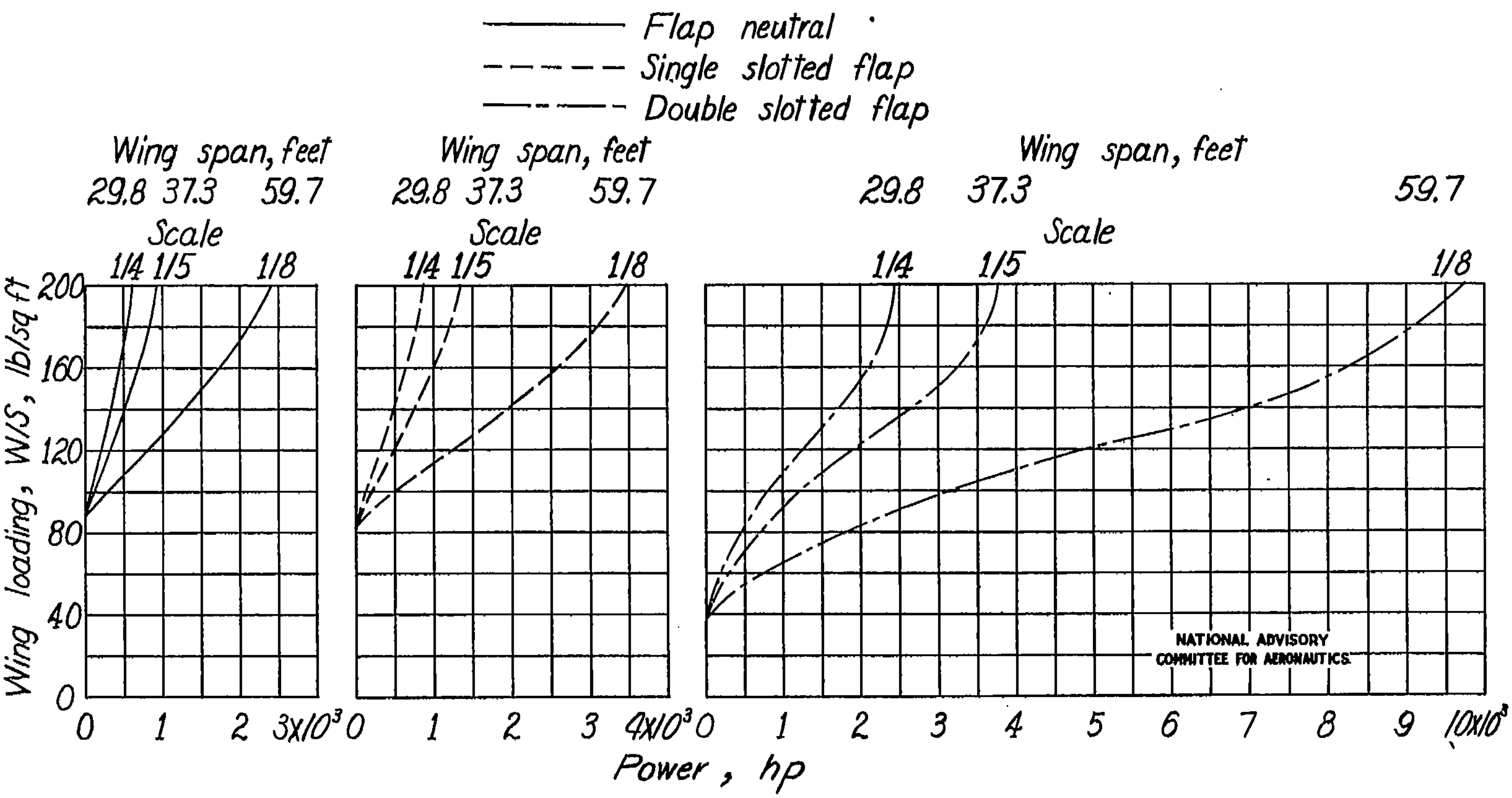

Figure 23.- Effect of scale and wing loading on the power required to maintain a indicated sinking speed of 25 fps at 0.85 $C_{L_{max}}$ for the model as a single-engine high-wing airplane. ($C_{L_{max}}$ estimated for $R_{eff} = 8 \times 10^6$.)